



STATICALLY BALANCED  
COMPLIANT WALLS

Hoessein Alkisaei



---

# STATICALLY BALANCED COMPLIANT WALLS

---

MASTER OF SCIENCE THESIS

For obtaining the degree of Master of Science in Civil Engineering at  
Delft University of Technology

H. Alkisaie, B.Sc.

January 20, 2016

Board of examiners:

Prof. Dr. ir. L.J. Sluys, Delft University of Technology  
Prof. Dr. ir. J.L. Herder, Delft University of Technology  
Dr. Ing. H. Bier, Delft University of Technology  
ir. G. Radaelli, Delft University of Technology



Copyright © 2016 by H. Alkisaie

All rights reserved. No part of the material protected by this copyright notice may be reproduced or utilized in any form or by any means, electronic or mechanical, including photocopying, recording or by any information storage and retrieval system, without the prior permission of the author.

Author email: [h.alki@live.com](mailto:h.alki@live.com) or [h.alkisaie@gmail.com](mailto:h.alkisaie@gmail.com)

# ACKNOWLEDGEMENTS

This work has been conducted at the Delft University of Technology in the form of a unique and triangular collaboration among three faculties: Civil Engineering, Mechanical Engineering, and Architecture. Extensive effort from all three fields has been provided in order to bring this study to a success.

Graduating is hardly straightforward. For many, this might sound familiar and obvious, but research teaches you how important it is to work systematically. Moreover, it is also taught me that candidates are required to be analytically strong, flexible, original, objective, controlled and extremely patient. Hurried activities can lead to undesired outcomes and delay in your progress. In addition, I believe that one of the most, if not the most, important characteristic researchers should have is courage. Decision-making, with the lack of a clear vision, pushes you sometimes to the limit and can become frustrating. Therefore, staying passionate and dedicated to what you are doing prevents you from giving up. But before all of that, always start by ensuring that you have the right people with the right skills to guide you through such process.

To Professor Bert Sluys, I am immensely grateful for the trust you have placed in me. I still remember the first time we talked about the kind of aspects and challenges we might face throughout the progress of this course. And yes, such a unique collaboration can be difficult sometimes. But your believe in me, caring guidance, motivating support, detailed feedback, and our fruitful discussions have been invaluable and kept me confident throughout the whole period. You have truly shown me what a true scientist is. *Dank u wel.*

To Professor Just Herder, I would like to show you my gratitude for sharing your pearls of wisdom with me during the course of this research. Your introduction talk to the world of Compliant Mechanisms and Static Balancing is still mind boggling to me and keeps me asking “what if?”... Your enthusiastic attitude and visionary input during our discussions were motivating and highly appreciated. *Dank u wel.*

To Dr. Henriette Bier, I would like to gratefully thank you for the expertise and insights you have provided. Our meetings and discussions started rather simple and always ended with multiple creative drawings and doodles, which nobody could understand except the two of us. This and your joyous personality have taught me that seeing a clear path among many blurry ones is true art. *Vielen Dank.*

To my daily supervisor ir. Giuseppe Radaelli, thank you a thousand times over for everything. I truly admire the way you have gradually made me familiar with the subject. I can imagine that it can be hard sometimes to guide a student with a different study background. But your stimulating assistance in understanding the theory, comprehensive guidance in executing experiments, our Skype meetings, text messages, and telephone calls, were excellent and truly made me feel at ease. I could have not wished for a greater daily supervisor. *Dank je wel, mijn vriend.*

I would also like to thank Professor Rolf Dollevoet and Dr. Michaël Steenberg for the fruitful discussions on the subject.

To all my friends and colleagues who have made my time in Delft unforgettable, I feel blessed with you.

At last, to my beloved parents, sisters and brother, who have asked me on daily basis when my graduation will take place, and who have continuously teased me on the subject, I am deeply thankful for the unconditional love and support that you guys have given me. The day you have all been waiting for has finally arrived.

HOESSEIN ALKISAEI  
JANUARY 2016

# CONTENTS

## Paper I

<b>1.Introduction</b>	<b>1</b>
<b>2.Method</b>	<b>2</b>
2.1. Sound barriers	2
2.2. Gravity compensation	3
2.3. Topology	3
2.4. Potential energy	4
2.5. Shape optimization	5
2.5.1. <i>Objective function</i>	5
2.5.2. <i>Isogeometric Shape Optimization (design parametrization)</i>	6
2.6. Design example	6
2.7. Material usage	7
<b>3.Results</b>	<b>9</b>
3.1. Optimization results	9
<b>4.Experiment</b>	<b>11</b>
4.1. Scaling	12
4.2. Optimization result and physical model	13
4.2.1. <i>Experimental setup</i>	14
4.3. Measurement results	14
<b>5.Discussion</b>	<b>14</b>
5.1. Evaluation of applied method	15
5.2. Evaluation of the results	15
5.3. Evaluation of the experiment	16
5.4. Real life application	16
5.5. Possible applications	17
<b>6.Conclusions</b>	<b>17</b>

## Paper II

<b>1.Introduction</b>	<b>23</b>
<b>2.Method</b>	<b>24</b>
2.1. Case study	25
2.2. Gravity compensation	25
2.3. Topology, boundary conditions and actuation types	25
2.4. Cross-sections	26
2.5. Material usage	26
2.6. Shape Optimization	27
2.6.1. <i>Objective Function and solution method</i>	28
2.7. Design example	28
<b>3.Results</b>	<b>31</b>
3.1. Optimization results	31
3.2. Satisfying results	32
3.3. Wind loading	38
<b>4.Experiment</b>	<b>40</b>
4.1. Optimization result and physical model	40
4.2. Experimental setup	42
4.3. Measurement results	42
<b>5.Discussion</b>	<b>46</b>
5.1. Evaluation of applied method	46
5.2. Evaluation of the results	46
5.3. Evaluation of the experiment	47
5.4. Real life application	47
5.5. Alternative applications	48
<b>6.Conclusions</b>	<b>48</b>

## Appendix A Theoretical

<b>A1.Potential energy</b> . . . . .	<b>53</b>
<b>A2.Static Balancing</b> . . . . .	<b>54</b>
A2.1. The potential energy . . . . .	55
A2.2. The Force . . . . .	56
A2.3. The Stiffness . . . . .	56
A2.4. Gravity balancer. . . . .	57
<b>A3.Compliant Mechanisms</b> . . . . .	<b>57</b>
<b>A4.Scale and Gravity contribution</b> . . . . .	<b>59</b>
A4.1. Static scale laws . . . . .	59
A4.2. Gravity contribution . . . . .	60
A4.3. Stiffness . . . . .	60

## Appendix B Numerical

<b>B1.Structural Optimization</b> . . . . .	<b>65</b>
B1.1. Topology optimization . . . . .	65
B1.2. Shape optimization . . . . .	65
B1.3. Size optimization . . . . .	66
<b>B2.Isogeometric Analysis</b> . . . . .	<b>66</b>
B2.1. NURBS . . . . .	66
<i>B2.1.1.Knot vectors</i> . . . . .	67
<i>B2.1.2.B-Splines</i> . . . . .	67
<i>B2.1.3.B-Spline Surfaces</i> . . . . .	69
<i>B2.1.4.B-spline solids.</i> . . . . .	69
<i>B2.1.5.Rational B-splines</i> . . . . .	69
<b>B3.Element formulation</b> . . . . .	<b>71</b>
B3.1. Kirchhoff-Love planar beams . . . . .	71
B3.2. Kirchhoff-Love Shells . . . . .	72
<b>B4.Numerical procedure</b> . . . . .	<b>74</b>
B4.1. Planar beams . . . . .	74
B4.2. Shell structures . . . . .	76
<b>B5.Numerical results</b> . . . . .	<b>77</b>
B5.1. Other potential geometries . . . . .	77
B5.2. Different material application . . . . .	79
B5.3. Failure. . . . .	80

## Appendix C Practical

<b>C1.Experiments</b> . . . . .	<b>85</b>
C1.1. Planar beam experiment. . . . .	85
C1.2. Shell beam experiment . . . . .	86
C1.3. PET-G Pull test . . . . .	92
<b>C2.Actuation</b> . . . . .	<b>95</b>
<b>C3.Noise</b> . . . . .	<b>97</b>
C3.1. Noise Barrier Materials . . . . .	97
<i>C3.1.1.Brick and masonry Block</i> . . . . .	98
<i>C3.1.2.Metals</i> . . . . .	98
<i>C3.1.3.Wood.</i> . . . . .	99
<i>C3.1.4.Transparent panels</i> . . . . .	99
<i>C3.1.5.Plastics</i> . . . . .	100
<i>C3.1.6.Composites</i> . . . . .	100
C3.2. Miscellaneous . . . . .	101

## Appendix D Patent . . . . . 105





**Pray. There is  
immeasurable power in it.**





Paper I



# Design of Large-Scale Compliant and Monolithic Gravity Balancers as Deformable Walls

H. ALKISAEI<sup>1</sup>, G. RADAELLI<sup>2,4</sup>, J.L. HERDER<sup>2</sup>, H. BIER<sup>3</sup>, L.J. SLUYS<sup>1</sup>

<sup>1</sup>*Dept. Structural Engineering, Delft University of Technology, Delft, The Netherlands*

<sup>2</sup>*Dept. Precision and Microsystems Engineering, Delft University of Technology, Delft, The Netherlands*

<sup>3</sup>*Dept. Architectural Engineering and Technology, Delft University of Technology, Delft, The Netherlands*

<sup>4</sup>*Laevo BV, Molengraaffsingel 12-14, Delft, The Netherlands*

---

## ABSTRACT

This paper presents the development of novel large-scale monolithic and compliant designs for gravity balancers with a prescribed displacement. The topology of the system consists of a planar beam with boundary and actuation conditions that are altered, depending on specific loading cases. The latter lead to different structural behaviour and are therefore investigated. Complex-shaped geometries are achieved by means of shape optimization procedures, which are based on minimizing the residuals between the desired and the actual potential energy path. The obtained designs are meant to act, in real-life application, as compliant sound barriers that are flattened when they are not needed and erected as soon as vehicles enter the scene. This prevents horizon pollution. The most satisfying geometry has a structural height of  $\pm 6m$ , a beam thickness of  $0.04m$ , and requires a maximum actuation force of  $-0.5\sim 1N$  to deform from the erected to the flattened state and vice versa. A scaled physical model made out of PET-G plastic has been successfully tested. The numerical predictions coincide well with the experimental results, and thus demonstrate the suitability of this method for further development and application.

*Keywords:* compliant mechanisms, interactive architecture, neutral stability, shape optimization, sound barriers, static balancing, zero-force

---

## 1. INTRODUCTION

Today architectural structures are increasingly implemented with characteristics that provide flexible adaptation to constantly changing needs and desires of people or environmental conditions. These structures are digitally designed, produced and operated, and are known as digitally driven architecture [1]. Relevant examples such as Scissor-Pair Transformable Structures developed at MIT [2], and other kinetic, reconfigurable systems [3], [4] indicate that the main challenges are their actuation and construction complexity.

2008-09, Hyperbody at Delft University of Technology and Festo AG have designed and built a 1:1 scale prototype of an Interactive Wall (IW), which was exhibited at the Hannover fair in 2009 for an interactive demonstration [5]. The IW is a flexible frame that is 1.09 meters wide, 0.53 meters deep and 5.30 meters tall. An elastic fabric is used to cover the frame to give the overall impression of a flexible, monolithic, and solid structure. Several motion sensors such as lighting and loudspeakers are integrated into the IW. With respect to kinetic transformation, the IW is actuated and positioned in desired states by means of electronic cylinders [6].

Inspired by the IW, Oosterhuis et al. [5] proposed the Barrier in Motion (BiM) in which sound barriers along train tracks are flattened to the ground as long as no trains are present. As soon as trains enter the area they trigger the

BiM to erect, so that noise is blocked effectively. This is advantageous considering that conventional sound barriers along car roads and train tracks permanently block the view due to their massive stature. However, the IW and BiM present several challenges with respect to materialisation and performance.

Firstly, the extensive and abundant amount of parts needed for construction introduce undesired complexities. Secondly, conventional rigid joints cause backlash, friction and wear [7], which can lead to poor repeatability, need for lubrication, high maintenance and assembly costs [8]. And finally, large structures that undergo large deformations demand a significant amount of force and are therefore often realized with integrated actuators of large sizes. In particular when moving vertically, i.e. against gravity. The aforementioned challenges are common in the fields of deformable and interactive structures.

An adequate way of dealing with the first two issues is by making use of compliant mechanisms and joints. Compliant mechanisms gain their motion from the deformation of the material and are able to undergo large deformations [9], [10]. They can be designed in monolithic manner [11], and therefore lead to the absence of sliding friction and the elimination of wear, noise, and the need for lubrication and eventually omit the disadvantages of conventional rigid joints [7]. In summary, compliant joints and mechanisms lead to reduced assembly, weight and lubrication costs [12].

Considering the third issue, statically balanced mechanisms undergo energy efficient motion and are in equilibrium throughout their entire range of motion. The potential energy level of a statically balanced mechanism is constant and implies low actuation forces as long as friction and other parasite forces can be neglected [13].

A constant potential energy can be achieved by balancing the change in potential energy with the introduction of a second energy storage element, e.g. counterweight or a spring. Mechanisms that statically balance the weight of an object are referred to as gravity balancers. These mechanisms allow weights to be moved up and down with little effort. Small-scale applications can be found in various examples [14]–[17]. By using the weight, and applying the gravity balancers method, a deformable large structure can be designed, which requires effortless actuation to position itself from one state to another. Compliant mechanisms are deformed due to the application of a force or displacement to the system. Consequently, energy will be stored in the elastic members in the form of elastic energy due to the stiffness of the material. This elastic potential energy can be used to obtain a constant potential energy level along the total range of motion. Some examples from literature of gravity balancers with compliant parts are discussed next.

Rijff et al. [18] developed a new method for the design of single degree of freedom gravity balancers where all rigid joints are replaced with compliant joints. They have basically connected rigid links with compliant joints and obtained a statically balanced compliant mechanism. Riele et al. [19] presented several gravity equilibrators that incorporated normal off-the-shelf springs that provided perfect static balance. This proved that gravity balancers could be constructed in cheap and simple manners. Radaelli et al. [20] presented a method for the design of compliant mechanisms with large deflections and prescribed load paths. They used shape optimization procedures for a planar beam, which is applied to the synthesis of a balancer for a pendulum. One of the beam-ends was clamped and the other exposed to a rotational actuation. In a follow up research, Radaelli et al. [21] extended the latter by obtaining a single complex-shaped beam on which a weight was attached. The beam was modelled as a monolithic planar beam that balances the weight along a prescribed vertical displacement with no constraints in the horizontal direction. However, the aforesaid research dealt with small-scale structures and no attention has been paid to large scale.

The goal of this research is to obtain novel geometries for statically balanced and compliant walls (CW), which consist of a monolithic planar beam with boundary conditions, and an actuation. These boundary and actuation types are altered for specific loading cases in order to investigate their influence on the structural behaviour. The compliant structure is required to deform from an erected to a flattened state and vice versa to conform the design of the Barrier in Motion. This deformation happens effortlessly since the weight of the structure is compensated by the naturally distributed stiffness of the material. Geometries that

satisfy the latter objectives are obtained by means of shape optimization procedures. Ultimately, the construction and validation of a scaled physical model will be presented as proof of principle.

After the introduction, the second section describes the topology and design characteristics of the considered geometries, the idea behind static balancing, and a thorough description of the optimization procedures. The third section presents the results of the most optimal shapes considering specific situations. The fourth section shows the experimental setup and results, followed by the discussion and conclusion in the fifth and sixth section, respectively.

## 2. METHOD

The current research analyses five different cases that represent the Compliant Wall (CW). The structural shapes are computationally obtained by means of Isogeometric Shape Optimization. The objective is to minimize the residual between the desired and actual potential energy path of the mechanism along a certain chosen range of motion. The following sections present specific and detailed information about the methods and materials that are used throughout this study. Ultimately, an optimization example is posed, which illustrates the sensitivities of the design parameter choices.

### 2.1. SOUND BARRIERS

Sound barriers are mostly employed along car roads and vary between 2 and 3 meters height. In densely populated areas the height variation ranges between 3 and 6 meters. Sound barriers along train tracks are in general lower than those along car roads. This is due to the fact that these barriers can be placed closer to the source in comparison with car roads. On the other hand, there are examples of 8 meters high sound barriers along train tracks. This is done to significantly increase the effectiveness of acoustic absorption. A third important application of sound barriers is at airports. These are placed along airstrips where planes take-off or land. In this situation, typical heights vary between 6 and 10 meters.

The surface-weight of the applied sound barrier is an important design component for the reduction of noise. A sound barrier with a surface-weight of  $10\text{kg}/\text{m}^2$  ensures a noise reduction of 15dB or more [22]. Structural weights between 40 and  $100\text{kg}/\text{m}^2$  lead to a reduction of 25dB or more, which is sufficient in most cases.

Therefore, this research aims for obtaining designs with structural heights between 4 and 7 meters that lead to a noise reduction of approximately 20dB or more, and are able to be deformed effortlessly from an erected to a flattened position and vice versa. A flattened position is defined as being lower than the train tracks. The latter is to prevent any form of horizon pollution. Furthermore, the focus is merely on sound barriers along train tracks,

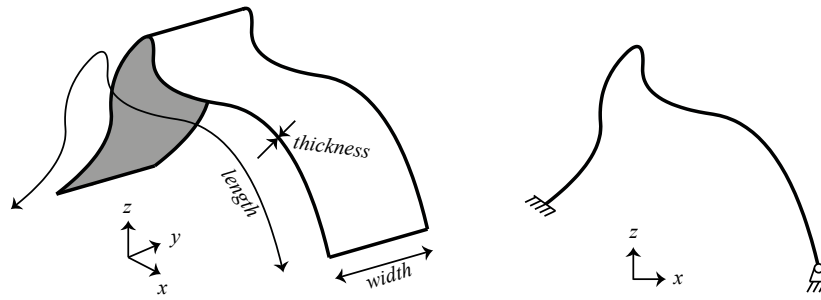


**Figure P1.1:** The topology considered in this study consists of a planar beam with a certain length, width and thickness. At each beam-end are specific boundary conditions applied. The results in this study will only present the two-dimensional side-view of the planar beam.

since sound barriers along car roads would be continuously positioned in the erected state due to the high traffic flux.

## 2.2. GRAVITY COMPENSATION

Self-weight plays a major role in the design process of large structures. In most of the cases it is decisive for the slenderness of specific structural elements. In this research the structural weight of the CW is compensated in order to achieve an effortless actuation along a certain path of motion. Various design methods for gravity compensation make use of the stiffness of springs to compensate centres of gravity [12]. However, this is not the case for the current investigation. Here it is chosen to compensate the structural self-weight by using the internally and naturally distributed material stiffness. It is therefore possible to obtain compliant and monolithic designs, since no external or additional springs are required. Consequently, the amount of parts needed for construction are reduced.

## 2.3. TOPOLOGY

In contrast to stiff and rigidly constrained conventional sound barriers, the application of the CW behaves in a compliant manner and undergoes large structural deformation, due to applied actuation conditions, in order to fulfil its purpose. Figure P1.1 presents the considered topology for this research, which is that of a single planar beam with a specific length, thickness, width, and a specific boundary condition at each end. Each actuation and

boundary type leads to a different behaviour and outcome. Figure P1.2 illustrates the five different cases that are considered in order to investigate the influences of different types of actuation and boundary conditions. The black and blue lines represent the initial and last deformed state, respectively. The red arrows present the type of actuation.

The first three cases from Figure P1.2 are exerted to a prescribed displacement  $v$ . Case I has two clamped beam-ends, Case II has a clamped and a pinned beam-end, and Case III has two pinned beam-ends. Case IV has a rotational actuation  $\theta$  at one beam-end and is clamped at the other. Case V is similar to Case IV except the clamped beam-end is substituted with a pin. This study is limited to situations in which the structure is exerted to one actuation type. Cases in which the beam-ends are displaced in vertical or horizontal sense are not presented, since they occur to be impractical for real-life application due to the significantly large space they occupy.

As can be seen from Figure P1.2, the five cases clearly depict relatively different deformed states due to the applied boundary and actuation conditions. For instance, pinned boundary conditions allow the structure to flatten completely, whereas clamped boundary conditions naturally do not. On the other hand, clamped boundary conditions lead to slim deformed states, which can be more practical in real-life. Furthermore, a rotational actuation at the foundation can be hidden from the eye. The latter is not possible for actuations applied to the body of the structure, like in the first three cases from Figure P1.2. It is therefore that rather simple observations, like these, already prove the

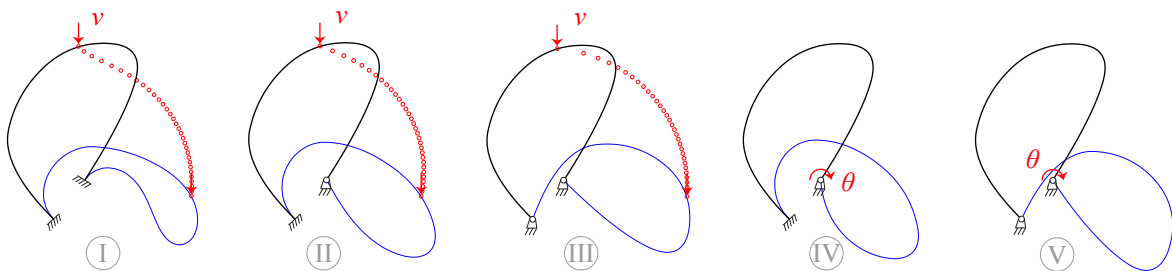


**Figure P1.2:** The five actuation schemes that are considered in this study. The first three schemes are exposed to a prescribed displacement  $v$ . The last two are exposed to a rotational actuation  $\theta$  at one of the fixations. The black and blue solid lines represent the initial and last deformed state of the structure, respectively.

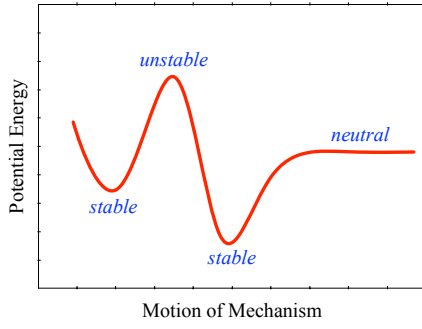


**Figure P1.3:** A potential energy level path of a mechanism. The local minima represent stable positions, while a local maximum represents an unstable position. If an energy path is constant it means that the mechanism is neutrally stable.

significant influence of different actuation and boundary conditions on the behaviour and appearance of the system.

#### 2.4. POTENTIAL ENERGY

A system with no exertion to acceleration is said to be in static equilibrium. At the same time, a system finds itself in a stable equilibrium position whenever small disturbances cause it to oscillate around its equilibrium. On the other hand, if small disturbances cause the system to diverge from its equilibrium state, it is then said to be unstable. Furthermore, systems that stay in the disturbed position are known as neutrally stable mechanisms. When the potential energy of a mechanism is plotted over its motion, each local minimum and maximum represents a stable and unstable equilibrium position, respectively. A neutrally stable mechanism gives a constant energy path, see Figure P1.3. The required force over a range of motion is obtained by taking the derivative of the potential energy with respect to its degree of freedom. This is shown in the following equation

$$F(x) = -\frac{\partial U_{total}}{\partial x}, \quad (P1.1)$$

in which  $F$ ,  $U_{total}$  and  $x$  represent the force, the potential energy and the relevant degree of freedom, respectively. Note, taking the derivative with respect to a rotation results in moment forces.

As earlier mentioned, the CW has basically two positions: erected (vertical) and flattened (horizontal). In this research the motion of the CW is expressed by means of potential energy. Figure P1.4 illustrates four potential energy paths that describe different behaviours of the CW. The graphs from Figure P1.4A and Figure P1.4B are known as bistable mechanisms. They consist of two local minima and of one local maximum in-between. Each local minimum, and thus stable position, represents an erected or flattened state for the CW.

Figure 1.4C represents a potential energy path with one local minimum, and thus one stable equilibrium position. This position can be the erected or the flattened state for the

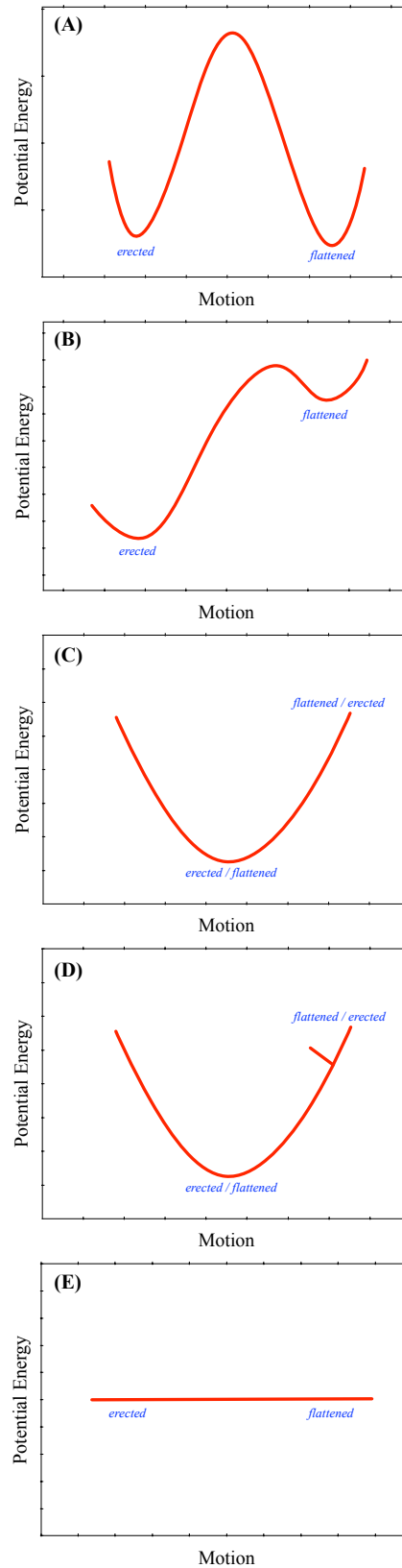


**Figure P1.4:** Five different energy load paths that could represent the behaviour of the Barrier in Motion. The first two graphs represent that of a bistable mechanism. The third and fourth represent that of a one-stable mechanism. The last represents that of a neutrally stable mechanism.



CW. Moving the structure away from its stable equilibrium will require a certain amount of force. The exact amount of required force depends on the steepness of the slopes of the potential energy path. As a result and by its own nature, the mechanism will fall back into its stable equilibrium position as soon as external forces are released.

It is also possible to include new stable equilibrium positions to the one- or bistable energy graphs. This is shown by the newly added stop in Figure 1.4D. In practice, this can be in the form of a mechanical lock for instance.

Figure 1.4E illustrates the behaviour of a CW with a neutrally stable potential energy along its range of motion. This indicates that the system is always positioned in an equilibrium, even when it is disturbed. Such systems require zero actuation force along their total range of motion, since Eq. (P1.1) holds.

Designing the CW as a bistable mechanism requires a significant amount of force to overcome the local maximum due to the large scale. Consequently, as soon as the local maximum is surpassed, the mechanism will fall by itself into the local minimum of that side. On the other hand, the local maximum can be lowered in order to lessen the required force to overcome this maximum. However, a neutrally stable mechanism results in a more energy efficient approach, which also attains zero-force actuation along the total range motion. It is therefore chosen in this study to design the CW as a neutrally stable mechanism.

## 2.5. SHAPE OPTIMIZATION

The topology, shape or dimensions of compliant mechanisms that need to satisfy an objective function for a set of parameters and constraints are obtained with the aid of structural optimization approaches. Topology optimization refers to the process of finding the topology, also known as the connectivity among constitutive elements, that fits the objective in the best manner. Shape optimization is the process of finding an optimal shape of the contour or surface that satisfies the objective in the best way. In size optimization the optimal size variables, e.g. thickness, cross-section, diameter, radii etc. are searched that fit the objective function best [12]. This research considers shape optimization and thus uses geometrical parameters as design variables to describe the geometry of the model. Three main aspects are considered next: the objective function formulation, the design parametrization and the solution method.

### 2.5.1. OBJECTIVE FUNCTION

A neutrally stable mechanism is one that possesses a constant potential energy with respect to its displacement and actuation requirements. The potential energy  $\mathbf{U}$  is defined as an array containing the determined energy level values  $U_i$  at each displacement step  $\delta_i$

$$\mathbf{U} = \begin{bmatrix} U_1(\delta_1) & U_2(\delta_2) & \dots & U_n(\delta_n) \end{bmatrix}. \quad (\text{P1.2})$$

The normalized potential energy graph  $\tilde{\mathbf{U}}$  is obtained by dividing the actual potential energy path  $\mathbf{U}$  by its mean value  $\bar{U}$

$$\tilde{U}_i = \frac{U_i}{\bar{U}} \quad \text{with } i = m..n, \quad (\text{P1.3})$$

$$\bar{U} = \frac{\sum_{i=m}^n U_i}{n - m + 1}, \quad (\text{P1.4})$$

in which  $\bar{U}$  is equal to the mean value of the elements in array  $\mathbf{U}$  for displacement steps  $i=m..n$ . The entries of the desired potential energy array  $\mathbf{U}_{ref}$  are set equal to the value one to represent a neutrally stable mechanism with respect to each displacement step for  $i=m..n$

$$\mathbf{U}_{ref} = 1. \quad (\text{P1.5})$$

The chosen objective function  $\Phi$  for this research can be seen as the minimization of the residuals between the normalized potential energy path  $\tilde{\mathbf{U}}$  and the desired potential energy graph  $\mathbf{U}_{ref}$

$$\Phi = \sqrt{\frac{\left( (\tilde{\mathbf{U}} - \mathbf{U}_{ref}) \right) \cdot \left( (\tilde{\mathbf{U}} - \mathbf{U}_{ref})^T \right)}{\left( \mathbf{U}_{ref} \cdot \mathbf{U}_{ref}^T \right)}}. \quad (\text{P1.6})$$

This objective function is equivalent to the normalized root-mean-square deviation. Figure P1.5 illustrates the actual normalized energy path  $\tilde{\mathbf{U}}$  and the desired reference energy path  $\mathbf{U}_{ref}$  in blue and red, respectively. The black bars depict the residual that needs to be minimized over a given range

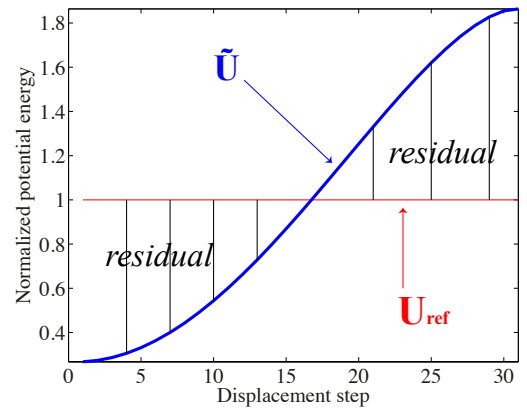


**Figure P1.5:** The actual normalized energy path of a mechanism is depicted by the blue solid line. The desired energy path is indicated by the red solid line. The black bars represent the residual that needs to be minimized between the two energy graphs.

of motion. Furthermore, the objective function reduces to

$$\Phi = \sqrt{(\tilde{\mathbf{U}} - \mathbf{1}) \cdot (\tilde{\mathbf{U}} - \mathbf{1})^T}, \quad (\text{P1.7})$$

after substitution of  $\mathbf{U}_{ref}$

### 2.5.2. ISOGEOMETRIC SHAPE OPTIMIZATION (DESIGN PARAMETRIZATION)

The Isogeometric Analysis (IGA) method [23] lends itself perfectly for the purpose of finding an optimal shape with specific mechanical properties [20]. It makes use of Non-Uniform Rational Basis Spline (NURBS) and avoids the problems of conversion between design description and analysis.

The coefficients of the basis functions are referred to as control points. These are represented by the red dots in Figure P1.6. Point A and B are the starting and the ending control point, respectively. Piecewise linear interpolation of the control points gives the control polygon. The latter is treated as if it is a linkage chain and is defined by the array

$$\mathbf{q} = [A_x \ A_y \ l_1 \ \theta_1 \ l_2 \ \dots \ l_6 \ \theta_6]. \quad (\text{P1.8})$$

This array contains the  $x$  and  $y$  coordinates of starting point  $A$ , the length  $l_i$  and its corresponding relative angle  $\theta_i$  of each polygon segment, see Figure P1.7. Ultimately, the B-spline, which is constructed by a linear combination of B-spline basis functions, is then shaped along the control polygon.

Note, the B-spline curve merely interpolates control points A and B and is therefore only tangent to the first and last segments of the control polygon.

The formulation of the elastic beam follows the Kirchhoff-Love plate theorem. This is an extension of the Euler-Bernoulli beam theory and assumes that a two-dimensional form can represent the mid-surface of a three-dimensional plate. The kinematic assumptions are: straight lines that are normal to the mid-surface remain

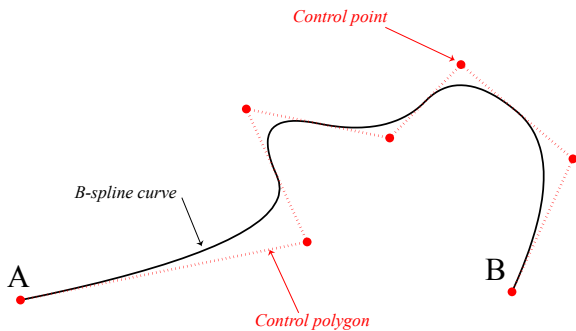


**Figure P1.6:** The B-spline is illustrated by the black solid line, which is a piecewise quadratic curve. This curve is shaped along the control polygon. The control points are indicated by the red dots. Control points A and B represent the starting and ending point, respectively.

straight after deformation, straight lines that are normal to the mid-surface remain normal to the mid-surface after deformation, and the thickness of the plate does not change during deformation. The elastic strain and kinetic energy functions are according to the linear isotropic elastic constitutive law of Euler-Bernoulli beams, given in [24]. Although linear mechanical properties are integrated, the numerical simulation solves a geometrically nonlinear problem for each displacement step. This incorporates normal and bending forces.

The optimization procedure is as follows. From the MATLAB® *Optimization Toolbox* the Sequential Quadratic Programming (SQP) optimization algorithm is chosen. A geometrical array  $\mathbf{q}_{initial}$  is taken to define the shape of an initial curve. The geometrical search space, the mechanical properties, and the specific actuation and boundary conditions are defined beforehand. The procedure starts at 50 different starting points randomly distributed around the search space using the Multistart option in the *Global Optimization Toolbox*. This study fixes starting control point  $A$  to zero and makes use of the last six control points. This results in 12 optimization parameters of which six are the lengths and six the relative angles of the control polygon segments. After optimization the 50 newly obtained curves are then ordered from the best to the worst. The best solution could, for instance, present a curve that crosses itself, which is physically infeasible. This indicates therefore that the predefined geometrical bounds and search space were too wide. The first option to resolve such cases is to analyse the practicability of the other 49 newly obtained solutions. If no satisfying curves are found, then a new procedure should be carried out with a smaller search space.

### 2.6. DESIGN EXAMPLE

The purpose of this section is to illustrate the clear contrast of the in- and output of an optimization procedure. The current example applies seven control points and thus six control polygon segments. This results in fourteen design parameters of which the first two are

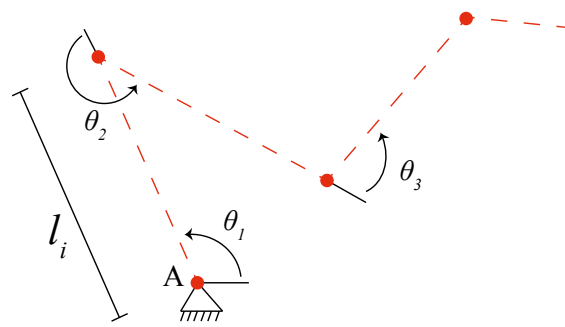


**Figure P1.7:** The control polygon is treated as if it is a linkage chain and is constructed by a piecewise linear interpolation of the control points. The angles of each segment is relative to its preceding one.

fixed to zero. The material density  $\rho$  is taken into account to incorporate gravitational forces, which is fully present before any displacement step is taken. The cross-sectional and mechanical properties of the planar beam, i.e.  $EI$  and  $EA$ , are kept constant over its total length.

An arbitrary shape is chosen and described by the polygon array

$$\mathbf{q}_{\text{initial}} = [A_x \ A_y \ l_1 \ \theta_1 \ \dots \ l_6 \ \theta_6] = \quad (\text{P1.9})$$

$$[0 \ 0 \ 0.1 \ 1 \ 0.1 \ 0.3 \ 0.1 \ 1.8 \ 0.1 \ 0.8 \ 0.1 \ 0.6 \ 0.1 \ 1].$$

The considered load case for this example resembles that of Case I, which has a prescribed vertical displacement  $v$  at the top and clamped beam-ends. The total prescribed displacement is equally subdivided into 31 displacement steps. The objective of the optimization procedure is to minimize the residuals between the actual and desired potential energy level in order to find a geometry that represents a neutrally stable mechanism. In this case, the optimization runs from the 7-th until the last displacement step. Figure P1.8 depicts a side view of the structure before and after optimization procedure. The black solid lines illustrate the unloaded state, while the blue solid lines represent the deformed state. The actual obtained energy paths  $\bar{U}$  and the required forces over the total range of motion, before and after optimization, are presented in Figure P1.9. These are measured at the point of actuation.

It is essential to be aware of the sensitivity of this approach. Choosing a different range of optimization, for instance, leads to a different outcome, as is presented in Figure P1.10. This case takes the same initial curve; only the optimization runs from the 14-th until the last displacement step. The corresponding energy and force graphs are presented as well.

Furthermore, slightly different initial shapes, thus  $\mathbf{q}_{\text{initial}}$ , lead to significantly different outcomes as well. Eq. (P1.10) and Eq. (P1.11) are arrays that contain slight differences in comparison with Eq. (P1.9). The shapes before and after optimization are presented in Figure P1.11 and Figure P1.12. The corresponding energy and force level graphs are redundant in these cases and are therefore not presented.

Note, other characteristics like, the type of actuation, type of boundary conditions, type of material, or beam thickness, have a significant influence on the outcome as well. For this reason, careful considerations should be taken during procedures and analysis.

## 2.7. MATERIAL USAGE

In practice a wide range of materials can be used, on different scales, to manufacture compliant mechanisms. Various types of plastics are often applied due to their capacity of undergoing large deformations and strains [10], [12], [25]. Fibre reinforced polymers have also proven to be great candidates for compliant applications [20]. However, taking into consideration that the CW will be built in the

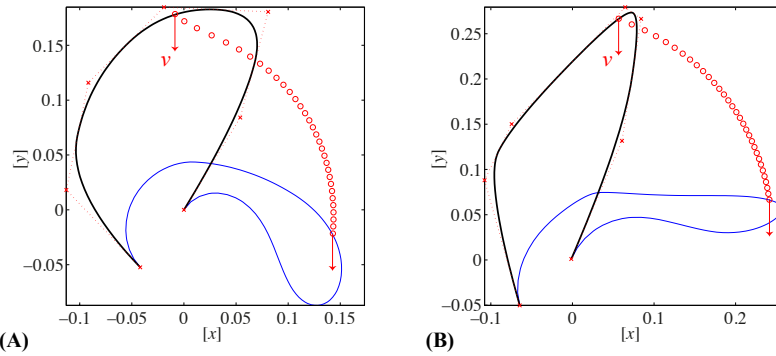


**Figure P1.8:** (A) illustrates the initial shape described by the array  $\mathbf{q}_{\text{initial}}$ . (B) depicts the outcome from optimization. The red and blue lines represent the initial and the last deformed state, respectively. This actuation is a prescribed displacement at the top. The beam-ends are clamped.

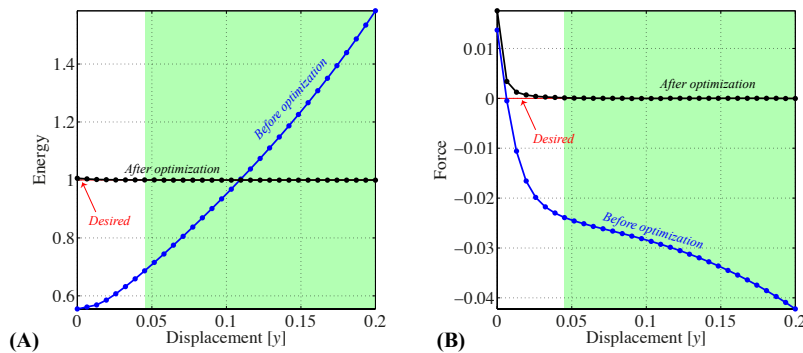


**Figure P1.9:** (A) presents the normalized energy paths before and after optimization. (B) illustrates the force graphs before and after optimization. The optimization range is indicated by the green area.

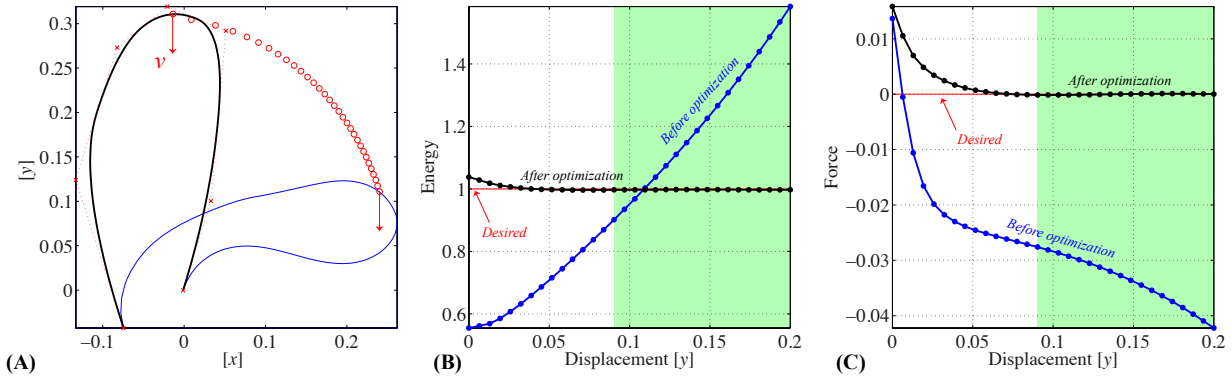


**Figure P1.10:** (A) depicts the shape after optimization. The initial and last deformed states are represented by the red and blue solid lines, respectively. (B) presents the normalized energy paths before and after optimization. (C) illustrates the force graphs before and after optimization.

$$\mathbf{q}_{\text{initial}} = [A_x \ A_y \ l_1 \ \theta_1 \ \dots \ l_6 \ \theta_6] = [0 \ 0 \ 0.2 \ 1 \ 0.1 \ 0.3 \ 0.2 \ 1.8 \ 0.1 \ 0.8 \ 0.1 \ 0.6 \ 0.1 \ 1]. \quad (\text{P1.10})$$

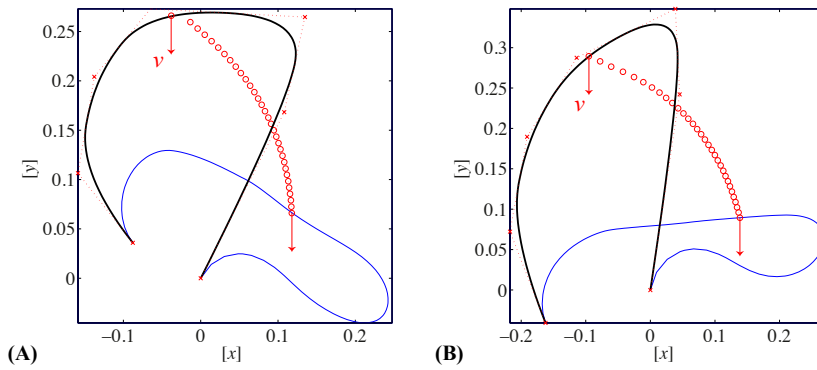


**Figure P1.11:** (A) presents the shape that is constructed by the array  $\mathbf{q}$  from Eq. (P1.10). (B) illustrates the shape after optimization. The initial and last deformed states are represented by the red and blue solid lines, respectively. This structure is exposed to a prescribed vertical displacement at the top, while having clamped beam-ends.

$$\mathbf{q}_{\text{initial}} = [A_x \ A_y \ l_1 \ \theta_1 \ \dots \ l_6 \ \theta_6] = [0 \ 0 \ 0.1 \ 10.1 \ 0.3 \ 0.3 \ 1.8 \ 0.1 \ 0.8 \ 0.1 \ 0.6 \ 0.1 \ 1]. \quad (\text{P1.11})$$

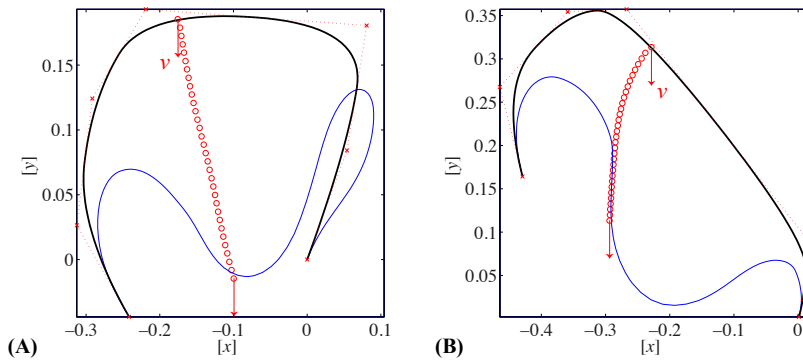


**Figure P1.12:** (A) presents the shape that is constructed by the array  $\mathbf{q}$  from Eq. (P1.11). (B) illustrates the shape after optimization. The initial and last deformed states are represented by the red and blue solid lines, respectively. This structure is exposed to a prescribed vertical displacement at the top, while having clamped beam-ends.

**Table P1.1**

Mechanical properties of PET-G plastic.

PARAMETER	VALUE	UNIT
$\rho$ (density)	1180 – 1330	kg/m <sup>3</sup>
$E_{flexural}$	1.24 – 2.76	GPa
Yield Strain	3.90 – 4.10	%
Ultimate Strain	5.00 – 350	%

natural environment, the choice has been made for PET-G plastic. This type of plastic can be heated and formed into any kind of shape, since it is a thermoplastic. It is widely available, cheap, 100% recyclable and naturally colourless with high clarity. It has good resistance against chemicals, against high impact and against scratches. Table P1.1 gives an overview of the mechanical properties of PET-G plastic.

### 3. RESULTS

The intention of this study is to obtain deformable, compliant, monolithic, and statically balanced wall geometries via shape optimization procedures. These structures are required to have a minimum height of 4m with a clear erected and flattened state. Five relatively different loading cases are considered. For each case the best-obtained result, which satisfies the requirements, is presented in this section.

#### 3.1. OPTIMIZATION RESULTS

The objective of optimization procedures is to minimize the residuals between the actual and the desired constant potential energy level. This leads consequently to zero-actuation force, since the derivative of a constant potential energy level gives zero force. For all five cases the total actuations are equally divided in 31 displacement steps. Furthermore, for all cases the optimization range runs from the 7-th until the last displacement step. The mechanical properties of the applied material, for all structures, are that of PET-G plastic and are given in Table P1.2. In some cases the thickness of the material did not provide sufficient stiffness to compensate the weight of the structure. This phenomenon proved to be directly related to type of actuation and boundary conditions. Consequently, optimization procedure experienced difficulties in finding converged solutions. Therefore, the thickness of the applied planar beam is manually adjusted, for each case, until a satisfying result is obtained. The next sections present the results.

Figures P1.13-P1.17 present the actuation scheme for each case. This is accompanied by the side views of the shapes, obtained from optimization procedures, in which the red, blue and black lines represent the initial, intermediate and final states, respectively. The corresponding force graphs

**Table P1.2**

Mechanical properties of PET-G plastic used for numerical analysis.

PARAMETER	VALUE	UNIT
$\rho$ (density)	1270	kg/m <sup>3</sup>
$E_{flexural}$	2.0	GPa
Yield Strain	4.00	%
Ultimate Strain	350	%

illustrate the required actuation force over the total range of motion. The maximum and minimum values, within the optimization range, are presented in Table P1.3. A positive force value indicates that the actuation is experiencing a pulling force in the direction of gravity. Contrarily, a negative force value specifies the required contribution of the actuation. In addition, force graphs with no gravity contribution are presented to manifest a clear contrast between the stiffness and the mass contribution of the system along the total range of motion.

It is evident that the actuation and boundary conditions have a direct influence on the behaviour of the structure. However, the practicability of the structure and its behaviour is of major significance for real life application. Firstly, not all structures have the same beam thickness. This is due to the fact that some structures need a larger thickness in order to provide sufficient stiffness to compensate the mass of the structure during motion. This is adjusted manually for each structure until a satisfying result is obtained. The configuration in Case III did not present any satisfying results. This is due to the fact that no sufficient material stiffness is provided since both beam-ends consisted of hinges. Generally, hinged beam-ends cause loss of structural stiffness contribution, which introduces complications in finding satisfying result.

Secondly, the required actuation force for each structure and case propagates differently. For instance, in Case I the actuation experiences at first a pulling force that is generated by gravitational forces. As soon as the actuation is initiated, the force graph drops immediately after one displacement step by a factor of 20. This occurrence happens less abrupt for the other cases. Eventually, for all cases except for Case III, the force graph goes to near perfect zero force as soon as the actuation and deformation of the structure enters the optimization range.

**Table P1.3**

The required actuation force for each structure.

CASE	VALUE	UNIT
I	-0.5 ~ 1	N
II	-5 ~ 3	N
III	-25000 ~ -34000	N
IV	-9 ~ 5	Nm
V	-47.5 ~ 8	Nm

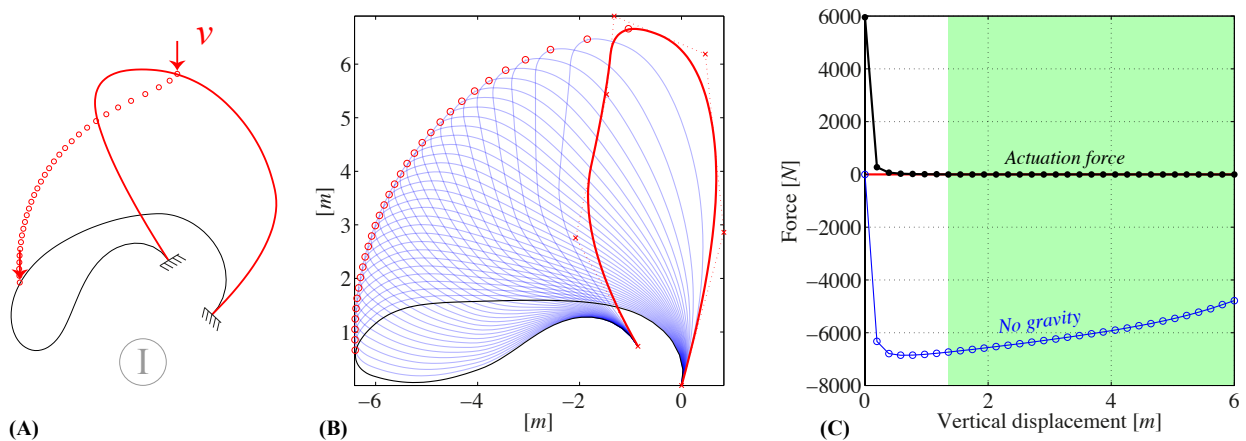


**Figure P1.13:** (A) the loading scheme. (B) the obtained shape after optimization. The red, blue and black solid lines represent the initial, the intermediate and the deformed state of the structure, respectively. (C) the force graphs with and without gravity contribution. The green area represents the optimization range. The material thickness and width are equal to  $0.04m$  and  $2m$ , respectively.

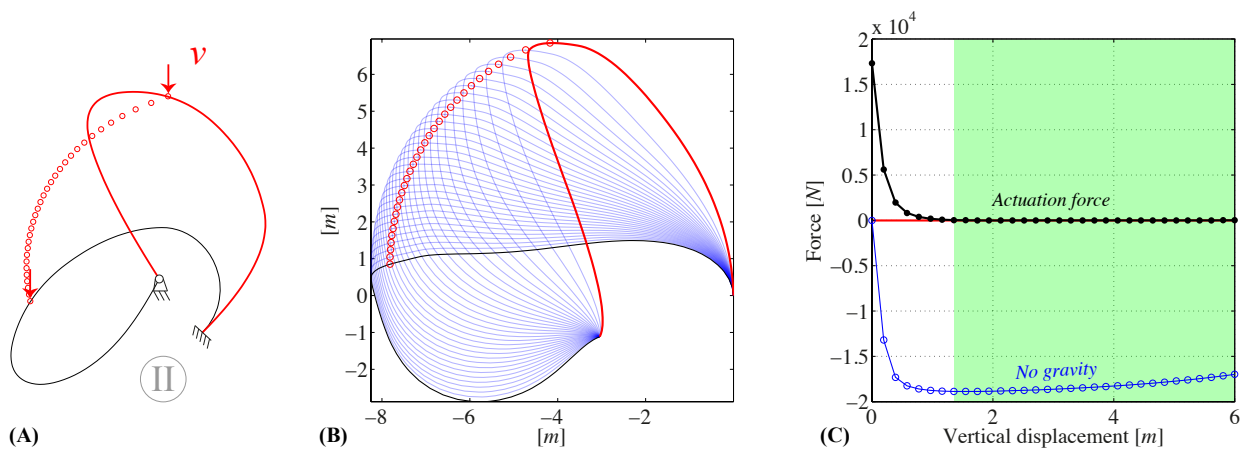


**Figure P1.14:** (A) the loading scheme. (B) the obtained shape after optimization. The red, blue and black solid lines represent the initial, the intermediate and the deformed state of the structure, respectively. (C) the force graphs with and without gravity contribution. The green area represents the optimization range. The material thickness and width are equal to  $0.07m$  and  $2m$ , respectively.

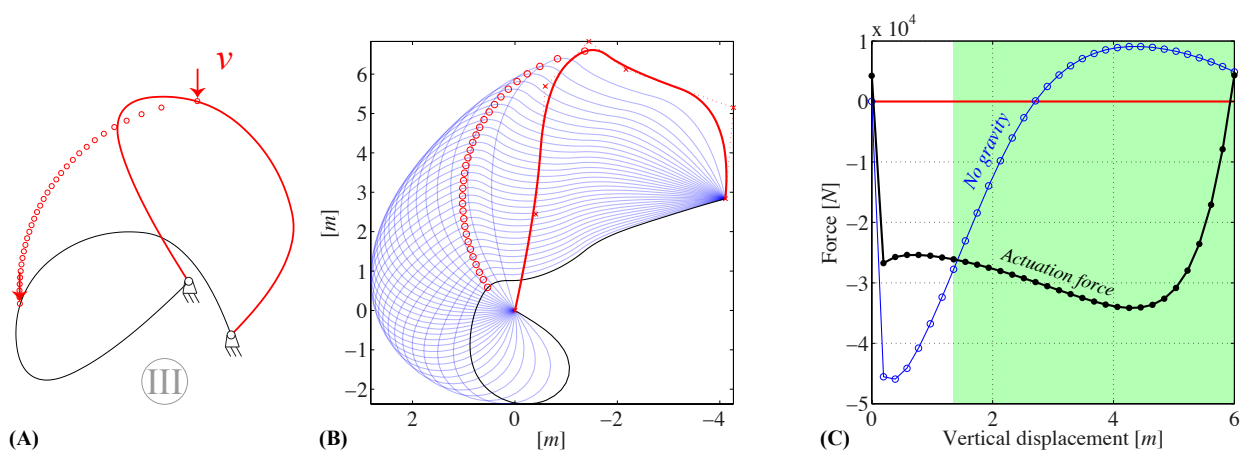


**Figure P1.15:** (A) the loading scheme. (B) the obtained shape after optimization. The red, blue and black solid lines represent the initial, the intermediate and the deformed state of the structure, respectively. (C) the force graphs with and without gravity contribution. The green area represents the optimization range. The material thickness and width are equal to  $0.07m$  and  $2m$ , respectively.

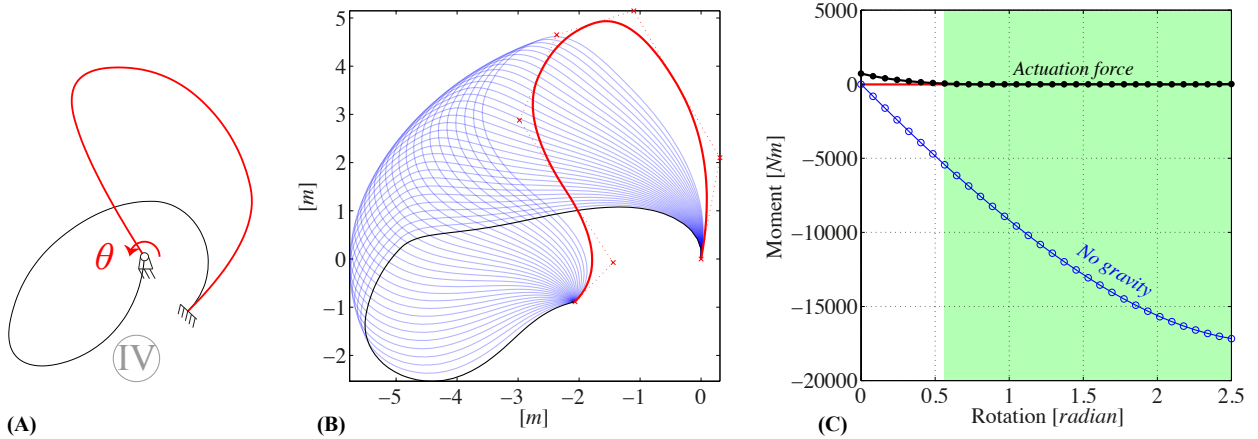


**Figure P1.16:** (A) the loading scheme. (B) the obtained shape after optimization. The red, blue and black solid lines represent the initial, the intermediate and the deformed state of the structure, respectively. (C) the force graphs with and without gravity contribution. The green area represents the optimization range. The material thickness and width are equal to  $0.04m$  and  $2m$ , respectively.

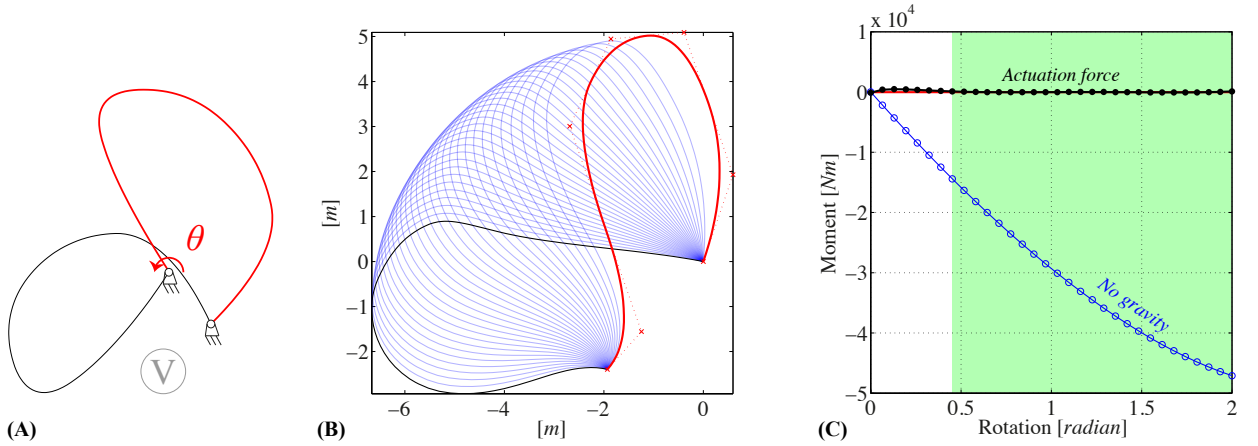


**Figure P1.17:** (A) the loading scheme. (B) the obtained shape after optimization. The red, blue and black solid lines represent the initial, the intermediate and the deformed state of the structure, respectively. (C) the force graphs with and without gravity contribution. The green area represents the optimization range. The material thickness and width are equal to  $0.07m$  and  $2m$ , respectively.

Thirdly, each structure results in a relatively different deformed state due to the applied actuation and boundary conditions. The initial and deformed state of the structure in Case I is meagre in comparison to the structures from other cases. This is due to the fact that both beam-ends are clamped and therefore do not allow any rotation at the foundations, whereas the other structures from the different cases require a significant amount of space at the surface due to the hinges at the beam-end(s). Consequently, structural parts of their deformed state lie largely below foundation level, which might be impractical for real life applications.

Fourthly, the influence of the actuation and boundary conditions can also be seen in the resulting material strain. Figure P1.18 presents the material strain due to structural deformation for each case. These graphs depict the strain levels at the outermost fibres of the planar beam for the last displacement step. All strain levels stay below the yield strain of 4% except that of Case III. Additionally, Figure

P1.18 visualizes clearly that relatively higher strain levels are reached at clamped boundaries in comparison with other types of boundary conditions. In this study the planar beam was experiencing strain levels between 2% and 3.5% at the clamped boundary conditions for Cases I, II and IV. Repetitive occurrence of such relatively high strain levels is undesired in practice since it would facilitate the introduction of fatigue issues.

#### 4. EXPERIMENT

This section presents the construction of an optimized deformable, compliant and monolithic gravity balancer. A physical model is evaluated to validate the presented method. The model resembles Case I, in which both beam-ends are clamped and a prescribed vertical displacement of  $-0.4m$  is applied at the top. The height and width of the model are  $0.5m$  and  $0.2m$ , respectively.

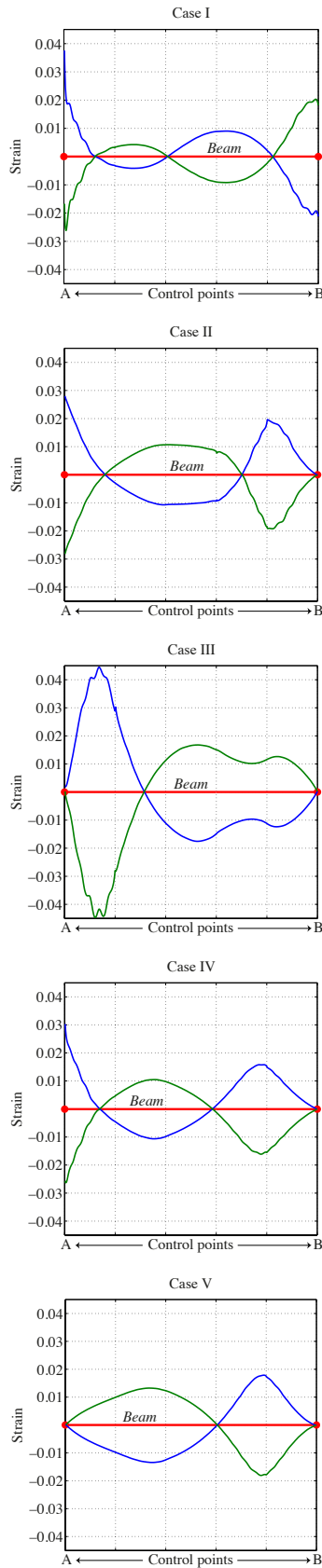


**Figure P1.18:** The material strain of the last deformed state is plotted along the longitudinal direction of the beam. The blue and green lines represent the strain at the inner- and outer fibres of the beam, respectively. Control points A and B represent the starting and ending point of the structure.

#### 4.1. SCALING

Before presenting the experimental results, it is key to have a notion of scaling effects concerning gravity and stiffness contribution. From theory [26] it is clear that the gravitational force  $S_F$  is proportional to the acceleration of gravity  $S_g$ , the density  $S_\rho$  and the volume  $S_l^3$  of a specific body

$$S_F = S_g S_\rho S_l^3, \quad (\text{P1.12})$$

$$S_g = \frac{\text{Gravity}_{\text{Model}}}{\text{Gravity}_{\text{Original}}}, \quad (\text{P1.13})$$

$$S_\rho = \frac{\text{Density}_{\text{Model}}}{\text{Density}_{\text{Original}}}, \quad (\text{P1.14})$$

$$S_l^3 = \frac{\text{height}_{\text{Model}}}{\text{height}_{\text{Original}}} \times \frac{\text{width}_{\text{Model}}}{\text{width}_{\text{Original}}} \times \frac{\text{thickness}_{\text{Model}}}{\text{thickness}_{\text{Original}}}. \quad (\text{P1.15})$$

Since acceleration of gravity and the density are held the same, Eq. (P1.12) reduces to

$$S_F = S_l^3, \quad (\text{P1.16})$$

implying that gravitational forces are proportional to the volume. Thus, the larger the volume of an object, the larger it is exposed to gravitational forces. Furthermore, for the stresses  $S_\sigma$  we can write

$$S_\sigma = S_g S_\rho S_l, \quad (\text{P1.17})$$

which can be reduced to

$$S_\sigma = S_l, \quad (\text{P1.18})$$

Thus, the stresses are proportional to the change in dimensions. Moreover, to understand the change in stiffness due to scaling we recall Hooke's Law

$$\varepsilon = \frac{\Delta l}{l} = \frac{\sigma}{E} = \frac{F}{AE}, \quad (\text{P1.19})$$

in which  $\sigma$  represents the stress,  $E$  the modulus of elasticity,  $F$  the applied force and  $A$  the loaded area. Then, the stiffness  $k$  can be written as

$$k = \frac{F}{\Delta l} = \frac{AE}{l}, \quad (\text{P1.20})$$



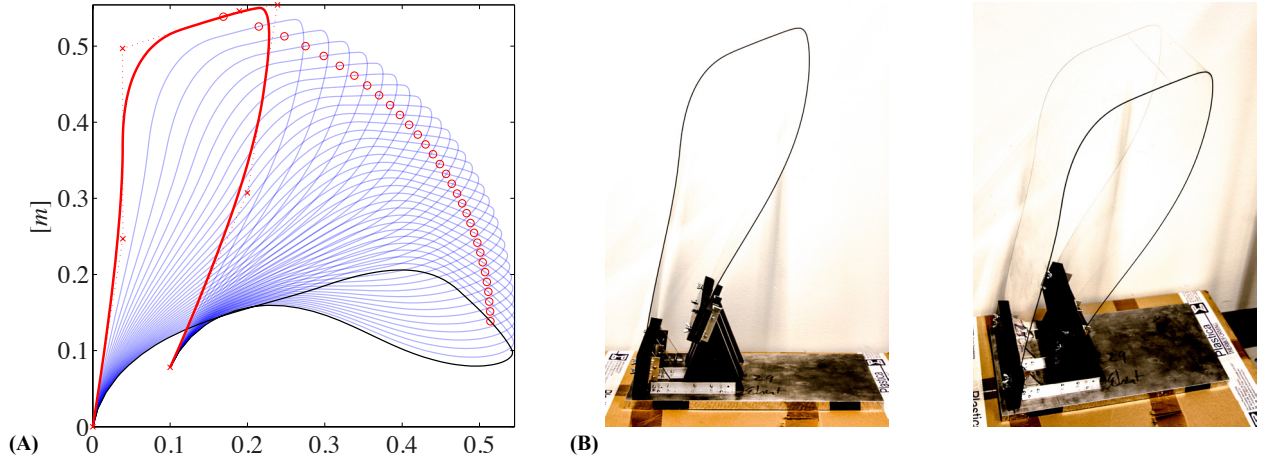


**Figure P1.19:** (A) the newly obtained shape for a physical model. (B) The actual physical model obtained by means of thermoforming.

and leads to

$$S_k = \frac{S_A S_E}{S_I} = \frac{S_I^2 S_E}{S_I} = S_I S_E. \quad (\text{P1.21})$$

The latter implies that if the material is kept the same, thus  $S_E = I$ , then the stiffness becomes proportional to the change in dimensions. Hence, the contribution of stiffness and gravitational forces are linearly and cubically affected, respectively, due to dimension changes.

It is therefore important to realize that constructing such structures will become a trade-off between the contribution of gravity and the stiffness. Especially when the contribution of gravitational forces is significantly less on a small scale, due the fact that gravitational forces decrease cubical, whereas the stiffness decreases linearly.

#### 4.2. OPTIMIZATION RESULT AND PHYSICAL MODEL

The numerical prescribed actuation is carried out in 31 equally divided displacement steps in which the optimization runs from the 7-th until the last step. Figure P1.19 illustrates the obtained optimization result and its corresponding physical model. The shape of the physical model is obtained by means of thermoforming. An initially flat PET-G plastic plate was placed onto a mould, heated and draped into the desired shape. The applied material has a plate thickness of  $1.5\text{mm}$ , a modulus of elasticity of  $2.32\text{GPa}$ , a material density of  $1270\text{kg/m}^3$  and a yield strain of 4%. Figure P1.20A depicts the corresponding numerical load path with and without gravitational contribution. There are no practical geometries obtained with near perfect zero force actuation for the chosen dimensions at this scale. Due to downsizing, the contribution of gravitational forces decreased cubically, whereas the stiffness decreased linearly. This resulted in a larger stiffness contribution than gravity,

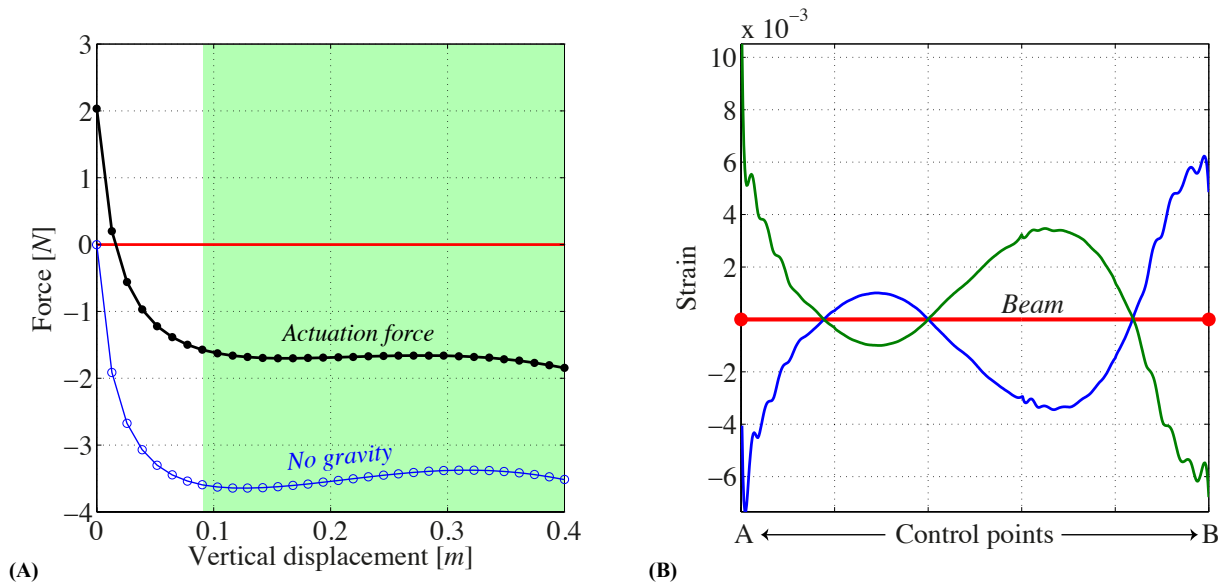


**Figure P1.20:** (A) the required actuation force to bring the physical model into deformation. The green area indicates the optimization range. (B) The material strain at the inner- and outer fibres of the beam for the last deformed state.

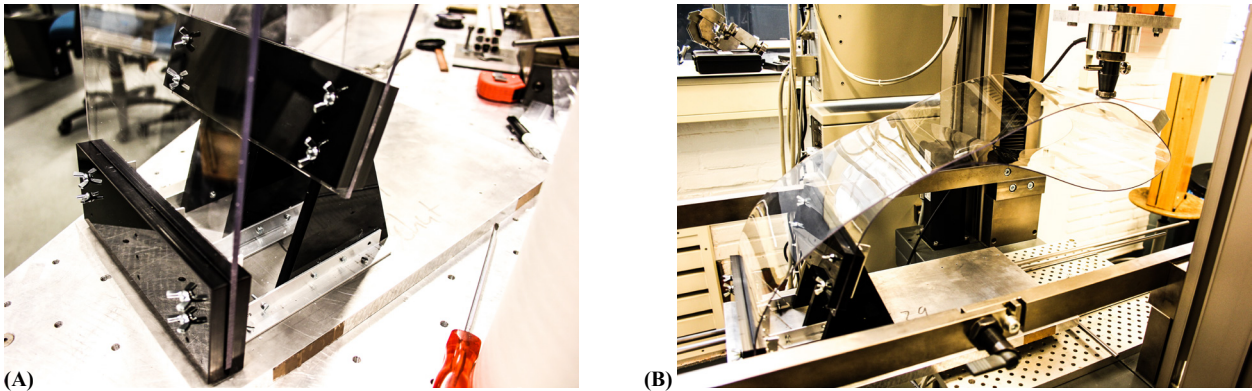


**Figure P1.21:** (A) a specifically designed foundation to clamp the structure at the fixations. (B) the physical model is tested with the aid of a compression bench, which measures the vertical displacement and the required force simultaneously.

which is why a certain actuation force is required over a large range of motion. This can be resolved by applying a smaller beam thickness, thus reducing the stiffness. However, the appropriate thickness was not constructible for the authors. On the other hand, the obtained force graph presents a near perfect constant force actuation. It is therefore possible to reduce the required actuation force by adding a certain mass to the point of application. Figure P1.20B illustrates the strains at the outermost fibres of the beam for every displacement step. These reach maximum strain levels of 1%.

#### 4.2.1. EXPERIMENTAL SETUP

An experimental setup is constructed to evaluate the performance of the physical model. Figure P1.21A presents a specifically designed foundation that is used to clamp the structure at the foundation. This foundation is attached to a relative heavy aluminium plate to prevent the structure from toppling during testing. The total setup is placed on straight rollers, which make it possible for the foundation to be displaced in horizontal sense. A compression bench is used to apply a vertical displacement to the structure and measure the required vertical force, see Figure P1.21B. The vertical displacement is applied in low speed during testing to be able to neglect inertia effects. As like in [21] is for the application of the vertical displacement a knife-edge applied

over the total width of the structure, see Figure P1.22. A double-sided tape is attached to keep the bar and knife-edge in its place.

#### 4.3. MEASUREMENT RESULTS

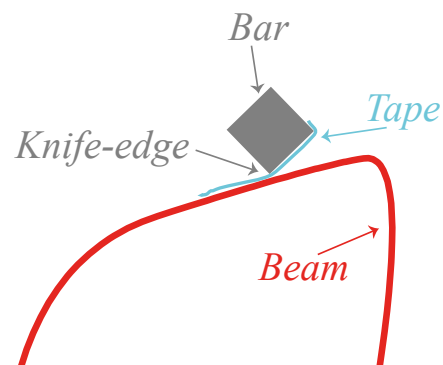
Figure P1.23 illustrates the measurement results, and show good overlap. These measurements are performed in two directions to obtain a hysteresis loop for the determination of energy loss. This loss is assumed to be equal in both directions. The blue and black lines represent the hysteresis loop obtained from the compression bench and the numerical load path obtained from optimization, respectively. The required force to deform the structure is  $\pm 1.68N$ . This implies that adding mass of  $1.68/9.8066=0.1713kg$  at the point of actuation can reduce this force to perfect zero, see Figure P1.24.

### 5. DISCUSSION

This section evaluates the applied method, the results and the experiment. Additionally, real life applications and application purposes for further development and research are discussed.



**Figure P1.22:** A knife-edge is used to apply the vertical displacement to the physical model during testing. This knife-edge is kept in its place with the aid of a double-sided tape.



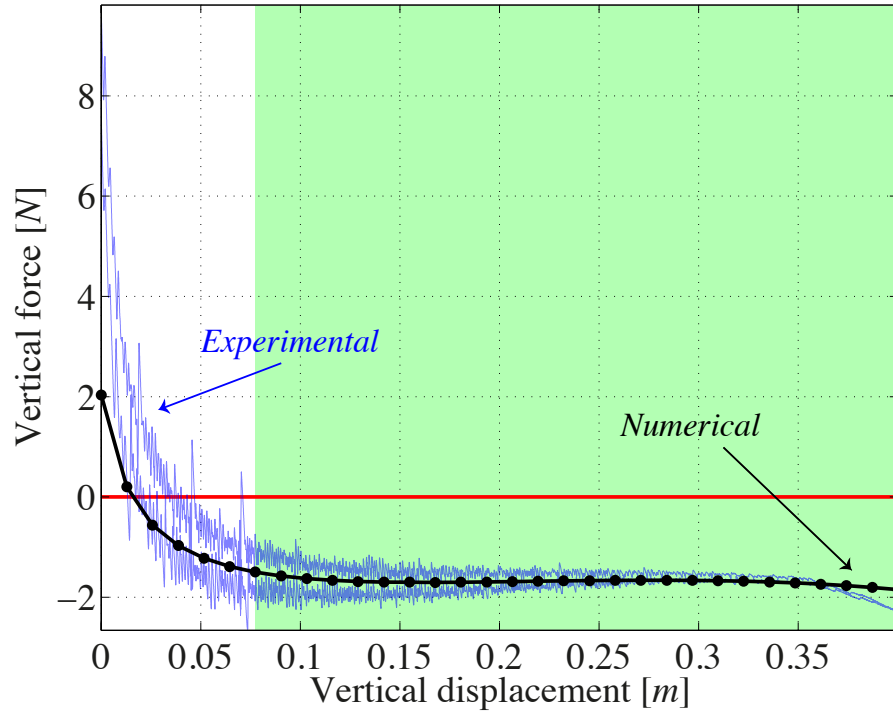


**Figure P1.23:** The measurement result obtained from the compression bench. The green area represents the optimization range. The experimental measurements are performed in two directions to obtain a hysteresis loop for the determination of energy loss.

### 5.1. EVALUATION OF APPLIED METHOD

This research applies Isogeometric Shape Optimization procedures to obtain statically balanced large-scale compliant structures that compensate their weight during motion by using their naturally distributed material stiffness. The numerical model works well in achieving geometries that satisfy a desired objective. However, it is not certain that the global minimum is found during optimization procedures. On the other hand, the multi-start option found enough satisfying local minima values that are small enough, which

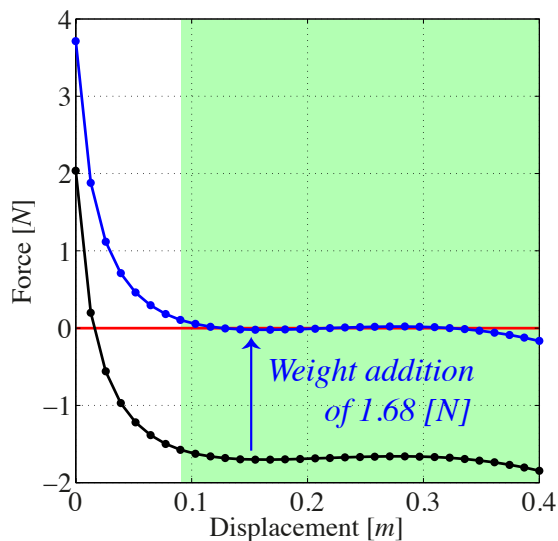


**Figure P1.24:** By adding a weight at the point of actuation application, the required actuation force will be reduced to perfect zero.

make finding the global minimum of no relevance. Still, there might remain unfound local minima that correspond to better results than the ones presented in this study. This is matter for future investigation.

Furthermore, the objective function used in this study is constructed for a single actuation and is not suitable for simultaneously applied actuations. Applying multiple actuations to the structural body leads to a more controlled structural deformation. The objective function for the latter case is, for instance, required to minimize the residuals between a desired potential energy path and the potential energy paths obtained from multiple actuations.

Moreover, instead of using a single beam element the numerical model can be extended to apply multiple beam elements in a monolithic manner. Or, it can be extended in such a way that it allows the implementation of various material types at local levels. Both extensions can help, for instance, in distributing the material stress in a more effective and evenly manner. Also, applying appropriate material types at structural parts that undergo large strains on a repetitive base can decrease fatigue phenomenon.

### 5.2. EVALUATION OF THE RESULTS

It is not straightforward that such complex shaped compliant structures indeed balance their weight along a certain range of motion. However, optimization procedures obtained structures with heights between 5 and 6 meters that require near perfect zero actuation force along their range of motion, and therefore the objective of this research is satisfied. An important factor to consider is the trade-off

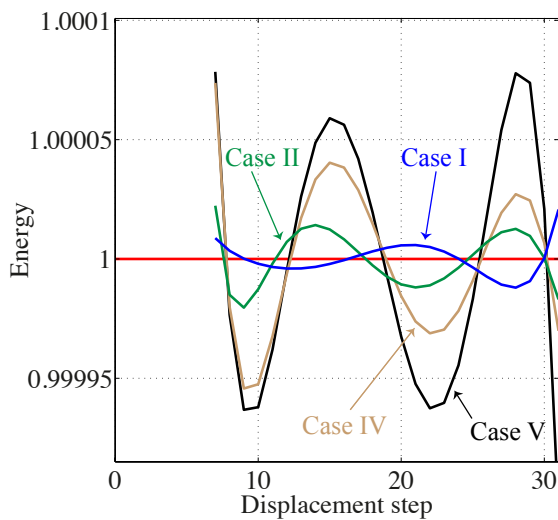


**Figure P1.25:** The normalized potential energy graphs of each structural deformation, except that of Case III. Each local minimum and maximum represents a stable and unstable position, respectively.

between the contributions of the weight and the stiffness of the applied material. As discussed, dimensional change has a linear and cubical effect on the contributions of stiffness and gravity, respectively. At the same time, more weight demands also more force to keep the structure into position during motion initiation.

Moreover, Figure P1.25 presents the potential energy graphs of the actuations for each case, except that of Case III. These represent the potential energy paths within the optimized range. Each local minimum and maximum characterizes a stable and unstable position, respectively. The structural deformation of Case I is the closest to a statically balanced mechanism. This is most certainly due to the applied actuation and boundary conditions. Thus, if a choice needs to be made, based on energy efficiency, then Case I is the right choice.

On the other hand, rotational actuations at the foundation can be hidden from the eye. This is not possible for actuations applied at the body of the structure. Nonetheless, an actuation at the body of the structure results in a more controlled behaviour, whereas rotational actuations at the foundation leave the height, for instance, uncontrolled. It is therefore that for real life application careful considerations should be made between the energy efficiency of a specific structure and its corresponding actuation and boundary conditions.

### 5.3. EVALUATION OF THE EXPERIMENT

It is chosen to use PET-G plastic as structural material for the physical model. The advantages of this material are low costs, widely available, 100% recyclable and good resistance against impact. Furthermore, this material can be shaped into any desired geometry by means of thermoforming, since it is a thermoplastic.

The differences between the experimental and numerical

values are considered to be small. The differences have some predictable causes. Thermoplastics, like PET-G, have strong nonlinear stress-strain relations. The numerical model, however, adopted a linear constitutive law. This numerical simplification causes slight load path differences between the model and experiment. Also, it is clear that at the beginning of the measurement a relatively higher noise is present. This is due to the fact that at initiation the horizontal velocity of the foundation is significantly higher than at the end.

Moreover, inaccuracies introduced during production procedures should be taken into account. For instance, during cooling down of the thermoformed shape, the material undergoes shrinkage due to thermal effects. This results in a slightly different geometry than designed, affecting the stiffness and thus behaviour of the system.

The foundation is made out of thick laser-cut plastic and provides sufficient rigidity. The rollers beneath the foundation provide low friction and sufficient stiffness. The double-sided tape kept the bar and knife-edge in their places as it should. Besides the compression bench are no further complex parts implemented in the test setup.

### 5.4. REAL LIFE APPLICATION

The differences between the numerical and experimental results have minor differences. The biggest source of errors comes from the application of a linear constitutive law during simulations, while PET-G plastics have a strong non-linear strain relation. An important consideration that must be made is that these differences can increase significantly when a structure is built at actual sale.

Furthermore, as is obtained from numerical simulations, the deformation of the structure demands a significant amount of space along a train track. This might not be available in practice and thus limit the CW from functioning fully.

Moreover, the application of real life actuations can be challenging. For Cases I, II and III an actuation mechanism that pulls or pushes the structure downwards, while moving along its own small rail track, is needed. Cases IV and V require an actuation mechanism that provides a torque to bring a beam-end into rotation. Therefore, in order to say which actuation type is practical and best along a train track, further research is required. Also, other types of actuation, like a tendon that is pulled on the inside of the structure, should be considered and investigated further.

Considering construction, thermoforming a physical model on small-scale is practical as shown in this research. However, thermoforming a large-scale and flat PET-G plate into a desired shape might not be possible yet. It is therefore required to investigate how these unique and complex geometrical shapes are actually constructed on large-scale.

Conventional sound barriers are required to have a surface mass of  $10\text{kg/m}^2$  in order to deal with low frequency noise. The obtained designs have a minimum thickness of  $40\text{mm}$ . This leads to  $0.04\text{m} \times 1270\text{kg/m}^3 = 50.8\text{kg/m}^2$ , which is more than sufficient.

Also, sound barriers are placed in the natural environment and face different weather conditions. This could influence the mechanical properties, and thus the performance of the material, over time. In addition, relaxation, creep and fatigue can also have a significant influence on the behaviour of the system. It is therefore important that these aspects are also considered.

Lastly, another important factor is stability. The obtained geometrical solutions are flat in the third dimension. Trains that pass by with high speed will generate high wind pressure and velocity. This occurrence would blow the CW over due to its low in-plane stiffness. Hence, thorough investigation is required to solve this issue.

### 5.5. POSSIBLE APPLICATIONS

Sound barriers represent one possible application for the presented method, which can be extended to other structures such as small- and large-scale bridges and roofs that need to reconfigure due to changing traffic or environmental conditions. Other kinds of small- and large-scale urban furniture that is offering temporary seating and shelter from sun and rain etc. can be as well considered. Such reconfigurable structures are relevant due to their potential to considerably improve efficiency of space use. Finding statically balanced monolithic solutions for these applications could be a future objective.

## 6. CONCLUSIONS

This research presents four computational loading cases that consist of large-scale and complex shaped geometries that are able to compensate their own weight along a large range of motion. Consequently, near perfect zero force is required for the total deformation. All four structures are satisfying and have a clear erected and flattened state, as is required for the application of the Barrier in Motion. These structures consist of a single monolithic, material isotropic and compliant planar beam. The thickness of the beam depends on the specific type of actuation and boundary conditions. Hinged beam-ends lead to a loss of stiffness contribution. Therefore, some structures are required to have a larger thickness in order to provide sufficient stiffness to compensate the weight. It is also shown that the loading case with clamped beam-ends and an actuation applied at the top of the structure is relatively the most energy efficient mechanism. This is mainly due the fact that this configuration did not face any loss of stiffness contribution. Nevertheless, the findings in this study are, especially due to the large-scale, a novel contribution to the field of statically balanced compliant mechanisms and structures.

The Isogeometric Shape Optimization procedures prove to be a great tool in finding satisfying two-dimensional geometries for uncommon objectives. For each loading case a different structural shape is found due to the type of actuation and boundary conditions.

An experimental model is constructed in order to validate the predicted numerical outcome. This physical model represents an optimized and downscaled version of the large-scale structure with clamped beam-ends and a prescribed displacement at the top. The physical shape of the structure is obtained by means of thermoforming in which an initially flat PET-G plastic plate was heated and draped onto a mould. This approach proves to be an adequate method for the production of small-scale compliant structures.

The numerical predictions coincide well with the experimental values and therefore demonstrate the applicability of the used method. The main sources of minor differences are the nonlinearity of the material, the shrinkage of the material due to cooling down after thermoforming, and hysteresis in the material. Nonetheless, these differences are expectable.

## ACKNOWLEDGEMENT

The authors would like to acknowledge the conceptual contribution of Hyperbody at Delft University of Technology and STW (HTSM-2012 12814: ShellMech). The authors would also like to acknowledge the Department of Structural Engineering - Delft University of Technology for the financial support of this project.

## REFERENCES

- [1] H. Bier and T. Knight, "Digitally-Driven Architecture," *Footprint*, no. 6, pp. 1–4, 2010.
- [2] D. Rosenberg, "Indeterminate Architecture : Scissor-Pair Transformable Structures," *Footprint*, no. 6, pp. 19–39, 2010.
- [3] S. Yiannoudes, "Kinetic Digitally-Driven Architectural Structures as ' Marginal ' Objects - a Conceptual Framework," *Footprint*, no. 6, pp. 41–54, 2010.
- [4] G. Flachbart and P. Weibel, Eds., *Disappearing Architecture*. Basel: Birkhäuser Basel, 2005.
- [5] K. Oosterhuis and G. Joosen, "Barrier in Motion," *IA#5 - Robotics in Architecture - All titles - Jap Sam Books*, 2013. [Online]. Available: <http://www.japsambooks.nl/en/books/all-titles/ia-5-robotics-in-architecture/101>. [Accessed: 18-Jul-2015].
- [6] M. Hosale and C. Kievid, "Modulating territories, penetrating boundaries," *Footprint*, no. 6, pp. 55–67, 2010.
- [7] Larry L. Howell, *Compliant Mechanisms*. Wiley, 2002.
- [8] B. P. Trease, Y.-M. Moon, and S. Kota, "Design of Large-Displacement Compliant Joints," *J. Mech. Des.*, vol. 127, no. 4, p. 788, Jul. 2005.
- [9] C. Thill, J. Etches, I. Bond, K. Potter, and P. Weaver, "Morphing skins," *Aeronaut. J.*, vol. 112, no. 1129, pp. 117–139, 2008.
- [10] S. Kota, J. Hetrick, and R. Osborn, "Design and application of compliant mechanisms for morphing," *24 Smart Struct. Mater.* 2003, vol. 5054, no. 734, pp. 24–33, 2003.
- [11] J. Luo, Z. Luo, S. Chen, L. Tong, and M. Y. Wang, "A new level set method for systematic design of hinge-free compliant mechanisms," *Comput. Methods Appl. Mech. Eng.*, vol. 198, no. 2, pp. 318–331, 2008.
- [12] J. A. Gallego Sanchez, "Statically Balanced Compliant

- Mechanisms,” Delft University of Technology, PhD Thesis, 2013.
- [13] J. L. Herder, “Energy-free systems: theory, conception, and design of statically balanced spring mechanisms,” Delft University of Technology, PhD Thesis, 2001.
- [14] A. Gopalswamy, P. Gupta, and M. Vidyasagar, “A new parallelogram linkage configuration for gravity compensation using torsional springs,” in *Proceedings 1992 IEEE International Conference on Robotics and Automation*, pp. 664–669.
- [15] V. Arakelian and S. Ghazaryan, “Improvement of balancing accuracy of robotic systems: Application to leg orthosis for rehabilitation devices,” *Mech. Mach. Theory*, vol. 43, no. 5, pp. 565–575, May 2008.
- [16] A. H. A. Stienen, E. E. G. Hekman, F. C. T. Van der Helm, G. B. Prange, M. J. A. Jannink, A. M. M. Aalsma, and H. Van der Kooij, “Freebal: dedicated gravity compensation for the upper extremities,” in *2007 IEEE 10th International Conference on Rehabilitation Robotics*, 2007, pp. 804–808.
- [17] “InteSpring Home.” [Online]. Available: <http://www.intespring.nl/>. [Accessed: 21-Jul-2015].
- [18] B. L. Rijff, J. L. Herder, and G. Radaelli, “An Energy Approach to the Design of Single Degree of Freedom Gravity Balancers With Compliant Joints,” in *Volume 6: 35th Mechanisms and Robotics Conference, Parts A and B*, 2011, pp. 137–148.
- [19] F. te Riele and J. Herder, “Perfect static balance with normal springs,” in *ASME 2001 Design Engineering Technical Conferences and Computers and Information in Engineering Conference*, 2001, pp. 9 – 12.
- [20] G. Radaelli and J. L. Herder, “Isogeometric Shape Optimization for Compliant Mechanisms With Prescribed Load Paths,” in *Volume 5A: 38th Mechanisms and Robotics Conference*, 2014.
- [21] G. Radaelli and J. L. Herder, “A Monolithic Compliant Large-Range Gravity Balancer,” in *14th World Congress in Mechanism and Machine Science*, 2015.
- [22] “Richtlijnen geluidbeperkende constructies langs wegen - CROW.” [Online]. Available: <http://www.crow.nl/publicaties/richtlijnen-geluidbeperkende-constructies-langs-we>. [Accessed: 06-Sep-2015].
- [23] T. J. R. Hughes, J. A. Cottrell, and Y. Bazilevs, “Isogeometric analysis: CAD, finite elements, NURBS, exact geometry and mesh refinement,” *Comput. Methods Appl. Mech. Eng.*, vol. 194, no. 39–41, pp. 4135–4195, Oct. 2005.
- [24] A. P. Nagy, M. M. Abdalla, and Z. Gürdal, “Isogeometric sizing and shape optimisation of beam structures,” *Comput. Methods Appl. Mech. Eng.*, vol. 199, no. 17–20, pp. 1216–1230, Mar. 2010.
- [25] G. K. Ananthasuresh, A. G. Schache, T. W. Dorn, and M. G. Pandy, “How Far are Compliant Mechanisms from Rigid-body Mechanisms and Stiff Structures?,” *Adv. Mech. Robot. Des. Educ. Res.*, vol. 14, pp. 83–94, 2013.
- [26] J. C. Cool, *Werktuigkundige Systemen*. Delft: Delftse Uitgevers Maatschappij b.v., 1992.









Paper II



# Design of Large-Scale, Statically Balanced and Compliant Shell Structures as Deformable Walls

H. ALKISAEI<sup>1</sup>, G. RADAELLI<sup>2,4</sup>, J.L. HERDER<sup>2</sup>, H. BIER<sup>3</sup>, L.J. SLUYS<sup>1</sup>

<sup>1</sup>*Dept. Structural Engineering, Delft University of Technology, Delft, The Netherlands*

<sup>2</sup>*Dept. Precision and Microsystems Engineering, Delft University of Technology, Delft, The Netherlands*

<sup>3</sup>*Dept. Architectural Engineering and Technology, Delft University of Technology, Delft, The Netherlands*

<sup>4</sup>*Laevo BV, Molengraaffsingel 12-14, Delft, The Netherlands*

---

## ABSTRACT

This study presents a novel approach to the design of compliant and monolithic shell structures that are able to compensate their weight along a large range of deformation by using the naturally distributed material stiffness. Gravity compensation is an example of static balancing and implies that near perfect zero actuation force is required to bring a system into motion. The structural behaviour is influenced by the different actuators, boundary conditions and cross-sectional curvatures. New shell structure geometries are obtained by means of shape optimization procedures. The latter influenced the geometrical design parameters and minimized the objective function value until a satisfying minimum was found. The newly obtained shell structures are meant to function as deformable sound barriers that flatten to the ground when no vehicles are near and erect as soon as vehicles enter the scene. The main reason for this application is to prevent horizon pollution. The most satisfying outcome from optimization procedures has a structural height of  $\pm 5m$ , a material thickness of  $0.02m$ , and requires  $-24 \sim 40N$  to be positioned from the erected to the flattened state and vice versa. This structure introduces a certain resistance at the beginning of deformation until a certain load bearing peak is reached. Subsequently, the load drops drastically and enters the statically balanced region in which the actuation force remains constant and near perfect zero as the displacement is increased. Also, this structure provides sufficient resistance against wind loading. For the validation of the applied method a physical model, made out of PET-G plastic, has been constructed and successfully tested. The experimental results coincide well with the predicted values and indicate the applicability of the method.

*Keywords:* compliant mechanisms, interactive architecture, neutral stability, tape-spring, shape optimization, shell, sound barriers, static balancing, zero-force

---

## 1. INTRODUCTION

Architecture consisting of building components that can adapt or respond to the changing parameters of user preferences, environmental aspects or mechanical changes are referred to as reconfigurable, responsive, adaptive or digitally driven architecture [1]. Due to the ability of structures to respond in an adaptive and efficient manner to external as well as internal stimuli [2], designs become increasingly lightweight and over-dimensioning becomes unnecessary. However, creating such buildings is challenging since many aspects need to be taken into account. Some of these aspects are: smart material technology, design scenarios, characterization and optimization [3]. Literature provides multiple examples of adaptive building components that deal with light [4], climate [5], noise [6] and earthquakes [7]. The Muscle Tower II project, for instance, developed by Hyperbody at Delft University of Technology is an example of a responsive kinetic large-scale structure [8]. Pneumatic cylinders, known as Festo ‘muscles’, were used to actuate this digitally driven tower.

Another responsive structure developed by Hyperbody at Delft University of Technology and Festo AG is the

Interactive Wall (IW). A 1:1 scale prototype was built and exhibited at the Hannover fair in 2009 to demonstrate its interactive features [9]. This prototype consists of a flexible frame, which is  $1.09m$  wide,  $0.53m$  deep and  $5.30m$  tall. In order to give the impression of a monolithic and flexible structure, an elastic fabric is used to cover the whole frame. The element of interactivity is implemented with the aid of motion sensors such as lighting and loudspeakers. Electronic cylinders are mounted at the foundation of the frame to introduce sensorial and physical transformation [10].

The IW became an inspiration for the design of the Barrier in Motion (BiM) by Oosterhuis et al. [9]. In contrast to conventional sound barriers, the BiM flattens to the ground as long as no vehicles are passing by. As soon as vehicles, like trains, enter the area they trigger the BiM to erect, in order to block noise effectively. As a consequence, such designs and mechanisms would not permanently block the view.

However, large dynamic structures, like Muscle Tower II and the IW, require an abundant amount of parts for construction. Also, conventional rigid joints cause backlash, friction and wear [11], which can lead to poor accuracy,

repeatability and therefore introduce high maintenance and assembly costs [12]. Furthermore, deforming large-scale structures over a large range requires a significant amount of force, which is often accomplished by the implementation of integrated actuations of undesirable sizes.

Alkisaie et al. [13] managed to computationally obtain large-scale statically balanced, compliant and monolithic designs as deformable walls for the application of a Compliant Wall. To reduce the extensive amounts of parts needed for construction they made use of the theory of compliant mechanisms [11]. The latter gain their motion from the deformation of the material due to an applied force or displacement to the system. And since compliant mechanisms can be designed in a monolithic manner [14], sliding friction, wear, noise or need for lubrication are eliminated. This eventually leads to reduced assembly, weight and costs [15]. Furthermore, in order to achieve an effortless deformation, they made use of the naturally distributed material stiffness to compensate the weight along the total range of deformation. This is known as gravity compensation [16]–[24] and is an example of static balancing. The different structural geometries presented by Alkisaie et al. consist of a single complex-shaped planar beam with actuations and boundary conditions at each beam-end, which are altered for specific loading cases. These structures have a clear erected and flattened position and are deformed with near perfect zero actuation force. However, the relative low in-plane stiffness of the planar beams did not provide sufficient resistance against high wind loading generated by trains that pass by.

A larger material thickness increases the stiffness of the planar beam. On the other hand, a higher stiffness is also achieved by curving the cross-section while the material thickness is kept the same. This is similar to tape-springs or shells. These structural elements are nowadays increasingly being used in the space industry for the deployment of small satellite aerals and array areas. Another example is a tape spring solar sail [26]. This sail can be wound around a hub before deployment and then self-deploy due to the composition of a membrane that is attached to a tape spring structure. The advantage of these approaches is that they preserve the simplicity of a monolithic structure. More examples of tape-springs and curved beams are discussed next.

Peterson et al. [27] show that tape springs are very suitable for large deformation bending. Kebabze et al. [28] have investigated a cylindrical shell that has two stable configurations. In line with the latter, Pellegrino [29] has reviewed the design and construction of physical bistable shell demonstrators and the embedded actuation layers that trigger configuration changes. Jennings et al. [30] show that curved cross-sections have a high stiffness until buckling occurs. Consequently, further deformation requires low forces since the stiffness at the deforming region is lowered to nearly zero. Guest et al. [31] describe a shell structure that has zero stiffness for any finite deformation along a twisting path. This means that the shell is in a neutrally stable

state of equilibrium. This is achieved due to a particular combination of geometry and initial stress. An analytical rigid model of the shell shows that no change occurs in the energy level along a path of twisted configurations. Experimental models of thin shell confirm the neutrally stable configurations that are predicted by theory. Seffen et al. [32] have presented a study in which tape springs are longitudinally and transversely curved. They also show that after buckling of the tape spring a constant bending moment is required for further deformation. This holds for *opposite-* and *equal-sense bending* response [26] with perfect geometry. However, initial imperfections lead to a smaller range of rotations and a non-constant actuation force. Vehar et al. [33] introduce tape springs as elements of fully compliant mechanisms by a closed-loop design. The localized folds and the unfolded straight segments serve as compact revolute joints and as links, respectively. They propose an actuated tape spring mechanism by incorporating shape memory alloy wire actuators. In addition, they discuss and present several potential applications for actuated tape spring mechanisms, like bistable, multi-stable, and variable stiffness mechanisms.

Thus, shell and tape-spring structures show resistance until buckling occurs. This resistance could be, for instance, used to withstand the high wind loads that are generated by trains that pass by. It is also shown that shells are able to have multiple stable positions, which can be improved to obtain neutral stability along the total range of motion.

The goal of this research is to obtain new geometries, which consist of a single shell, that balance their own weight along a certain chosen range of deformation, for the Compliant Wall (CW). In addition, these geometries are required to provide a certain resistance against wind loading. Shape optimization procedures are used to obtain structural geometries that satisfy these requirements. These structures are exposed to different actuations, boundary conditions and cross-sectional curvatures. A scaled physical model is constructed and tested as proof of principle.

This paper is structured as follows. The next section describes the different topologies, actuation schemes and cross-sectional curvatures. Also, the different design characteristics, fundamental ideas behind gravity compensation, and optimization procedures are presented. The third, fourth and fifth sections illustrate the obtained results, the executed experiment and the discussion part, respectively. Finally, the conclusion is found in the sixth section.

## 2. METHOD

This study computationally analyses 18 different cases that represent the Compliant Wall (CW). Each case describes a monolithic and compliant shell structure with a specific topology, actuation and definite boundary conditions. To obtain the particular shapes of the structures use is made of Isogeometric Shape Optimization procedures.

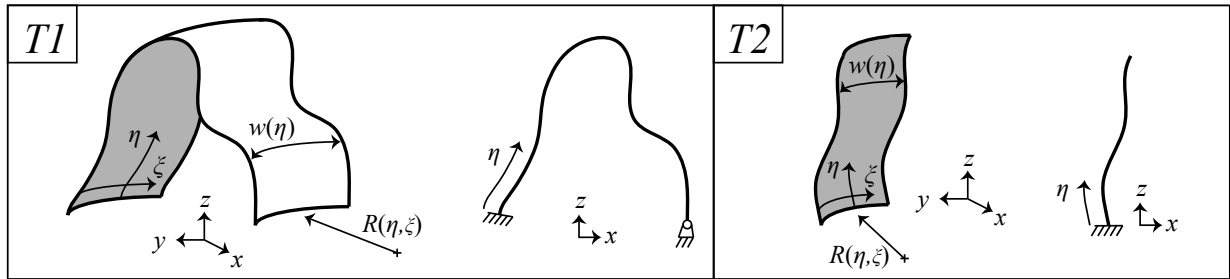


**Figure P2.1:** The two global topologies that are considered in this study. Topology *T1* has two fixations at foundation level, whereas topology *T2* has only one. Both topologies have curved cross-sections that can alter along the  $\eta$  axis. The width of the structures can alter along the  $\zeta$  axis. The curvature  $R$  is a function of the  $\eta$  and  $\zeta$  axis.

The latter changed the design parameters of the structural shape and minimizes the objective function value until a satisfying minimum is found. Consequently, the satisfying results present deformable structures that require near perfect zero force actuation along a certain chosen range of deformation. This section describes specific and detailed information about the used methods and materials, and is concluded by an optimization example that highlights the sensitivities of design parameter choices.

### 2.1. CASE STUDY

Most sound barriers are employed along car roads and vary between 2 and 3m height. This range is adjusted for densely populated areas and lies between 3 and 6m. Sound barriers along train tracks can be placed closer to the source of noise and are therefore in general lower than those along car roads. Nonetheless, there exist examples of barriers with 8m heights along train tracks. The reason for this is to significantly increase the effectiveness of acoustic absorption. Lastly, sound barriers are also placed along airstrips where planes take-off or land and have typical heights between 6 and 10m.

The surface-weight of an applied sound barrier is one of the most important design components to reduce noise effectively. According to the Dutch guidelines for noise reducing structures [34] a surface-weight of  $10\text{kg}/\text{m}^2$  reduces noise with 15dB or more. Surface-weights between 40 and  $100\text{kg}/\text{m}^2$  reduce noise with 25dB, which is sufficient in most cases.

Accordingly, this study intends to obtain three-dimensional structural designs with curved cross-sections and structural heights between 4 and 7m in order to reduce noise with 15dB or more. In addition, these structures are required to be able to deform effortlessly from an erected to a flattened position to prevent horizon pollution. Please note that the main focus is on sound barriers along train tracks, since car roads demand sound barriers to be continuously positioned in the erected state due to the high traffic flux.

### 2.2. GRAVITY COMPENSATION

Numerous design methods make use of the stiffness of external springs to compensate stationary centres of

gravity to move weights up and down with little effort [15]. This research, on the other hand, makes use of the naturally distributed stiffness of the applied material to compensate the weight of the structure along the total range of deformation. Thus, no additional or external springs are required to achieve an effortless structural deformation of the CW.

### 2.3. TOPOLOGY, BOUNDARY CONDITIONS AND ACTUATION TYPES

In an earlier research Alkisaie et al. [13] investigated the influence of specific combinations of actuation and boundary conditions on the behaviour of structures, which consisted of monolithic and compliant planar beams. Diversely, the topologies in this study are that of a single monolithic and compliant beam but with a curved cross-section. Figure P2.1 illustrates the considered global topologies for this study. The advantage of the first topology is that it offers the possibility to apply actuation and boundary conditions at foundation level, which can be hidden from the eye in practice. On the other hand, the advantage of the second topology is that it does not require a relatively large space or a second fixation at the foundation in order to stand. However, the actuation needs to be applied on the body for the second topology and cannot be hidden as like for *T1*.

It is also chosen to expose both topologies to different boundary conditions and actuation types. Note, this research restricts itself to one actuation mechanism per structure. Topology *T1* has a rotational actuation  $\theta$  at one of the structural-ends and a pin or a clamp at the other. Differently, topology *T2* has a vertical displacement  $v$  applied at the top and a consistently clamped support, see Figure P2.2. These different boundary and actuation type combinations will be further referred to as the five schemes in this study.

Moreover, the width  $w$  and the curvature  $R$  of the applied material are not restricted to be constant along the respective dimensions of the structure. In fact, the width is a function of the length axis  $\eta$  while the curvature is a function of the length axis  $\eta$  and the width axis  $\zeta$ . More depth will be provided in section 2.6.

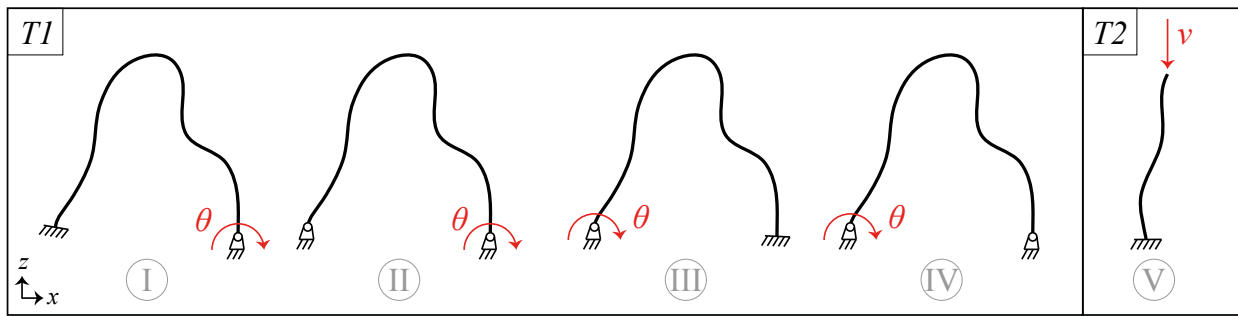


**Figure P2.2:** The five loading schemes that are considered in this research. All structures from topology  $T1$  are exposed to a rotational actuation  $\theta$  at one of the fixations. Topology  $T2$  is exposed to a prescribed vertical displacement  $v$  at the top while being clamped at the foundation.

#### 2.4. CROSS-SECTIONS

The stiffness of a shell is mostly influenced by its curvature and its width. The latter two are especially significant when shell structures are exposed to deformation. It is therefore that the influence of the orientation of the curvature on the deformation of the structure is investigated as well during this research. Figure P2.3 depicts a three-dimensional impression of the possible different curvature orientations at the supports of the global topologies. Please note that the

moment [26]. Shells are said to undergo *opposite-sense bending* if the longitudinal and transverse curvatures are in the opposite sense. On the other hand, *equal-sense bending* induces that the longitudinal and transverse curvatures are in the same sense, see Figure P2.4.

If a shell is exposed to an equal-sense bending, the cross-section flattens, which is a nonlinear behaviour, while the applied moment increases linearly. Suddenly, when the cross-section at the localized deformation area becomes

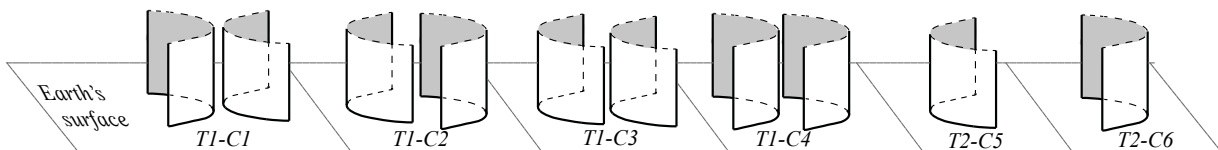


**Figure P2.3:** The different cross-sectional configuration that the two global topologies can have. This figure merely illustrates transverse curvatures. However, the structures will also have a longitudinal curvature. Note, the two sides of the first four configurations will come together at some point in the height in order to resemble topology  $T1$  correctly.

two sides of the first four configurations come together at some point in the height to correctly resemble topology  $T1$ . Also, Figure P2.3 merely illustrate structures with transverse curvatures. However, these can also have a longitudinal curvature, like in Figure P2.2.

The behaviour of tape springs or shells is highly nonlinear when exposed to bending. For small rotations the bending moment shows a linear relation as the tape or shell bends into a smooth curve. However, for large deformations the behaviour will depend on the sign of the occurring bending

approximately straight the applied moment decreases very quickly. Then the moment force remains constant for any further rotation. Contrarily, the linear force behaviour is significantly shorter for shells, which are exposed to opposite-sense bending. A sudden load bearing peak occurs early and causes the moment to decrease very quickly. Finally, the fold will then have the same characteristics as the fold for the equal-sense bending. From here, the moment  $M$  remains constant as the rotation is further increased. In addition, for both loading cases, the unloading path practically coincides with the loading path.

Ultimately, the five schemes, in combination with the different cross-sectional orientations, lead to a total of 18 different cases for investigation. Table P2.1 illustrates which specific cross-sectional orientation is applicable to the specific scheme and which is not by the plus and minus sign, respectively. All 18 cases are computationally analysed in this study to eventually determine whether they satisfy the requirements of the CW.

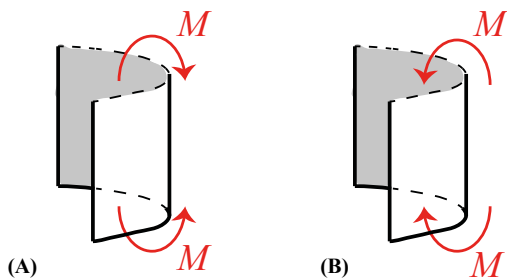


**Figure P2.4:** Perspective view of shells exposed to end moments. (A) illustrate *opposite-sense bending*, (B) *equal-sense bending*.

#### 2.5. MATERIAL USAGE

A wide range of materials can be used, on different

**Table P2.1**

The combinations of different cross-sections and loading schemes. The + and - indicate whether the specific combination is possible or not. In total, this leads to 18 cases for investigation.

SCHEME	CROSS-SECTIONS						CASES
	C1	C2	C3	C4	C5	C6	
I	+	+	+	+	-	-	4
II	+	+	+	+	-	-	4
III	+	+	+	+	-	-	4
IV	-	-	-	-	+	+	2
V	-	-	-	-	+	+	2

scales, to manufacture compliant structures. These are mostly advantageous for applications that undergo large deformations and strains [12], [15], [35]. On the other hand, fibre reinforced polymers also proved to be good candidates for compliant applications [23]. However, this study takes into consideration that the CW will be built in the natural environment. It is therefore decided to apply PET-G plastic. The advantage of the latter is that it can be heated and formed into any kind of shape, since it is a thermoplastic. Besides, it is widely available, cheap, 100% recyclable and naturally colourless with high clarity. Furthermore, it has good resistance against chemicals, against high impact and against scratches. Table P2.2 gives an overview of the mechanical properties of PET-G plastic.

## 2.6. SHAPE OPTIMIZATION

The Isogeometric Analysis (IGA) method [36], is an effective tool for the investigation of specific structural shapes with certain mechanical properties. This method makes use of Non-Uniform Rational B-Splines (NURBS) and avoids the problems of conversions between design description and analysis. This study applies the following preferences. For the construction of a three-dimensional geometry a *control net*, as depicted in Figure P2.5, is described first. This is symmetric in the  $y$ - $z$  plane. The *control points* of the control net are illustrated by the black and red dots. The red and green lines are referred to as the spine and wing segments of the control net, respectively. Each segment has its own length and relative angle. The black lines are constructed, by a piecewise linear interpolation of the outer control points, in order to close the control net. The angle of each spine segment is relative to its preceding one in the  $x$ - $z$  plane, while the angles of the wings are described

in the planes that are perpendicular to the corresponding spine segment. Eventually, the actual three-dimensional geometry is constructed by shaping a surface along the control net in which the spine and the wings form the longitudinal and transverse curvatures, respectively. Note, the actual geometry is only interpolatory and tangent at the red dots and at their corresponding wings. Moreover, the actual geometry consists of a predefined amount of finite shell elements that employed standard Gaussian quadrature rules.

The control net is defined by the array (P2.1)

$$\mathbf{q} = [ l_{s,1} \dots l_{s,4} \theta_{s,1} \dots \theta_{s,4} l_{w,1} \dots l_{w,5} \theta_{w,1} \dots \theta_{w,5} ],$$

in which  $l$  and  $\theta$  stand for the length and angle of the

**Table P2.2**

Mechanical properties of PET-G plastic.

PARAMETER	VALUE	UNIT
$\rho$ (density)	1180 - 1330	$kg/m^3$
$E_{flexural}$	1.24 - 2.76	GPa
Yield Strain	3.90 - 4.10	%
Ultimate Strain	5.00 - 350	%
$\nu$ (Poisson)	0.37 - 0.44	[-]

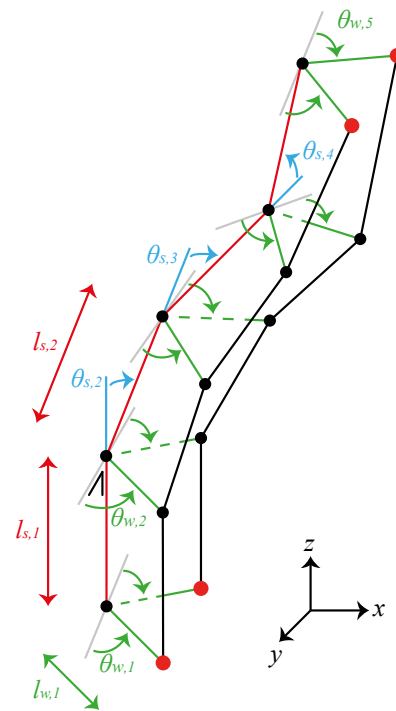


**Figure P2.5:** The control net. This consists of spine (red) and wing (green) segments. The angle (blue) of a spine segment is relative to its preceding one. The angle of the wings (green) is perpendicular to the spine segment. The control net is symmetrical in the  $y$ - $z$  plane. The dots represent the control points.

respective segment. Moreover, the subscripts  $s$  and  $w$  denote the spine and wing of the net, respectively. This study only considers shape optimization procedures, which implies that only geometrical design variables are taken into account and manipulated. This leads to a total of 18 design parameters if all the entries from the control net array are considered during optimization procedures.

The mechanical properties of the shells are formulated according the Kirchhoff-Love plate theorem [37], [38]. These properties are kept constant throughout deformation and optimization. In addition, a linear isotropic elastic constitutive law is implemented to describe the behaviour of the material. Geometrical nonlinear calculations are carried out due to the large deformations of the structures.

### 2.6.1. OBJECTIVE FUNCTION AND SOLUTION METHOD

The intention of the optimization procedure is to achieve a near perfect zero actuation force by adjusting the geometrical design parameters of the structure. The objective function  $\Phi_F$  that is used in this research, is given by

$$\Phi_F = \sum_{i=m}^n |F_i|, \quad (\text{P2.2})$$

in which  $F_i$  represents the actuation force at displacement step  $i$ . The summation that runs over the range  $i = m..n$  results in an objective function value that needs to be minimized. This range is further referred to as the optimization range. From the MATLAB® *Optimization Toolbox* the Nelder-Mead simplex direct search algorithm is used during optimization procedures to find a minimum of the objective function. This method starts at an initial estimate and continuously adjusts this estimate in order to find a lower minimum. Eventually and after successful execution an objective function value near zero is found, which consequently indicates relative low actuation forces. Then the procedure returns a newly obtained control net array that corresponds with the found minimum.

In some cases designers can be restricted to geometrical bounds. This could lead to the choice not to take all design parameters into account during optimization procedures. A drawback of the latter is that the flexibility of adjusting the geometry of a specific structure, by optimization procedures, is reduced. Consequently, finding satisfying results becomes more difficult. For instance, it might happen that the optimization procedure is prohibited to adjust the curvature of the cross-section. This can lead to structures that do not provide sufficient structural stiffness to compensate the structural weight along a certain chosen range of motion. On the other hand, it can also lead to structures with too large stiffness contribution. The outcome would surely not result in near perfect zero actuation force. However, in such cases it can be satisfying for designers to obtain a near perfect constant actuation force. In that event it is then suggested to execute a second optimization procedure, but

with an adjusted objective function  $\Phi_p$ . This is given by

$$\Phi_p = \sum_{i=m}^n |F_i - P|, \quad (\text{P2.3})$$

$$P = \frac{\sum_{i=m}^n F_i}{n - m + 1}, \quad (\text{P2.4})$$

in which  $P$  represent the average actuation force value over a certain chosen range  $i = m..n$ . The latter objective function can be seen as the general formulation in which  $P$  is substituted by the value zero or by the average actuation force value. Please note that substituting  $P$  by zero gives Eq. (P2.2). Additionally, subsequent optimization procedures that use Eq. (P2.3) minimize and flatten fluctuations in newly obtained force graphs.

### 2.7. DESIGN EXAMPLE

This section presents an optimization example of a monolithic and compliant shell structure, which is exposed to a prescribed vertical displacement at the top. Also, the structure has a clamped foundation and therefore resembles scheme V eventually. The initial array is given by

$$\mathbf{q}_{\text{initial}} = \begin{bmatrix} 1 & 1 & 1 & 1 & 0.2 & 0.4 & -0.6 & 1.5 & \dots \\ 1 & 1 & 2 & -1 & -1.3 & 1 & -1 & -0.5 \end{bmatrix}, \quad (\text{P2.5})$$

which is constructed in such a way that the shell structure would have different longitudinal and transverse curvatures. The material density  $\rho$  and Earth's gravitational forces  $g$  are taken into account, present before any displacement takes place, and are set equal to  $1270 \text{ kg/m}^3$  and  $9.80166 \text{ m/s}^2$ , respectively. Furthermore, the modulus of elasticity is  $2 \text{ GPa}$ , the Poisson's ration is  $0.4$ , and the material thickness  $0.01 \text{ m}$ . The geometry consists of  $4 \times 16$  finite shell elements and the optimization range runs from the 10-th until the last displacement step.

Figure P2.6 illustrates the structural geometries. The lefter figures depict the initial geometry, while the righter ones depict the optimized outcome. The most upper figures depict the control net for the respective geometry. Furthermore, the geometries in yellow and in blue represent the un-deformed and deformed state of the structure, respectively.

The changes between the initial and optimized geometry are most visible in the  $x$ - $z$  and  $y$ - $z$  views. For instance, it can be seen from the  $x$ - $z$  view that the region, where the material undergoes large bending, is shifted closer to the foundation. Due to this shift, the deformed state of the optimized geometry is closer to the ground in comparison with the deformed state of the initial geometry. Also, the



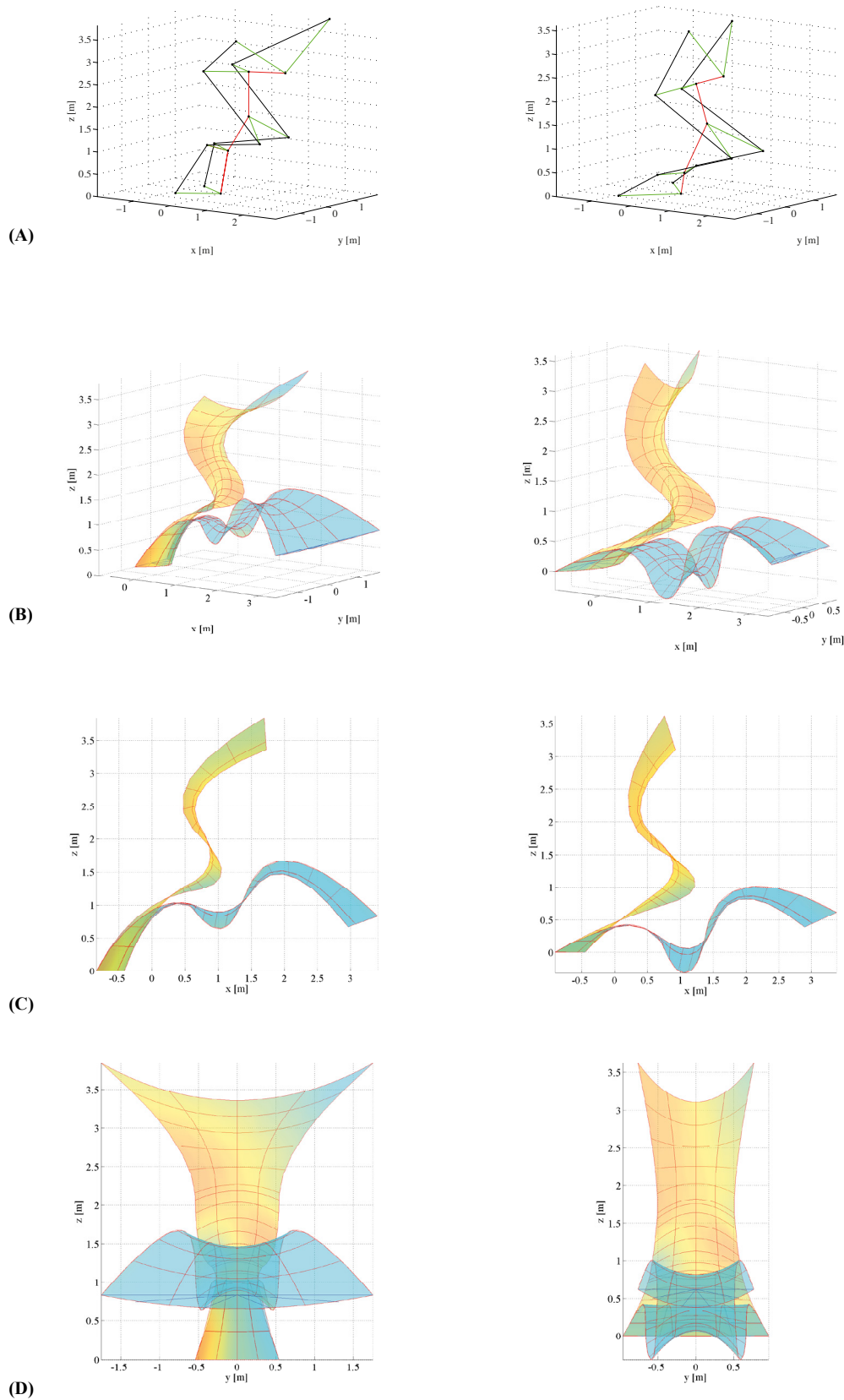


**Figure P2.6:** The lefter figures present the initial shape. The righter figures depict the shape after optimization. For this run, a prescribed vertical displacement is applied at the top while the foundation is clamped. The geometry consists of 4x16 shell elements and 3<sup>rd</sup> order polynomials for basis functions. Row (A) illustrates the control net of the respective geometries.

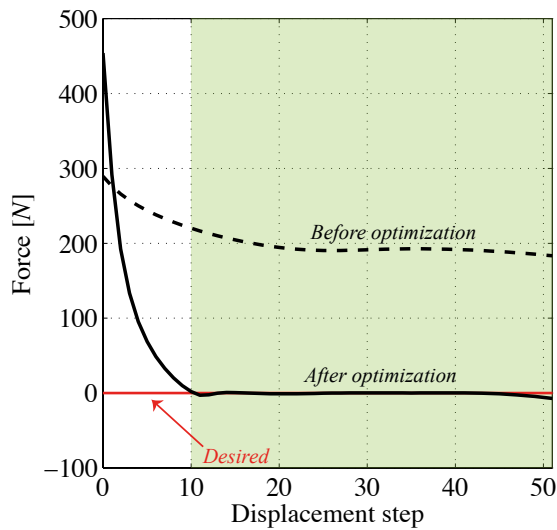


**Figure P2.7:** Force-displacement graph. The dashed line illustrate the force graph before optimization. The solid line represent the force graph after optimization and it shows that the actuation reduces to zero as soon as it enters the optimization range (green).

$y$ - $z$  view clearly illustrates that the geometry has become smaller at the top after optimization. Figure P2.7 depicts the required actuation force before and after optimization. The green area represents the optimization range. The required actuation force is being measured at the application point of the displacement, see Figure P2.8. Actuation and boundary conditions are applied at the blue dot, after which rigid bar elements, indicated by the blue solid lines, transfer the constraints or displacements to the structural body. This is done to form rigid edges. Please note as well that for each displacement step a finite element calculation, which incorporates normal and bending forces, is being executed to obtain the force-displacement graphs.

It is important to keep in mind that outcomes are highly sensitive to initial data. A slightly different initial control

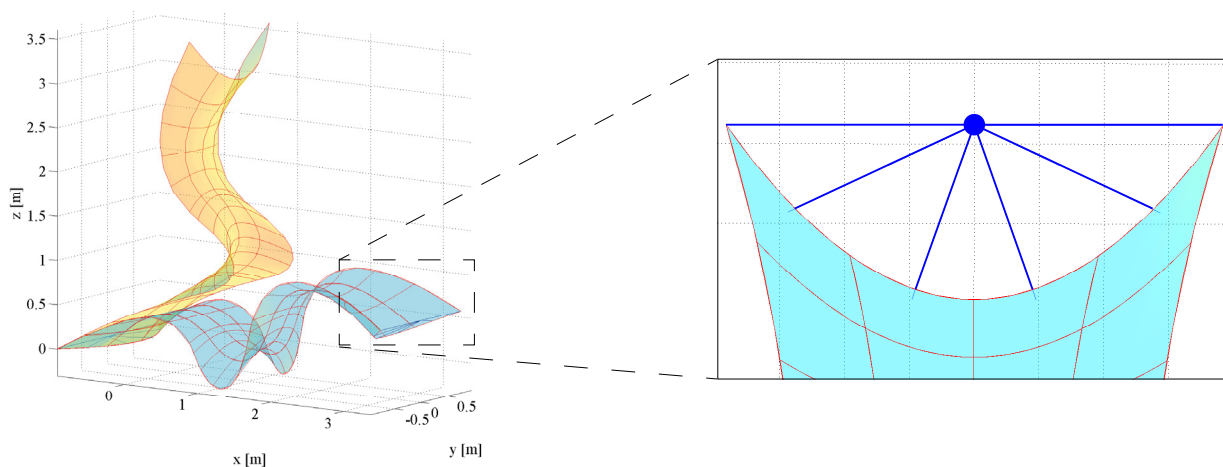


**Figure P2.8:** The application of actuation and boundary conditions. The conditions are applied at the blue dot after which rigid elements, indicated by the blue solid lines, transfer the condition to the structure. This is done for both structural ends. Note, the finer the mesh, the more rigid elements.

net, for instance, leads to a completely different result. This is also the case when a different optimization range is chosen [13]. Moreover, the refinement of the finite element mesh plays a major role during numerical procedures. For instance, the mesh used for the optimization example consists of  $4 \times 16$  shell elements with 3<sup>rd</sup> order polynomials for basis functions. Elevating the polynomial order, refining the mesh, or a combination of these two are known as  $p$ -,  $h$ -, and  $ph$ -refinement, respectively [36]. These are analogues to refinements in standard finite element analysis. Figure P2.9 presents a mesh refinement. To illustrate their great influences on analysis, it was decided to apply these refinements to the optimization example. Figure P2.10 depicts the load paths obtained after different refinements. Note that the black solid graph line represents the earlier obtained result from optimization with  $4 \times 16$  shell elements. The other graph lines are due to refinements and did not undergo any optimization procedure. The newly obtained results clearly depict that the load paths of the relatively fine meshes are close to each other. Further mesh refinement, or even order elevation did not lead to significantly different results. Also, the initial shape is perfectly preserved when refining. However, the computation time of very fine meshes becomes a major drawback. For instance, it takes, a computer with an 8-core Intel Xeon 2.80GHz Processor and 24GB RAM Memory, 12 hours and 30 minutes to finish a single structural analysis run for a geometry with  $180 \times 180$  shell elements and 5<sup>th</sup> order basis functions. On the other hand, meshes with  $10 \times 80$ ,  $60 \times 120$ , and  $100 \times 140$  shell elements and 3<sup>rd</sup> order basis functions require 2, 17, and 40 minutes, respectively, to finish. Thus, the difference in computation time is highly significant between the latter three meshes and the finest one. Though, the gain from the finest mesh is not noteworthy. It is therefore that this study manually applies refinements to specific cases until no significant improvements or differences are noticed. Then, from these fine meshes the coarsest one is chosen for optimization procedures in order to save computation time.

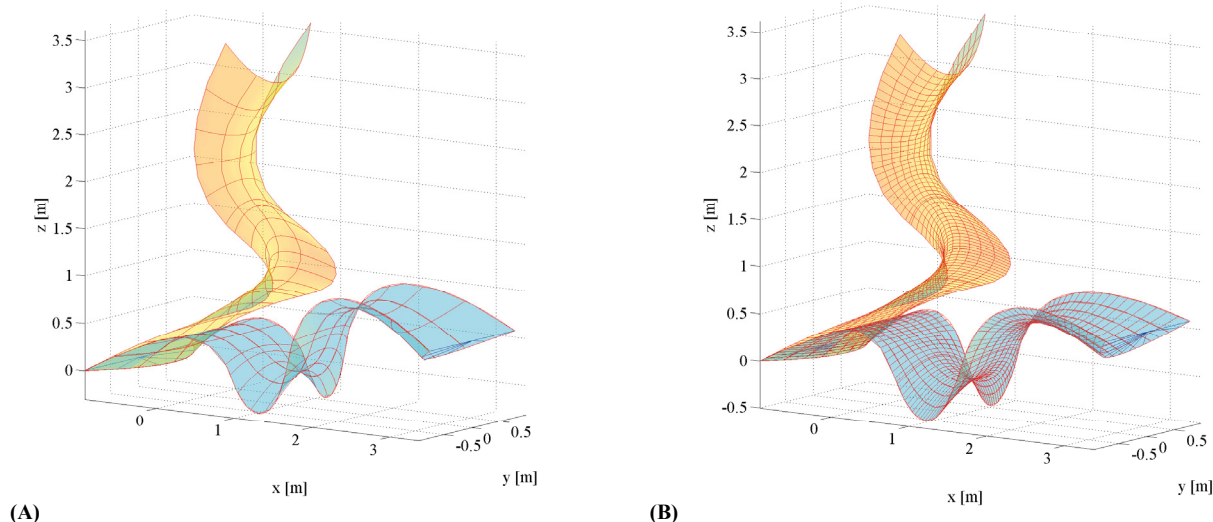


**Figure P2.9:** Mesh refinement. (A) illustrates a geometry with 4x16 shell elements, while (B) depicts a geometry with 10x80 shell elements. This is one of the benefits of the used method: the shape is perfectly preserved.

to a horizontally distributed surface loading in order to investigate whether they supply sufficient resistance against wind loads.

### 3. RESULTS

The aim of this study is to obtain novel wall geometries that are deformable, monolithic, and statically balanced. The cross-section of these geometries are curved and therefore resemble shells. New geometries are obtained with the aid of Isogeometric Shape Optimization procedures. The results are required to show a clear erected and flattened state, have a minimum structural height of 4m, and demand near perfect zero actuation along their range of motion. This research analyses 18 different cases of which the results that meet the requirements are presented with great detail in this section. Ultimately, these satisfying results are exposed

#### 3.1. OPTIMIZATION RESULTS

The objective of optimization procedures in this research is to minimize the objective function value by adjusting the design parameters of the structure. An optimization outcome with a significantly small objective function value indicates that a specific mechanism is being deformed with near perfect zero actuation force. Thus, Eq. (P2.2) is used during optimization procedures. For all cases the applied actuation is equally divided in 51 displacement steps. The optimization range and material thickness are

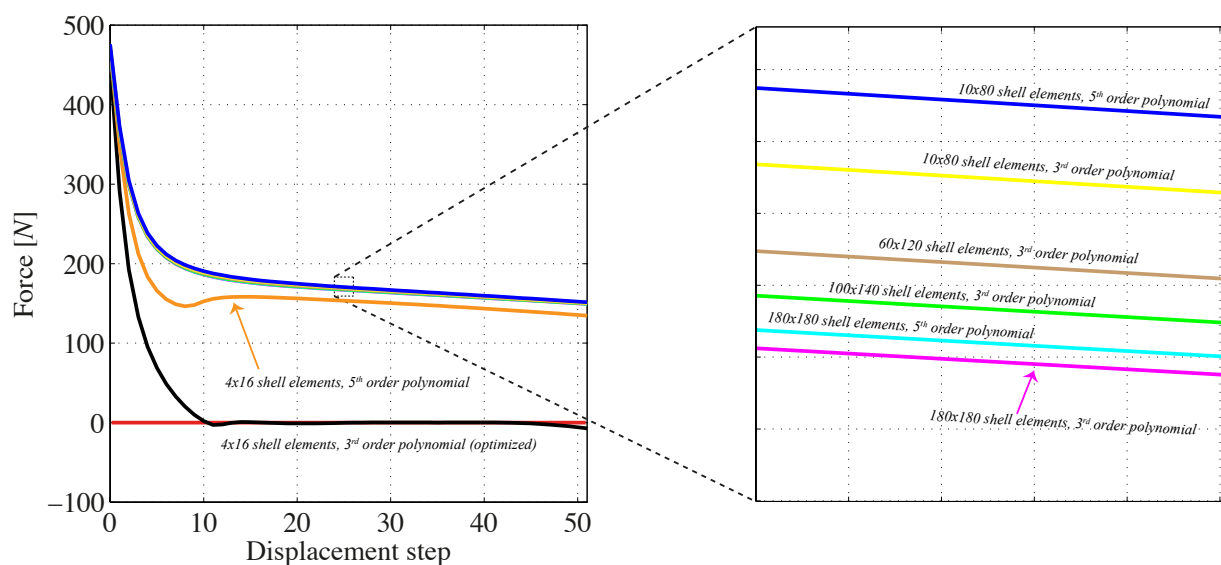


**Figure P2.10:** Load graphs of refined meshes. The black solid line presents, once again, the load graph from the optimization example. The coloured load graphs are obtained by mesh-refinement. Thus, the latter are not optimized.

specific to respective cases. The mechanical properties of the applied material are given in Table P2.3 and are that of PET-G plastic. Furthermore, all optimization procedures are executed with a fine mesh that consisted of 10x80 shell elements and 3<sup>rd</sup> order polynomials for basis functions, unless stated otherwise. Also, not all cases consider all design parameters during optimization. This is done in order to obtain geometrically acceptable results. Table P2.4 presents the results of all 18 cases qualitatively. Ratings are used to indicate whether the result is satisfying, medium satisfying or dissatisfying. These are based on whether the results meet the earlier stated requirements and are denoted by the +, the ± and the - sign. Additional commentary is provided for each case to explain the rating. Next, the most promising results are presented and discussed in more detail.

### 3.2. SATISFYING RESULTS

The structures from Cases I-C1, I-C2, V-C5, and V-C6 have a clear erected and flattened state, no colliding structural parts, and demand near perfect zero actuation force over a large range of deformation, see Figures P2.11-P2.14. However, there are differences in material thickness, geometry, and structural behaviour, which are important for the practicability of the structure.

In general, topology *T1* is required to have a larger material thickness than topology *T2*. This is mainly due to two aspects. Firstly, the curvature of the material for topology *T1* is required to be approximately flat at the top in order to allow deformation to run smoothly. And secondly, when the material of the structure did not provide sufficient thickness, the flat regions started to sag during deformation, which is obviously undesired. These two aspects are not observed for topology *T2* since it is not an arched structure.

Furthermore, the geometries of the structures differ strongly in relation to each other. All geometries are initially 2m wide and have a certain curved cross-section. The optimization procedure influences the length of the wings and the curvature of the cross-section in order to satisfy the objective. Eventually, the width of the structure altered as well. Moreover, the type of bending, which the structural elements are exposed to, also have a major influence on the width and curvature. For instance, the structural material around both fixations from Case I-C2 are exposed to equal-sense bending. Consequently, the region near the rotary actuated fixation deforms easily and quickly into a flat plate and prevents sufficient load transfer to the other fixation. It

is therefore that the optimization increased the curvatures at the regions near to the fixations in order to increase the stiffness to have a sufficient load transfer. However, this resulted in a relatively narrow geometry that did not flatten completely to the Earth's surface. On the other hand, the regions around the fixations of Case I-C1 are exposed to opposite-sense bending. This is a rather rigid and stiff structure due to the opposite positioned curvatures. As a consequence, optimization flattens the cross-sections in order to enable deformation. Case V-C5 and V-C6 do not experience the preceding phenomenon. Although Case V-C5 resulted in a relatively narrow geometry as well, which is probably due to the trade-off between the contribution of the structural mass and structural stiffness in order to compensate the weight along the path of deformation.

Also, for each case a force-displacement graph is obtained. Positive force values imply that no actuation is required to deform the structure, whereas negative force values indicate the opposite. Table P2.5 presents the required actuation forces quantitatively. Furthermore, to have a manifestation of the contribution of the stiffness and/or the weight a force graph without gravitational forces is plotted as well. The latter basically presents the contribution of structural stiffness over the total range of motion. The difference between the latter graph and the actual actuation graph is equal to the contribution of the structural mass. All four cases have similar force-displacement behaviour except Case V-C6. The latter presents a certain resistance at initiation until a load bearing peak is reached, after which the force drops considerably. Afterwards, as soon as the material becomes flat over the total width at the deforming region, the force remains constant as the displacement is increased. This behaviour is in line with theory about opposite-sense bending and is therefore expected to happen. In general, all structural parts that are exposed to bending tend to become flat at the deforming region in order to perform smooth structural deformation.

Another important factor is the type of applied actuation and boundary conditions. Structure with a clamped fixation and a prescribed vertical displacement prove to give better statically balanced motion in comparison with structures with hinged and rotary actuated boundary conditions. This is due to the fact that structural parts maintain their rigidity more firmly during deformation since clamped boundary conditions prevent geometrical deformation near the fixations to a large extent.

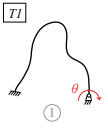
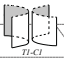
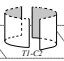
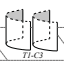
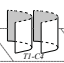
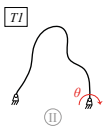
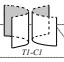
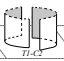
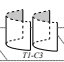
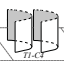
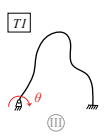


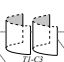
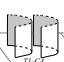
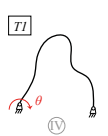




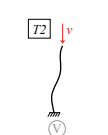
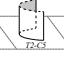
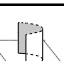
The material strain due to deformation is different for each deformed structure. The amount of deformation, rotation or displacement, which the structural parts undergo, also influence the strain levels. The first principal strain levels for all deformed structures remain below the yield strain of 4% except that of Case I-C1. The latter reaches strain levels of 12% at the clamped fixation. Such high strain levels are far into the plasticity range and therefore undesired. It is also observed that Case V-C6 experiences high strain levels of approximately 3.5% at the

**Table P2.3**  
Mechanical properties of PET-G plastic used for simulations.

PARAMETER	VALUE	UNIT
$\rho$ (density)	1270	kg/m <sup>3</sup>
$E_{flexural}$	2.0	GPa
Yield Strain	4.00	%
Ultimate Strain	350	%
$\nu$ (Poisson)	0.4	[-]

**Table P2.4**

The results obtained from optimization procedures. The schemes and cross-sectional configurations are presented. It is also stated how many design parameters are taken into account during optimization. The rating indicates whether the specific case was successful in obtaining structural shapes that satisfy the objectives. The +, ±, and - denote satisfying, medium satisfying and unsatisfying, respectively. Comments are given to explain the rating.

SCHEME	CROSS-SECTION	# DESIGN PARAMETERS	RATING	COMMENTS
		14 design parameters The spine lengths are fixed	+	Both regions at the fixations are exposed to equal-sense bending. This prevented sufficient load transfer from the actuated to the other fixation.
		14 design parameters The spine lengths are fixed	±	Both regions at the fixations are exposed to equal-sense bending. This prevented sufficient load transfer from the actuated to the other fixation.
		14 design parameters The spine lengths are fixed	±	The two sides of the structure cross each other at foundation level. Further, a major part of the structure is flat.
		18 design parameters	±	One fixation is exerted to opposite-sense bending and the other to equal-sense bending. The latter flattened quickly and prevented proper deformation.
		14 design parameters The spine lengths are fixed	-	Near zero actuation force is not achievable. Geometrically not satisfying.
		14 design parameters The spine lengths are fixed	-	Near zero actuation force is not achievable. Geometrically not satisfying.
		18 design parameters	-	Near zero actuation force is not achievable. Geometrically not satisfying.
		14 design parameters The spine lengths are fixed	-	Near zero actuation force is not achievable. Geometrically not satisfying.
		18 design parameters	-	The two sides collide with each other and therefore no satisfying results are obtained.
		18 design parameters	-	The two sides collide with each other and therefore no satisfying results are obtained.
		18 design parameters	-	The two sides collide with each other and therefore no satisfying results are obtained.
		18 design parameters	-	The two sides collide with each other and therefore no satisfying results are obtained.
		14 design parameters The spine lengths are fixed	-	The curvature of the left side flattens quickly and loses its stiffness, while the right side stays rigid.
		18 design parameters	-	Near zero actuation is not achievable. Both sides act as two rigid parts.
		18 design parameters	±	Near zero actuation is not achievable. Both sides act as two rigid parts.
		18 design parameters	-	Both sides cross each other.
		18 design parameters	±	The geometry of the structure is narrow.
		18 design parameters	+	The actuation goes to zero when the deforming region flattens completely.

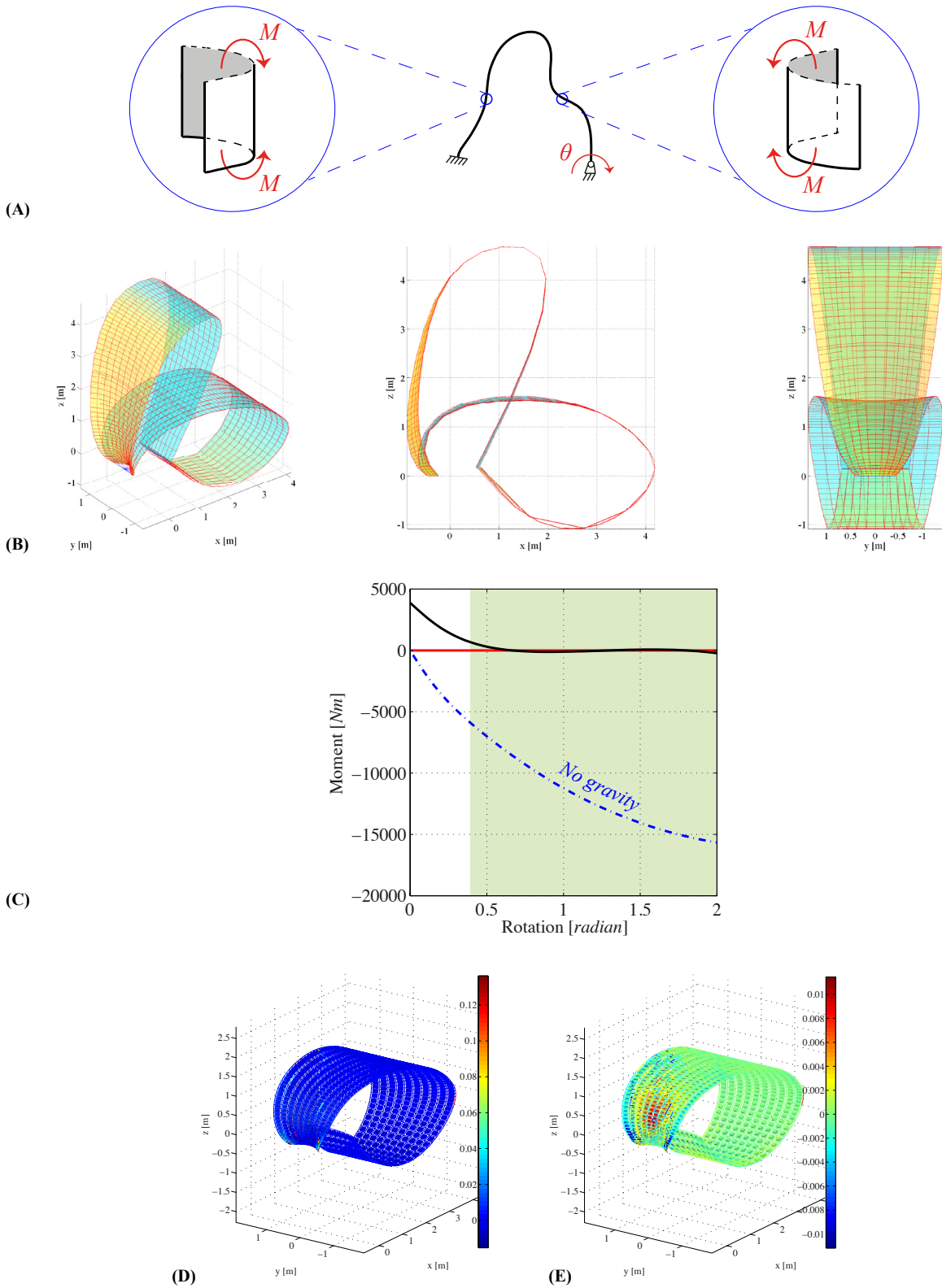


**Figure P2.11:** Case I-C1. (A) illustrates the scheme and the cross-section of each side. It also illustrates what type of bending these sides are exerted to. (B) presents the geometry that is obtained from optimization. (C) the actuation force that is required to bring the structure into motion. The contribution of the material stiffness is indicated by the graph line that does not incorporate the weight of the structure. The difference between blue and black graphs is equal to the contribution of the weight. The green area represents the optimization range. (D) and (E) present the first and second principal strains, respectively. The material thickness of this structure is equal to  $0.04m$ .

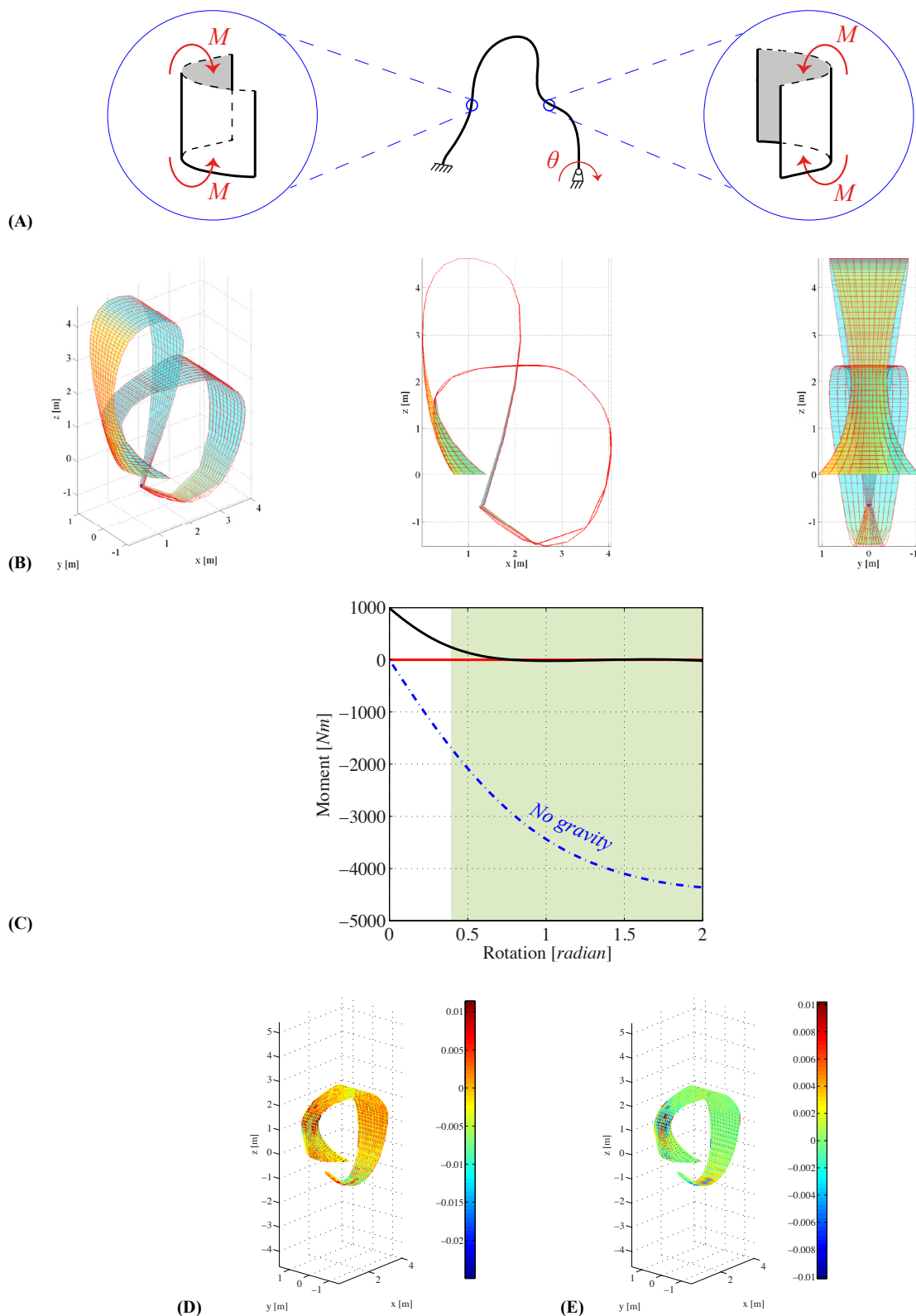


**Figure P2.12:** Case I-C2. (A) illustrates the scheme and the cross-section of each side. It also illustrates what type of bending these sides are exerted to. (B) presents the geometry that is obtained from optimization. (C) the actuation force that is required to bring the structure into motion. The contribution of the material stiffness is indicated by the graph line that does not incorporate the weight of the structure. The difference between blue and black graphs is equal to the contribution of the weight. The green area represents the optimization range. (D) and (E) present the first and second principal strains, respectively. The material thickness of this structure is equal to  $0.03m$ .

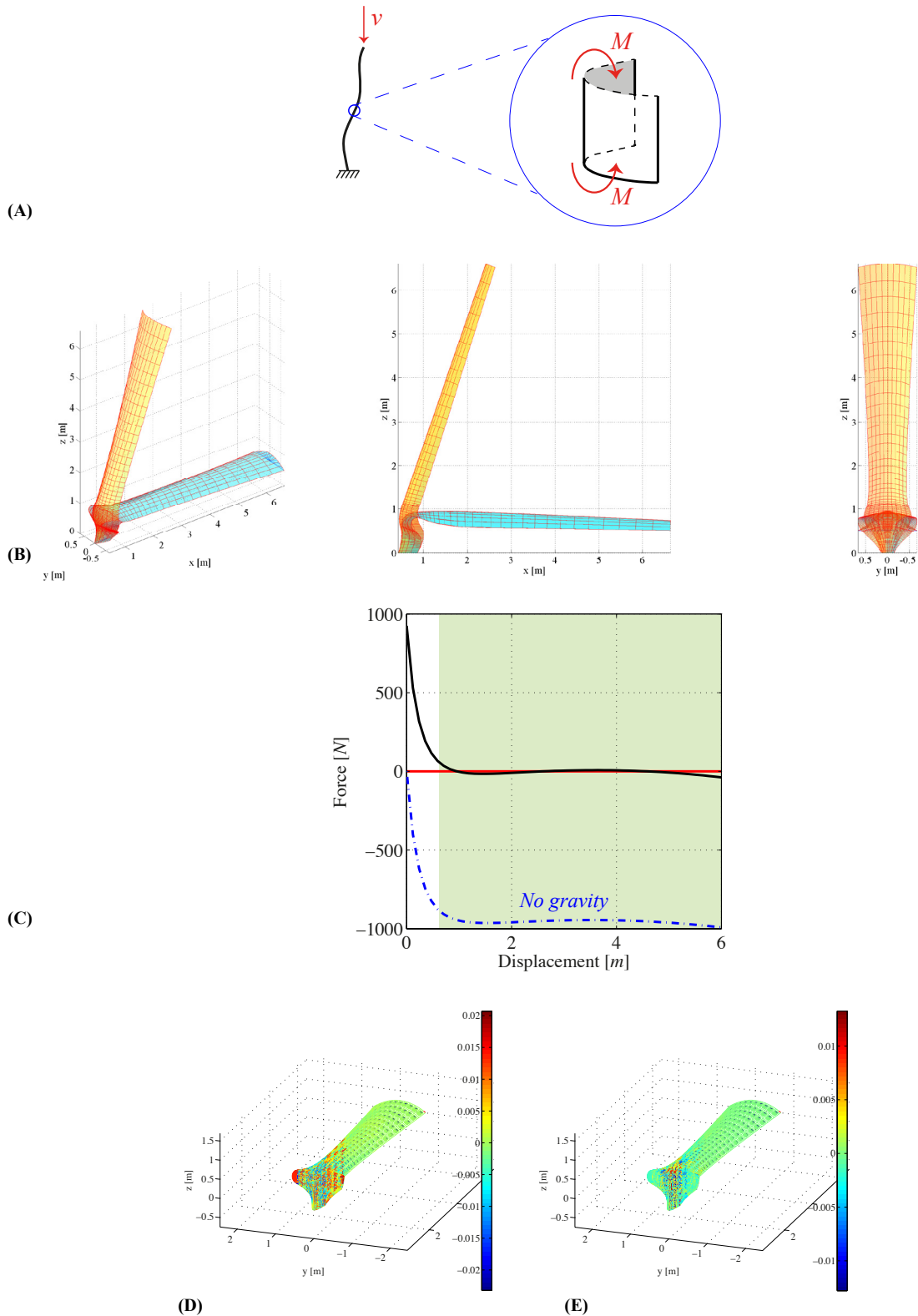


**Figure P2.13:** Case V-C5. (A) illustrates the scheme and the cross-section of the structure. It also illustrates what type of bending this cross-section is exerted to. (B) presents the geometry that is obtained from optimization. (C) the actuation force that is required to bring the structure into motion. The contribution of the material stiffness is indicated by the graph line that does not incorporate the weight of the structure. The difference between blue and black graphs is equal to the contribution of the weight. The green area represents the optimization range. (D) and (E) present the first and second principal strains, respectively. The material thickness of this structure is equal to  $0.02m$ .



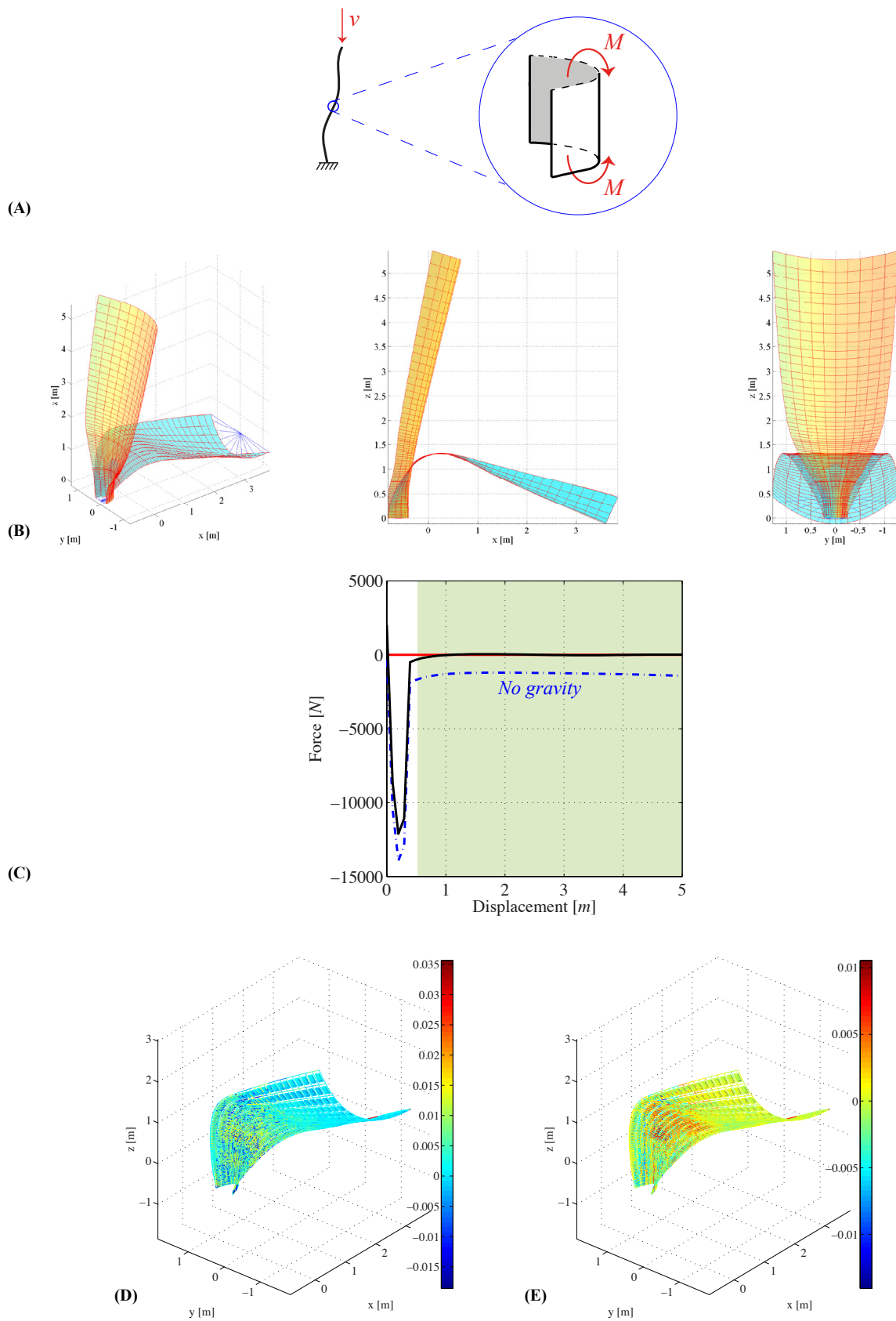


**Figure P2.14:** Case V-C6. (A) illustrates the scheme and the cross-section of the structure. It also illustrates what type of bending this cross-section is exerted to. (B) presents the geometry that is obtained from optimization. (C) the actuation force that is required to bring the structure into motion. The contribution of the material stiffness is indicated by the graph line that does not incorporate the weight of the structure. The difference between blue and black graphs is equal to the contribution of the weight. The green area represents the optimization range. (D) and (E) present the first and second principal strains, respectively. The material thickness of this structure is equal to  $0.02m$ .

**Table P2.5**

The required actuation force within the optimization range for each structure.

CASE	VALUE	UNIT
I-C1	-120 ~ 70	Nm
I-C2	-20 ~ 8	Nm
V-C5	-15 ~ 8	N
V-C6	-25 ~ 40	N

clamped boundary condition. This occurrence is predictable since the curvature of the cross-section near to the clamped fixations is not permitted to alter. This basically means that the deforming region is not allowed to become flat in order to deform smoothly. Thus, the rigidity and stiffness of these regions are maintained, which leads to relatively high strain levels in the deformed state of the structure. Such high strain levels should be prevented in practice. Especially for structures that are deformed on a repetitive basis, since this would introduce relaxation and fatigue issues and endanger the functionality of the structure. Another interesting structural behaviour is that of Case V-C5. The highest strain levels are not observed at the clamped fixation, but at the outermost fibres of the flanges at the deforming region. This is due to the fact that the curvature at that region deformed drastically from a high value to approximately zero, thus flat. Still, the strain levels are approximately 2%. To prevent structural damage at high strain level regions it is possible to apply material types at those regions that are able to undergo high strain levels. However, the implementation of different materials will surely influence the deforming behaviour of the structures. Therefore, new optimization simulations will be required then, which incorporate these different types of materials, in order to obtain new structural geometries that deform in a statically balanced manner as well.

### 3.3. WIND LOADING

When trains pass by they generate a great amount of wind loading that travels with high velocity. Structures that are built along train tracks are, obviously, required to withstand the generated wind loading. It is therefore that this study exerts the newly obtained structural geometries to a horizontally distributed loading to analyse their behaviour as a rough estimate. The most extreme wind load value for

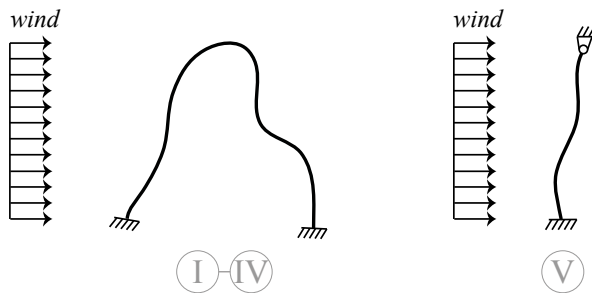


**Figure P2.15:** The loading schemes for wind simulation.

**Table P2.6**

The boundary conditions that are applied to the fixations (structural ends) of the geometries for wind simulation.

CASE	FIXATION 1	FIXATION 2
I-C1	$\delta_x = \delta_y = \delta_z = 0$ $\varphi_x = \varphi_y = \varphi_z = 0$	$\delta_x = \delta_y = \delta_z = 0$ $\varphi_x = \varphi_y = \varphi_z = 0$
I-C2	$\delta_x = \delta_y = \delta_z = 0$ $\varphi_x = \varphi_y = \varphi_z = 0$	$\delta_x = \delta_y = \delta_z = 0$ $\varphi_x = \varphi_y = \varphi_z = 0$
V-C5	$\delta_x = \delta_y = \delta_z = 0$ $\varphi_x = \varphi_y = \varphi_z = 0$	$\delta_x = \delta_y = \delta_z = 0$ $\varphi_x = \varphi_z = 0$ $\varphi_y = \text{free}$
V-C6	$\delta_x = \delta_y = \delta_z = 0$ $\varphi_x = \varphi_y = \varphi_z = 0$	$\delta_x = \delta_y = \delta_z = 0$ $\varphi_x = \varphi_z = 0$ $\varphi_y = \text{free}$

buildings in the Netherlands is equal to 2650Pa. This is used for buildings that have structural heights of 200m and are constructed at coastal areas. For this study, the latter wind loading is taken as a simplification to represent the high wind loading that is generated by trains. The horizontally distributed loading is gradually increased and remains horizontal during simulation. Also, it is assumed that the structures are positioned in the erected state when trains pass by. Therefore, the actuations of the structures are fixed at this stage. This is also the case during wind simulation. Figure P2.15 illustrates a schematic representation of the latter. The structures from schemes I until IV are clamped at both fixations, while the structure from scheme V is clamped at the foundation and fixed by a hinge at the top. Table P2.6 presents the specific boundary conditions that are applied to the structures of the different cases that are analysed during wind simulation.

Figure P2.16 presents the applied distributed loading versus the horizontal displacement of the structures. The latter is measured at a height of 3m. Figure P2.17 depicts the geometrical results and their corresponding first and second principal strains from wind simulations. During simulation

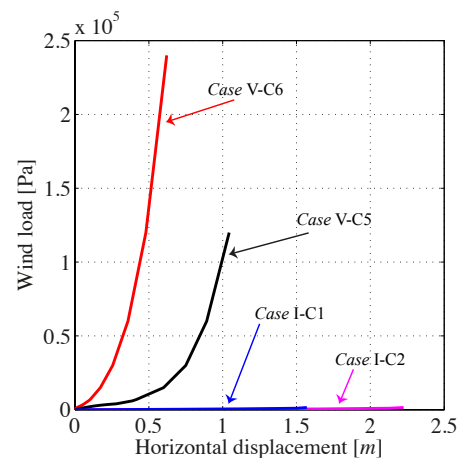


**Figure P2.16:** Results from wind simulation. The horizontal displacement is measured at a height of 3m for each respective structure.

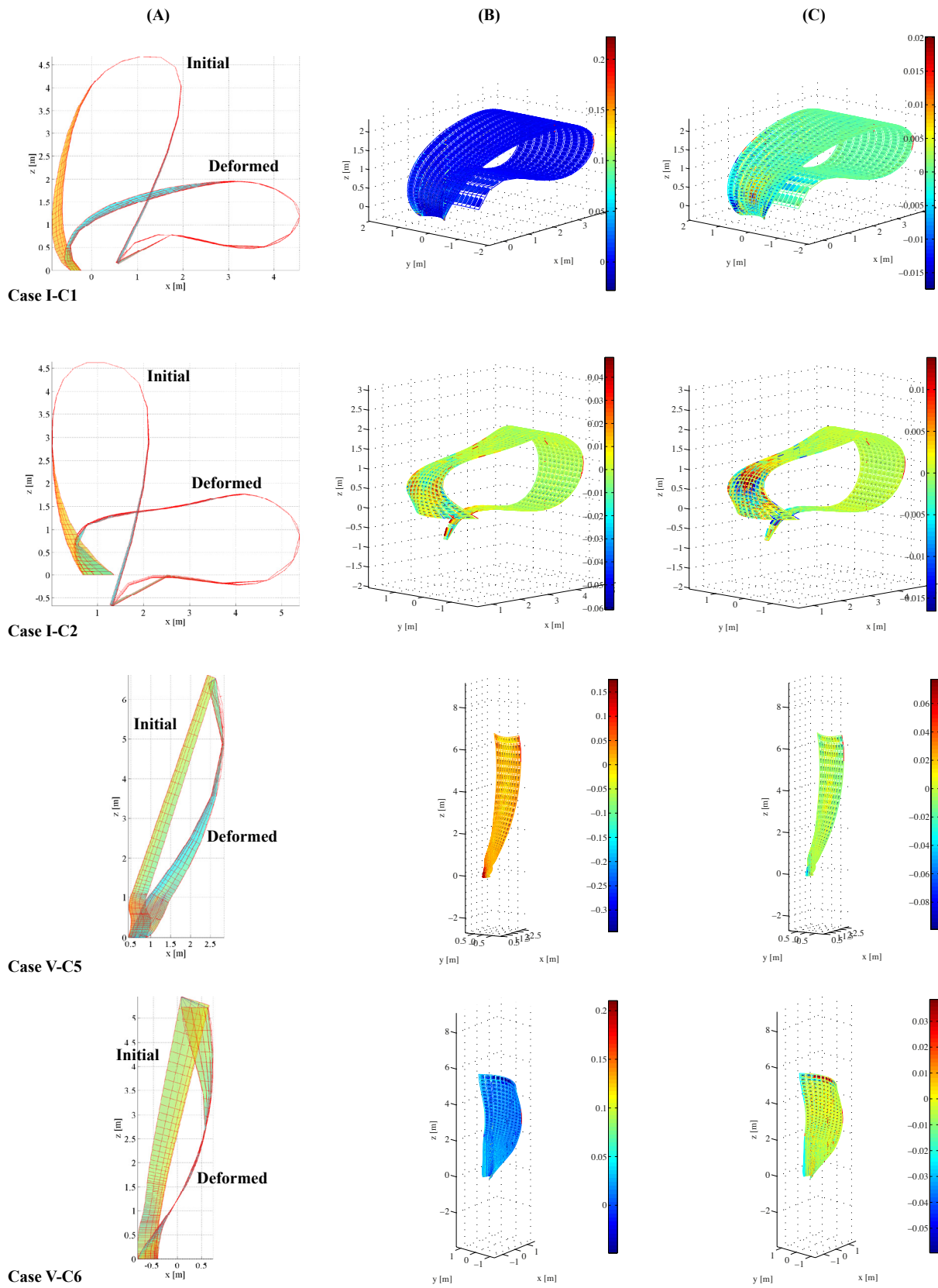


**Figure P2.17:** The results from wind simulations. Column (A) presents the initial and deformed state of the structures. Columns (B) and (C) illustrate the first and second principal strains, respectively.

and from the results it immediately becomes clear that the arched structures are not braced in the height. This allowed the structures to sway easily due to the applied horizontal wind loading. Also, more wind loading is captured due to their arched topology. Thus, no sufficient resistance is provided by these structures.

On the other hand, the structures with a single fixation at the foundation are braced in the height due to the applied boundary condition at the top. This proves to be a more effective solution against horizontal distributed loading. However, there are behavioural differences between the structures from Case V-C5 and Case V-C6. Firstly, the structure from Case V-C5 is exposed to an opposite-sense bending and therefore has a load bearing peak at some point. Observably, the cross-section at a height of approximately  $5m$  flattens as the distributed loading increases. Consequently this region lost its rigidity. The structure from Case V-C6 is exposed to an equal-sense bending and did not show any load bearing peak. However, the structure from the latter case did flatten over a large range of its geometry. This is due to the fact that the curvature is positioned towards the source of the distributed loading. Consequently, the distributed loading pushes the curved cross-section open and causes it to flatten. Although the structure from Case V-C6 showed to be withstanding the horizontally distributed loading to a large extent, special attention should be paid to the boundary condition at the top, since the latter is also required to withhold the large forces that are introduced due to the surface loading.

The maximum material strain levels in the deformed state of the structures remain below the yield strain of PET-G plastic, except that of Case I-C1. The structure of the latter case is easily blown to the surface. This results in strain levels of approximately 20% at the region near to the clamped fixations. Such levels are undesirable in practice

and should be prevented.

## 4. EXPERIMENT

This section presents the construction of a shell, which demands near perfect zero force actuation along a large range of deformation. This model is evaluated to validate the presented method. The physical model resembles the structure from Case V-C6 in which the fixation at the foundation is clamped and a prescribed vertical displacement of  $-0.65m$  is applied at the top. The maximum height and width of the model are approximately  $0.6m$  and  $0.25m$ , respectively. The prescribed displacement is carried out in 51 equally divided displacement steps in which the optimization runs from the 10-th until the last displacement step. The numerical mesh consists of  $10 \times 80$  shell elements with 3<sup>rd</sup> order polynomials for basis functions.

### 4.1. OPTIMIZATION RESULT AND PHYSICAL MODEL

The applied mechanical properties are that of PET-G plastic and the material thickness was set to  $1mm$ . At this scale it was not possible to obtain satisfying geometries that have a perfect zero actuation force. This is mainly due to scaling effects. When geometries are downsized, the contribution of stiffness and weight decrease linearly and cubically, respectively [13]. Thus, for most outcomes this means that the contribution of stiffness is larger than that of the weight. It is therefore decided to execute a subsequent optimization procedure with the objective to find a geometry that requires a constant actuation force, thus using Eq. (P2.3). Ultimately, a force-displacement graph is obtained in which the actuation force is close to perfect zero actuation force. This is presented in Figure P2.18 and

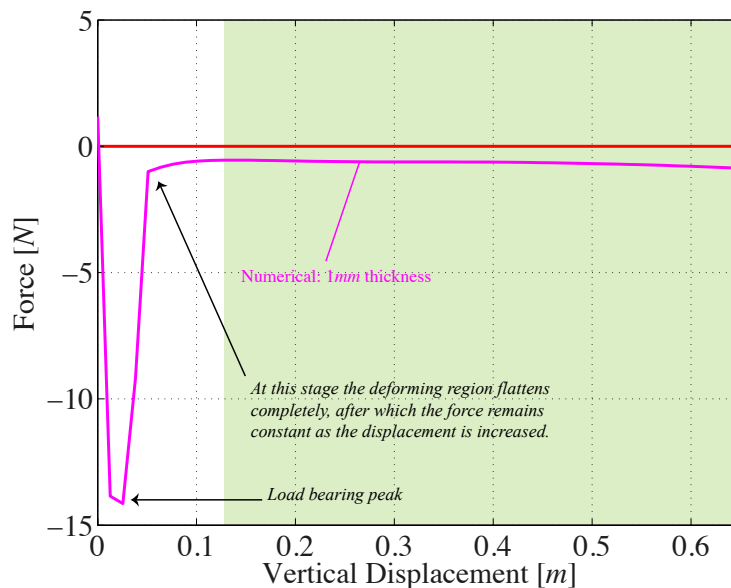


**Figure P2.18:** The force-displacement graph of the scaled model obtained from numerical simulation. The green area presents the optimization range. The material thickness is equal to  $1mm$ .

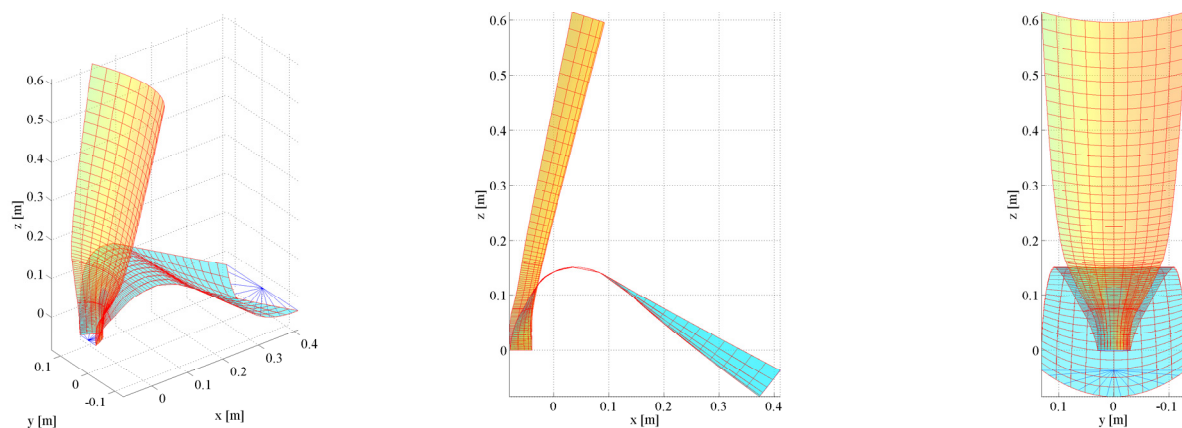


**Figure P2.19:** The obtained structural shape for a physical model. This resembles the loading case of V-C6, in which the foundation is clamped while a prescribed vertical displacement is applied at the top of the structure. The geometry consists of 10x80 shell elements with 3<sup>rd</sup> order polynomials for basis functions.

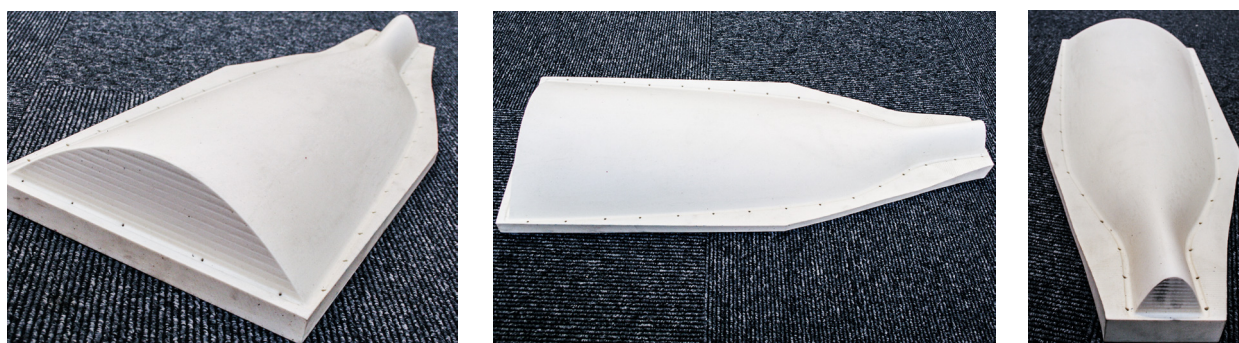


**Figure P2.20:** The eventual mould that is obtained from a drill machine. The material is NECURON-301<sup>®</sup>. Holes are drilled along the contour of the geometry in order to increase the vacuum force.



**Figure P2.21:** The physical model. The material is PET-G plastic. (A) presents the model in its initial and erected state. (B) illustrates a front view of the structure in its deformed state. (C) presents the structure in its deformed state. It is also noticeable that the structure is in a stable position and it does not require any external force or weight to stay in that position. (D) illustrates a top view of the deformed state.

is similar to that of Case V-C6. Once again, the positive force values indicate that no actuation is required to deform the structure, whereas negative force values impose the opposite. Figure P2.19 illustrates the eventually obtained geometry from optimization procedure. The numerical geometry is exported as an IGES file and imported in SolidWorks®. The latter offers standard *Mould Tools* that provide aid in creating a mould file, which can directly be sent to a mill machine afterwards. Figure P2.20 depicts the eventual mould, which is made of NECURON®-301. Subsequently, an initially flat PET-G plastic plate is placed on top of the mould, heated and then vacuum-formed onto the mould. Along the contours of the geometry holes are drilled in the mould in order to increase the vacuuming effect. Ultimately, the eventual physical model is cut out of the formed plate, see Figure P2.21.

#### 4.2. EXPERIMENTAL SETUP

In order to clamp the physical model at the bottom a specifically designed foundation is built and attached to a relatively heavy aluminium plate, see Figure P2.22. The relative heavy aluminium plate is implemented to prevent toppling during testing. The foundation is 54mm high and is built out of nine Medium-Density fibreboard (MDF) panels with a thickness of 6mm each. The physical model is elongated at the bottom so that clamping is made possible, see Figure P2.22B and Figure P2.22C. The prescribed vertical displacement is applied with the aid of a compression bench that is able to measure the required actuation force and the performance of the physical model simultaneously, see Figure P2.23. This bench is attached to the physical model by using a bar as a knife-edge [13], [24], see Figure P2.24A. The bar and knife-edge are kept in their place due to the application of a double-sided tape. To obtain a hysteresis loop for the determination of energy loss, measurements are performed in two directions. It is assumed that these losses are equal in both directions. Furthermore, to be able to neglect inertia effects the vertical displacement is applied in low speed during testing. And since the compression bench is only able to displace itself in a vertical sense, the physical model required to be displaced in a horizontal sense in order to execute testing in the correct manners. This is achieved by placing the physical model and its aluminium plate on a set of straight rods, see Figure P2.24B. The lower and upper two rods are chosen to be significantly longer than the middle ones in order to reach the long range of horizontal displacement.

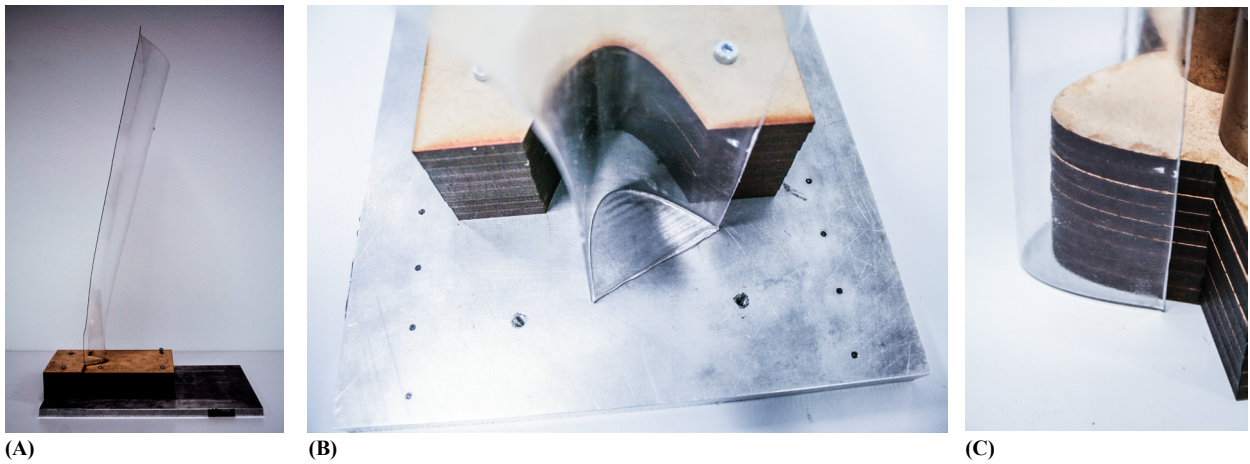
#### 4.3. MEASUREMENT RESULTS

Figure P2.25 illustrate the measurement results of two specimens and show good overlap with each other. Negative and positive force values indicate that the compression bench experiences compressive and pulling forces, respectively. It is clearly observed that the specimens supply a certain resistance at the beginning, as expected, until a load

bearing peak is reached. In physical terms, the curvature of the cross-section at the deforming region starts to flatten from the centre towards the outer edges of the wings. As a consequence, the compressive force drops drastically until the deforming region becomes approximately flat over the total width. Accordingly, the actuation force remains constant as the displacement is increased. In fact, the experimental measurements show that the load path of the model crosses the zero line at approximately  $x=0.5m$ , which implies a stable position without the addition of an external weight. This was seen in Figure P2.21C.

The purple graph line represents the load path obtained from numerical simulation and it does not overlap very well with the experiment. This is mainly due to the material thickness of the eventual physical model and is explained as follows. Before the initially flat PET-G plastic plate is heated, it is clamped at its four edges. Then, the heating element is initiated, which causes the plate to become limp and soft. This is then placed onto the mould while the vacuum mechanism is activated simultaneously. Consequently and due to the height differences of the mould, the soft plastic plate needs to be enlarged in order to fit the geometry of the mould. This leads to a local material thickness reduction of 10 or even 20%. This depends on the specific location on the mould. The material thickness of the eventual model lies between 0.9 and 1mm at relatively low mould heights, whereas the material thickness lies between 0.8 and 0.9mm at relatively high mould heights. Thus, the material thickness is overall reduced. Therefore, a subsequent structural analysis is carried out with the same geometry, but with a different material thickness, see Figure P2.26. It is easily observed that the new load graphs coincide better with the experiment. Also, a material thickness reduction of 0.1mm, at this scale, leads to a force reduction of approximately 50%, which is significant. Moreover, the differences between the experimental and numerical results might also be due to shrinkage that is introduced during cooling down. Such a phenomenon most likely has an influence on the mechanical properties of the material. Also, no holes are drilled within the contours of the actual geometry of the physical model, which might have reduced the effectiveness of the vacuum force within that region. Therefore, the eventual shape did not fit the mould perfectly. However, this is investigated further and it is noticed that the differences are negligible. This is also the case for inaccuracies that might have been introduced during handicraft production procedures.

According to numerical simulations, the strains in the material remain below the yield strain level, see Figure P2.27. This is obtained for the geometry with a material thickness equal to 1mm. During experiments, the strains in the material become highly visible for the eye at the centre of the deforming region, see Figure P2.28. This is in accordance with what is predicted by the numerical simulations.



**Figure P2.22:** The foundation is made of 9 MDF plates. Each plate is 6mm thick. These are attached to a relatively heavy aluminum plate in order to prevent the model from toppling during testing. (B) and (C) illustrate the elongation at the bottom of the physical model to make clamping possible.



**Figure P2.23:** The physical model during a compression test. The compression bench displaces itself in a vertical sense and measures the vertical displacement and the force simultaneously. The foundation of the model is displaced in horizontal direction due to straight rollers.

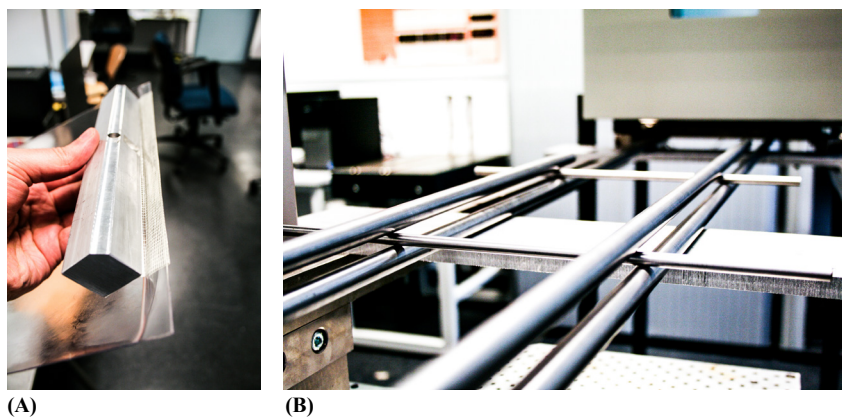


**Figure P2.24:** (A) a bar and knife-edge is used to apply a vertical displacement to the model. A double sided tape is used to keep the knife-edge in its place. (B) illustrates the rollers that are placed below the physical model to make horizontal displacement possible.

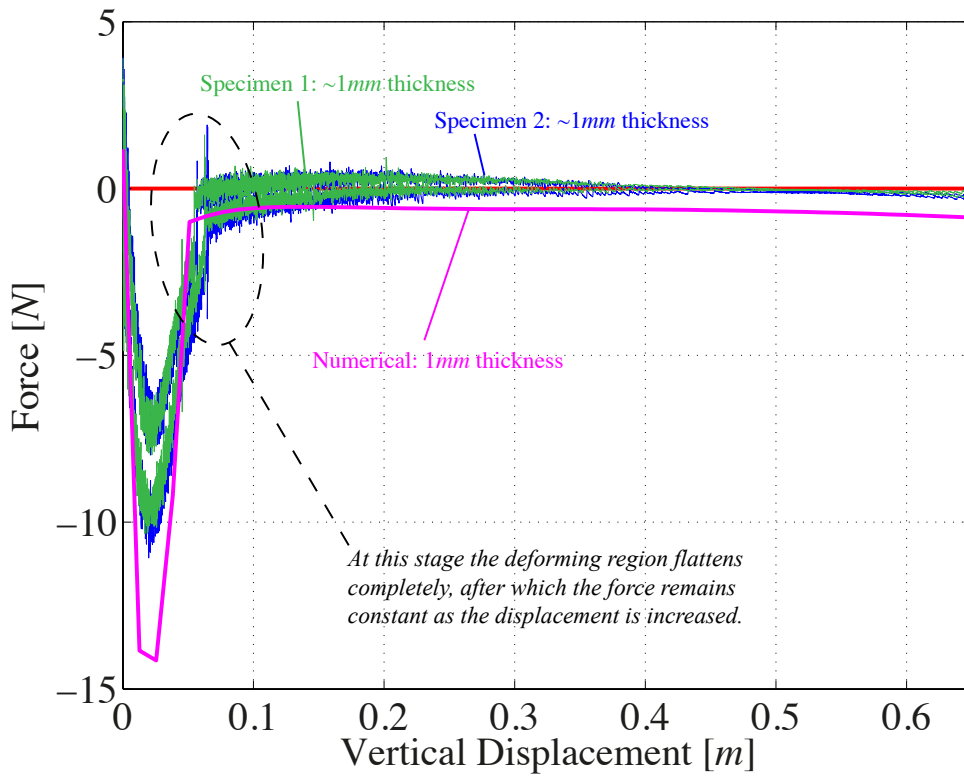


**Figure P2.25:** The force-displacement graphs of the experiment. The blue and green lines are obtained from the compression bench. These are performed in two direction to obtain a hysteresis loop for the determination of energy losses. The purple line is obtained from numerical simulation.

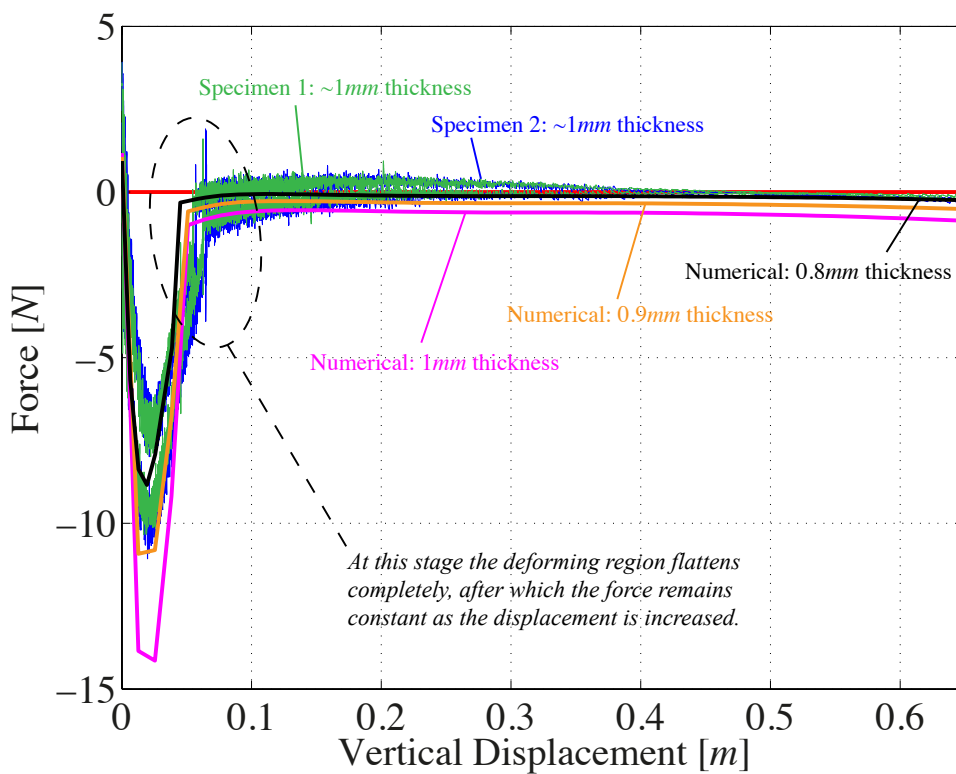


**Figure P2.26:** The material thickness has reduced due to vacuum-forming. Some areas have a thickness of 0.9mm and others of 0.8mm. The latter is especially measured at high mould areas. The orange and black lines illustrate the load graphs obtained from numerical simulations, but with different thicknesses.



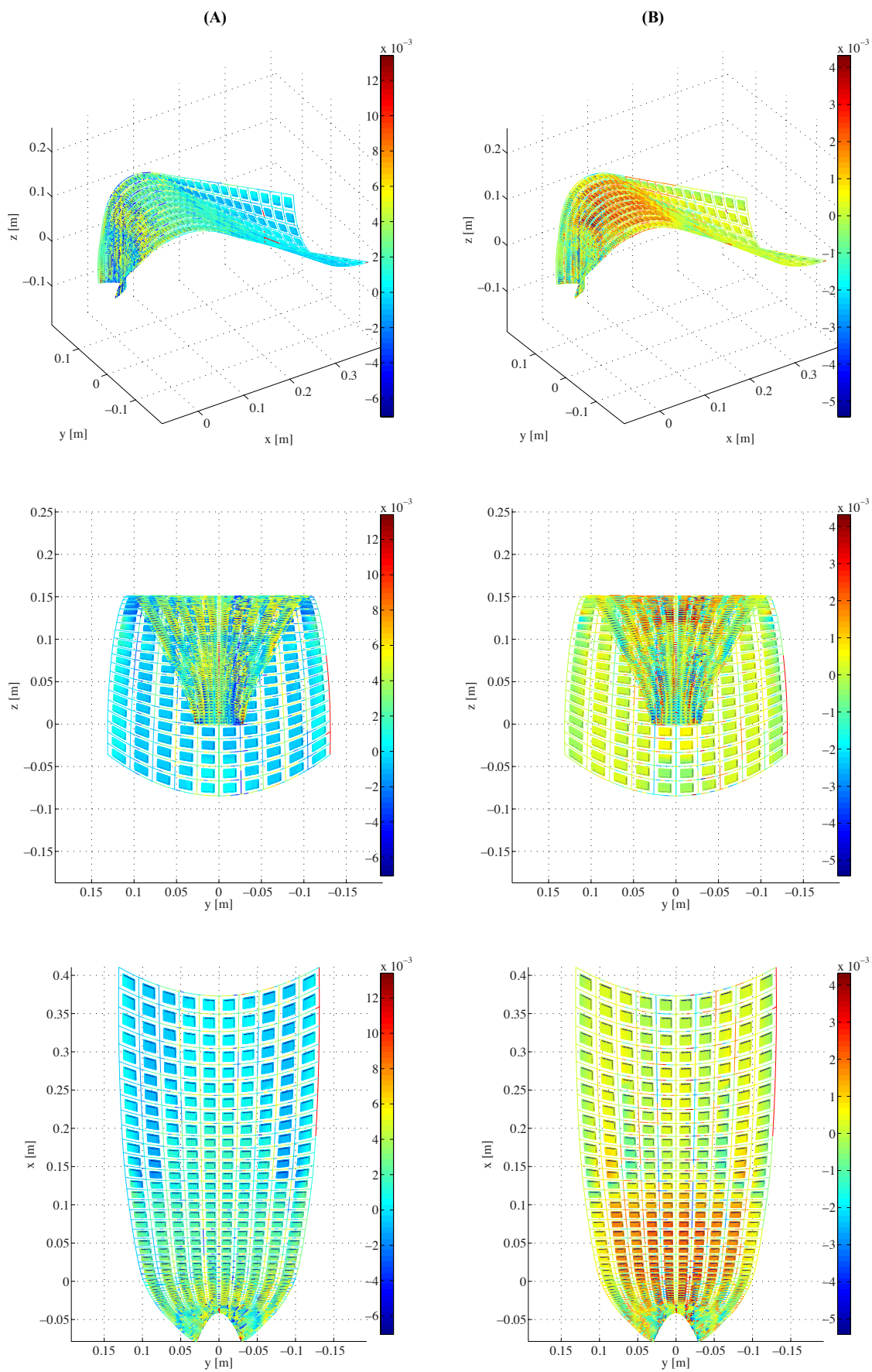
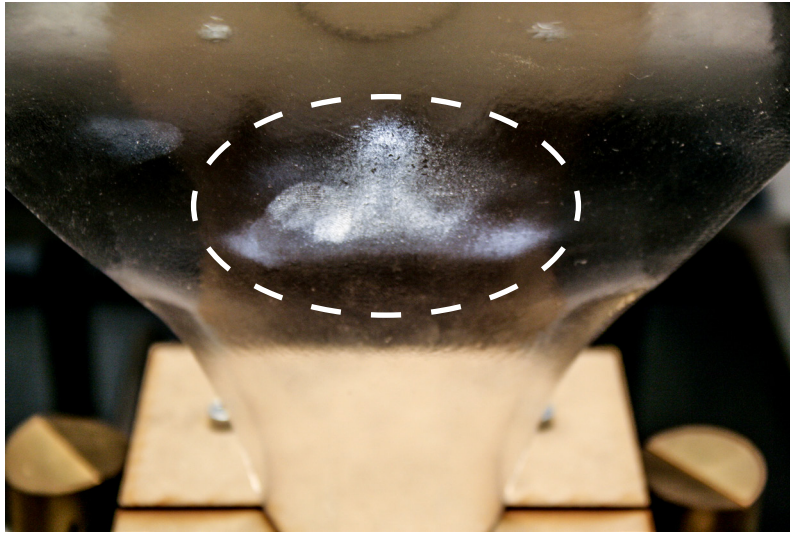


Figure P2.27: The material strain in the physical model. Columns (A) and (B) present the first and second principal strains, respectively.



**Figure P2.28:** The material strain in the physical model after testing. This is in accordance with what is predicted by the numerical model.

## 5. DISCUSSION

This section evaluates the applied method, the obtained numerical results and the experiment. Furthermore, attention is also paid to real life applications and purposes.

### 5.1. EVALUATION OF APPLIED METHOD

This study uses Isogeometric Shape Optimization procedures to obtain statically balanced large-scale compliant shell structures that compensate their weight along a certain range of motion by using the naturally distributed material stiffness. The numerical model works adequately in obtaining structural geometries that satisfy the desired objective. The optimization procedure alters the design parameters continuously in order to decrease the objective function value. When a minimum is found, the optimization stops and presents the geometry that corresponds to the newly obtained design parameters. Whether the newly obtained objective function value is small enough was up to the users experience. However, it is by no means certain that the global minimum is found. Thus, there might be better results than the ones presented in this research. This matter is for future investigation.

Moreover, this study applies merely one actuation per structure at a time. Applying multiple actuations simultaneously can be beneficial for the behaviour of the structure during deformation. However, the objective functions that are considered in this research do not suffice. Therefore, new objective functions are required, which minimize the objective function values of the multiple actuations in order to obtain a statically balanced motion.

Also, the numerical model can be extended in such a manner that multiple structural elements can be applied in a monolithic manner. Additionally, further research can also consider implementing different material types along the geometry of the structure. These extensions can help in

distributing the material stress in a more evenly manner, or prevent localized high strain levels.

Lastly, it is observed that the amount of used finite shell elements and the order of polynomials for basis functions, during simulation, influenced the outcome significantly. Therefore, several mesh sizes are benchmarked, after which a choice is made based on the experience of the user. This is due to the fact that there is no clearness in this study about which mesh size is the correct one, except it should not be too coarse. Besides, extremely fine meshes require a significant amount of time to finish procedures and are, therefore, avoided. However, it is wise that further research looks into speeding up numerical simulations in order to obtain results that are even closer to reality than the ones presented in this research.

### 5.2. EVALUATION OF THE RESULTS

The obtained structural geometries in this study are not easily attainable by hand and most certainly not straightforward. Nonetheless, optimization procedures are of great aid in obtaining shell structures with heights between 4 and 7m. Furthermore, these structures require near perfect zero actuation force over a large range of deformation. Therefore, these findings satisfy the objective of this research. However, special attention needs to be paid to the curvature of the cross-sections of each structure. A structure that has two fixations at the foundation of which the structural regions near both fixations are exposed to equal-sense bending, prevent the load to be transferred sufficiently from the actuated fixations to the constrained fixation. This forces optimization procedures to increase the stiffness, thus the curvature of the cross-sections, which leads to narrow geometries that do not deform as smoothly as desired. On the other hand, when structural regions near both fixations are exposed to opposite-sense bending, then both sides act as two rigid structural elements. This prevents smooth deformation unless the curvature of the

cross-sections is flattened to a certain degree. Consequently, the stiffness of the structure is reduced, which influences the integrity of the structure against high wind loading. In general, structures with boundary conditions at foundation level do not brace the structures in the height. Therefore, no sufficient resistance against wind loading is provided by these structures. On the other hand, the structure with a single fixation at the foundation, which is exposed to an opposite-sense bending, presents a certain resistance at the beginning of deformation. This resistance increases until a load bearing peak is reached, after which the load drops drastically. At a certain moment, the deforming region becomes approximately flat and the force remains constant as the displacement is increased. This behaviour is in line with theory and therefore expected. However, the load bearing peak is around  $12000N$ , which basically means that in practice an actuation needs to provide this amount of force before it enters the near perfect zero force region. Alternatively, the decision could be made that the structure is only deformed within the region that requires low actuation forces. However, this needs to be investigated further for wind loading.

It is also observed that the material strain reaches high levels at regions near clamped fixations. This is mainly due to the curved cross-section. Such high levels can introduce fatigue, creep and relaxation issues, which should be avoided in practice. An option would be to flatten those regions. However, this will lead to stiffness reduction at these regions and therefore influence the statically balanced behaviour of the structure during deformation. Thus, careful consideration should be made concerning localized high strain levels.

Lastly, the application of a rotational actuation at foundation level can be hidden from the eye, whereas the actuation applied on the body cannot. However, the application of a prescribed displacement at the top of a structure leads to a more controlled structural deformation. This is due to the bracing effect that the actuation at the top introduces. Furthermore, the structures that are exposed to a prescribed displacement at the top result after deformation in a clear flattened position, which is not achievable for those that are exposed to a rotational actuation at one of the fixations. Therefore, further research is required in order to decide which mechanism is more applicable in practice.

### 5.3. EVALUATION OF THE EXPERIMENT

For the physical model it is chosen to use PET-G plastic as structural material. Its advantages are low costs, widely available, 100% recyclable and good resistance against impact. Additionally, this material can be formed into any shape by means of thermoforming.

The obtained results from experiments have successfully validated the approach method. However, there are predictable minor differences between the results of the experiment and the numerical model. PET-G is a thermoplastic and has a strong nonlinear stress-

strain relation. The numerical model uses a numerical simplification by adopting a linear constitutive law, which causes slightly different load paths between the simulation and the experiment. These differences are probably significantly larger at a large scale and thus important to consider in further research.

Moreover, the forming procedure has a significant influence on the mechanical properties of the material. For instance, the thickness of the initially flat PET-G plastic plate is equal to  $1mm$ . Placing a soft and limb plastic plate onto the mould while a vacuum mechanism is activated obtains the eventual shape. This procedure causes the surface area of the plate to be enlarged due to the heights of the mould. This results in a plate thickness reduction between 10 and 20% depending on the location on the mould. An overall plate thickness reduction of  $0.1mm$  leads to an actuation force reduction of approximately 50% for the numerical simulations, which is significant. Another phenomenon that influences the mechanical properties is shrinkage. This is due to thermal effects during cooling down. Furthermore, the physical model does not fit the mould perfectly since the vacuum force is not highly effective within the contours of the actual geometry, but the differences prove to be negligible. However, it is recommended to search for methods that are able to maintain the initial material thickness during production process and prevent any type of thermal effects.

The construction of the foundation is made out of laser-cut MDF plates and provides sufficient rigidity. The double-sided tape functions as it should and keeps the knife-edge in its place. There are besides the compression bench no further complex parts implemented in the test setup.

### 5.4. REAL LIFE APPLICATION

The differences that are observed between the experimental and the numerical model can be significantly larger at actual scale and should be taken into account.

Also, the application of the CW in real life demands a significant amount of space along train tracks. This might not be available and therefore prevent the system from functioning fully. Furthermore, real life actuations can be a challenge. The structures with a prescribed displacement at the top require an actuation that pushes or pulls the structure downwards. This is not straightforward and probably not possible yet and requires further investigation. On the other hand, rotational actuations that provide a torque are available and are probably easier to implement.

The construction of the physical model proves to be practical at a small-scale, regardless of the inaccuracies that occur. However, constructing the obtained results at actual scale is not possible with the presented method. On the other hand, construction methods that are similar to those of casted concrete could be sufficient for the realization of these compliant shell structures. Nevertheless, this requires further investigation.

Conventional sound barriers need to have a material

surface mass of  $10\text{kg/m}^2$  in order to handle low frequencies effectively. Furthermore, a structure is required to have a surface mass between 40 and  $100\text{kg/m}^2$  in order to reduce noise by 25dB. The presented structural geometries in this research have a material thickness between 0.02 and 0.04m, which lead to a surface weight of  $0.02\text{m} \times 1270\text{kg/m}^2 = 25.4\text{kg/m}^2$  and  $0.04\text{m} \times 1270\text{kg/m}^2 = 50.8\text{kg/m}^2$ , respectively. Thus, these structures provide sufficient noise reducing effect.

Another important aspect is the environment in which the compliant walls will be built. The mechanical properties of the PET-G plastic can be influenced by the changing weather conditions and lead to structural damage. Especially when structures are deformed on a repetitive base. Thorough consideration is therefore of great importance.

Lastly, the newly obtained structural geometries are exposed to a horizontal distributed loading that represents wind loading. However, wind propagates in reality in a chaotic manner and might therefore cause the structures to twist, for instance. This is not considered in this study, but needs thorough attention in further research.

#### 5.5. ALTERNATIVE APPLICATIONS

The presented method can be used in other possible shape changing applications, like small- and large-scale bridges or structural elements that reconfigure due to changing traffic or environmental conditions. This can be extended to different scales of urban furniture, which offer temporarily seating and shelter from sun and rain for instance. Their ability to reconfigure makes such structures relevant, since their potential can considerably improve the efficiency of space use. To make these structures monolithic and their reconfigurations statically balanced could also be a future objective.

## 6. CONCLUSIONS

This study presents several computational structural geometries, which deform in a statically balanced manner from an erected to a flattened position and vice versa. The cross-sections of the structures are curved, thus representing shells. The statically balanced behaviour is obtained by using the naturally distributed material stiffness to compensate the weight of the structure along the total range of deformation. The structural topologies consist of a single monolithic, material isotropic, and compliant shell in which both structural ends are exposed to different actuation and boundary conditions. Further, it was also possible to position the curvature of the cross-section in a different position. The combination of the different curvatures, actuation and boundary conditions lead to a total of 18 cases for investigation. The outcomes show that the load is not transferred sufficiently from the actuated to the constrained structural end for structures in which both structural ends are exposed to equal-sense bending. On

the other hand, when both structural ends are exposed to opposite-sense bending, the respective ends behave rigidly and prevent smooth deformation unless the curvature of the cross-sections is flattened. Moreover, the most controlled structural deformation is presented by structures that are not arched. These have a single clamped fixation at the foundation and a prescribed displacement at the top. From the latter, the most promising structure is the one, which is exposed to an opposite-sense bending. This introduces a certain resistance at the beginning until a load bearing peak is reached. Then, the load drops drastically and enters the statically balanced region. In summary, the latter structure satisfies the requirements of the Compliant Wall, withstands high wind loading, and provides sufficient material surface weight to reduce train noise effectively. Ultimately, the presented findings in this study are a novel contribution to field of statically balanced compliant mechanism and structures, but as well to the field of shell or tape-spring dynamics.

The obtained structural geometries are complex-shaped and not easily attainable by hand. The Isogeometric Shape Optimization procedure is a great aid in finding satisfying three-dimensional geometries that satisfy the objective.

For the validation of the applied method a physical model is built. This represents a downscaled version of a structure that has a single clamped fixation at the foundation and a prescribed displacement at the top. The three-dimensional physical shape is obtained by means of vacuum forming in which an initially flat PET-G plastic plate is heated and placed onto a mould while a vacuum mechanism is activated simultaneously. This method is satisfying for the production of small-scale compliant structures with curved cross-sections.

The experimental and numerical results coincide well, but presented minor differences. These are due to the shrinkage during cooling down of the material after vacuum forming, and due to nonlinearities of the material. Inaccuracies that are introduced by handicraft production and the test setup are not visible for the eye and therefore negligible.

## ACKNOWLEDGEMENT

The authors would like to acknowledge the conceptual contribution of Hyperbody at Delft University of Technology, and the Department of Structural Engineering. The authors would also like to acknowledge STW (HTSM-2012 12814: ShellMech) for the financial support of this project.

## REFERENCES

- [1] H. Bier and T. Knight, "Digitally-Driven Architecture," *Footprint*, no. 6, pp. 1–4, 2010.
- [2] V. K. Wadhawan, "Smart structures: blurring the distinction

- between the living and the nonliving,” *Monogr. Phys. Chem. Mater.*, 2007.
- [3] C. M. J. L. Lelieveld, “Smart Materials For The Realization Of An Adaptive Building Component.” TU Delft, PhD Thesis, Delft University of Technology, 08-Feb-2013.
- [4] Z. Drozdowski, “The Adaptive Building Initiative: The Functional Aesthetic of Adaptivity,” *Archit. Des.*, vol. 81, no. 6, pp. 118–123, Nov. 2011.
- [5] R. C. G. M. Loonen, M. Trčka, D. Cóstola, and J. L. M. Hensen, “Climate adaptive building shells: State-of-the-art and future challenges,” *Renew. Sustain. Energy Rev.*, vol. 25, pp. 483–493, Sep. 2013.
- [6] T. Bein, J. Bös, L. Kurtze, and T. Doll, “Noise Insulation applying Active Elements onto Facades,” *Forum Acusticum, Budapest*, 2005.
- [7] P. Teuffel, “From adaptive to high-performance structures,” *ISSS 2011: 6th International Symposium on Steel Structures, Seoul, Korea, 3-5- November 2011*. Korean Society of Steel Construction (KSSC), 03-Nov-2011.
- [8] S. Yiannoudes, “Kinetic Digitally-Driven Architectural Structures as ‘ Marginal ’ Objects - a Conceptual Framework,” *Footprint*, no. 6, pp. 41–54, 2010.
- [9] K. Oosterhuis and G. Joosen, “Barrier in Motion,” *IA#5 - Robotics in Architecture - All titles - Jap Sam Books*, 2013. [Online]. Available: <http://www.japsambooks.nl/en/books/all-titles/ia-5-robotics-in-architecture/101>. [Accessed: 18-Jul-2015].
- [10] M. Hosale and C. Kievid, “Modulating territories, penetrating boundaries,” *Footprint*, no. 6, pp. 55–67, 2010.
- [11] Larry L. Howell, *Compliant Mechanisms*. Wiley, 2002.
- [12] B. P. Trease, Y.-M. Moon, and S. Kota, “Design of Large-Displacement Compliant Joints,” *J. Mech. Des.*, vol. 127, no. 4, p. 788, Jul. 2005.
- [13] H. Alkisaie, G. Radaelli, J. L. Herder, H. Bier, and L. J. Sluys, “Design of Large-Scale Compliant and Monolithic Gravity Balancers as Deformable Walls,” MSc Thesis, Delft University of Technology, 2016.
- [14] J. Luo, Z. Luo, S. Chen, L. Tong, and M. Y. Wang, “A new level set method for systematic design of hinge-free compliant mechanisms,” *Comput. Methods Appl. Mech. Eng.*, vol. 198, no. 2, pp. 318–331, 2008.
- [15] J. A. Gallego Sanchez, “Statically Balanced Compliant Mechanisms,” PhD Thesis, Delft University of Technology, 2013.
- [16] A. Gopalswamy, P. Gupta, and M. Vidyasagar, “A new parallelogram linkage configuration for gravity compensation using torsional springs,” in *Proceedings 1992 IEEE International Conference on Robotics and Automation*, pp. 664–669.
- [17] V. Arakelian and S. Ghazaryan, “Improvement of balancing accuracy of robotic systems: Application to leg orthosis for rehabilitation devices,” *Mech. Mach. Theory*, vol. 43, no. 5, pp. 565–575, May 2008.
- [18] A. H. A. Stienen, E. E. G. Hekman, F. C. T. Van der Helm, G. B. Prange, M. J. A. Jannink, A. M. M. Aalsma, and H. Van der Kooij, “Freebal: dedicated gravity compensation for the upper extremities,” in *2007 IEEE 10th International Conference on Rehabilitation Robotics*, 2007, pp. 804–808.
- [19] “InteSpring Home.” [Online]. Available: <http://www.intespring.nl/>. [Accessed: 21-Jul-2015].
- [20] B. L. Rijff, J. L. Herder, and G. Radaelli, “An Energy Approach to the Design of Single Degree of Freedom Gravity Balancers With Compliant Joints,” in *Volume 6: 35th Mechanisms and Robotics Conference, Parts A and B*, 2011, pp. 137–148.
- [21] F. te Riele and J. Herder, “Perfect static balance with normal springs,” in *ASME 2001 Design Engineering Technical Conferences and Computers and Information in Engineering Conference*, 2001, pp. 9 – 12.
- [22] R. Barents, M. Schenk, W. D. van Dorsser, B. M. Wisse, and J. L. Herder, “Spring-to-Spring Balancing as Energy-Free Adjustment Method in Gravity Equilibrators,” *J. Mech. Des.*, vol. 133, no. 6, p. 061010, Jun. 2011.
- [23] G. Radaelli and J. L. Herder, “Isogeometric Shape Optimization for Compliant Mechanisms With Prescribed Load Paths,” in *Volume 5A: 38th Mechanisms and Robotics Conference, Buffalo, New York*, 2014.
- [24] G. Radaelli and J. L. Herder, “A Monolithic Compliant Large-Range Gravity Balancer,” *14th World Congr. Mech. Mach. Sci., Taipei, Taiwan*, pp. 25–30, 2015.
- [25] K. A. Seffen and S. Pellegrino, “Deployment dynamics of tape springs,” *Proc. R. Soc. A Math. Phys. Eng. Sci.*, vol. 455, no. 1983, pp. 1003–1048, Mar. 1999.
- [26] M. E. Peterson and T. W. Murphey, “Large Deformation Bending of Thin Composite Tape Spring Laminates,” in *54th AIAA/ASME/ASCE/AHS/ASC Structures, Structural Dynamics, and Materials Conference*, 2013.
- [27] E. Kebabze, S. . Guest, and S. Pellegrino, “Bistable prestressed shell structures,” *Int. J. Solids Struct.*, vol. 41, no. 11–12, pp. 2801–2820, Jun. 2004.
- [28] S. Pellegrino, “Bistable shell structures,” in *46th AIAA/ASME/ASCE/AHS/ASC Structures, Structural Dynamics & Materials Conference*, 2005, pp. 1 – 8.
- [29] A. L. Jennings, J. Black, and A. N. Gutierrez, “Geometry and Moments of Bent Tape Springs,” in *54th AIAA/ASME/ASCE/AHS/ASC Structures, Structural Dynamics, and Materials Conference*, 2013.
- [30] S. Guest, E. Kebabze, and S. Pellegrino, “A zero-stiffness elastic shell structure,” *J. Mech. Mater. Struct.*, vol. 6, no. 1–4, pp. 203–212, Jun. 2011.
- [31] K. A. Seffen, Z. You, and S. Pellegrino, “Folding and deployment of curved tape springs,” *Int. J. Mech. Sci.*, vol. 42, no. 10, pp. 2055–2073, Oct. 2000.
- [32] C. Vehar, S. Kota, and R. Dennis, “Closed-Loop Tape Springs as Fully Compliant Mechanisms: Preliminary Investigations,” in *Volume 2: 28th Biennial Mechanisms and Robotics Conference, Parts A and B*, 2004, pp. 1023–1032.
- [33] “Richtlijnen geluidbeperkende constructies langs wegen - CROW.” [Online]. Available: <http://www.crow.nl/publicaties/richtlijnen-geluidbeperkende-constructies-langs-we>. [Accessed: 06-Sep-2015].
- [34] G. K. Ananthasuresh, A. G. Schache, T. W. Dorn, and M. G. Pandy, “How Far are Compliant Mechanisms from Rigid-body Mechanisms and Stiff Structures?,” *Adv. Mech. Robot. Des. Educ. Res.*, vol. 14, pp. 83–94, 2013.
- [35] T. J. R. Hughes, J. A. Cottrell, and Y. Bazilevs, “Isogeometric analysis: CAD, finite elements, NURBS, exact geometry and mesh refinement,” *Comput. Methods Appl. Mech. Eng.*, vol. 194, no. 39–41, pp. 4135–4195, Oct. 2005.
- [36] A. P. Nagy, S. T. Ijsselmuiden, and M. M. Abdalla, “Isogeometric design of anisotropic shells: Optimal form and material distribution,” *Comput. Methods Appl. Mech. Eng.*, vol. 264, pp. 145–162, Sep. 2013.
- [37] A. P. Nagy, M. M. Abdalla, and Z. Gürdal, “Isogeometric sizing and shape optimisation of beam structures,” *Comput. Methods Appl. Mech. Eng.*, vol. 199, no. 17–20, pp. 1216–1230, Mar. 2010.





Appendix A  
Theoretical





## A1. POTENTIAL ENERGY [1], [2]

The potential energy of a mechanical system can be described as the capacity to do a task with respect to its purpose or configuration. The curve of the potential energy is similar to the hill topography in the ball-on-the-hill analogy.

If a system has no acceleration, it is then said to be in a state of equilibrium. This state of equilibrium is said to be stable when a small external disturbance only causes oscillations about the equilibrium state. On the other hand, if a small external disturbance causes the system to diverge from its equilibrium, then the equilibrium state is said to be unstable. However, if the system stays in the disturbed position, the equilibrium state is said to be neutral.

**Figure A1.1** explains the latter visually. The ball in position A is resting in a stable equilibrium. If the ball is shifted by a small amount, it then tends to return to position A or oscillate around it. On the other hand, position B represents an unstable equilibrium. If the ball is shifted with a small amount, it will diverge from its equilibrium position and move to a different position. The third position, position C, is similar to position A. The last position, which is position D, represents neutral stability. Any disturbance in position D will cause the ball to move to its disturbed position only.

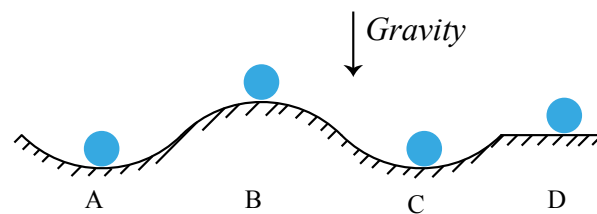


**Figure A1.1:** 'Ball on the hill' analogy.

Mechanisms can also be designed with these different potential energy characteristics. When a mechanism consists of one stable position, it merely has one local minimum in its energy graph, see Figure A1.2B. By adding a mechanical stop in the energy graph, one may create two stable positions, Figure A1.2A.

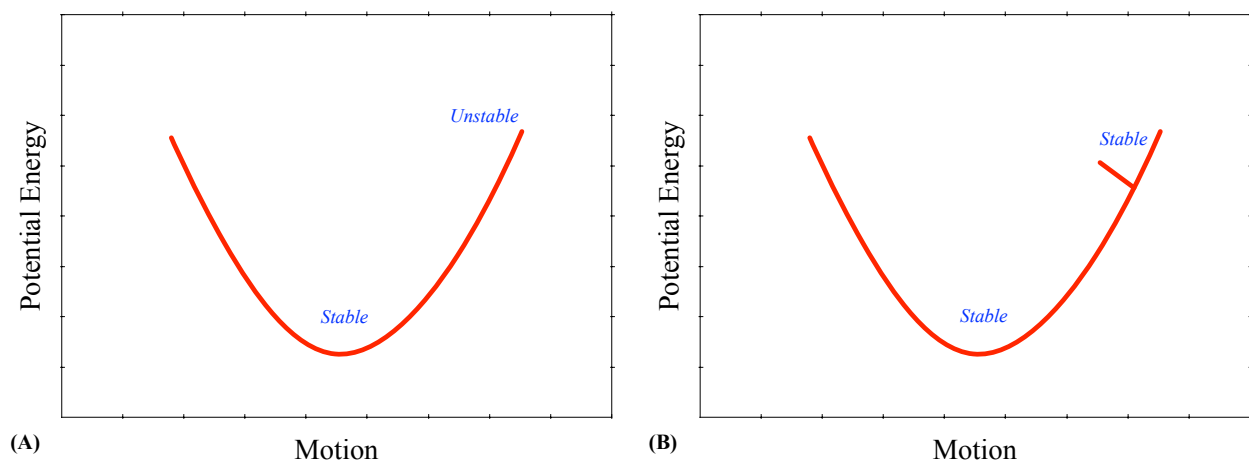


**Figure A1.2:** Energy graphs of one-stable mechanisms. (A) has only one stable position, (B) has two stable positions due to an additional mechanical stop.

If a mechanism has two stable equilibrium positions, it is said to be bistable. Since two local minima enclose a local maximum, these two stable positions will have an unstable position in between, see Figure A1.3. Thus, bistable mechanisms will consist of two stable positions and at least one unstable position. Note, the two stable positions in Figure A1.3 can have different levels in relation to each other. And like in the previous graph, a mechanical stop can also be implemented.

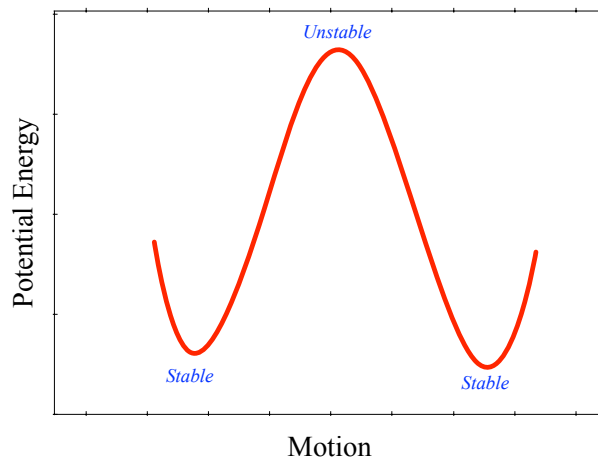


**Figure A1.3:** Energy graph of a bistable mechanism.

Finally, a mechanism can also be represented by a neutrally stable energy graph, see Figure A1.4. The mechanism is stable along the total range of motion.

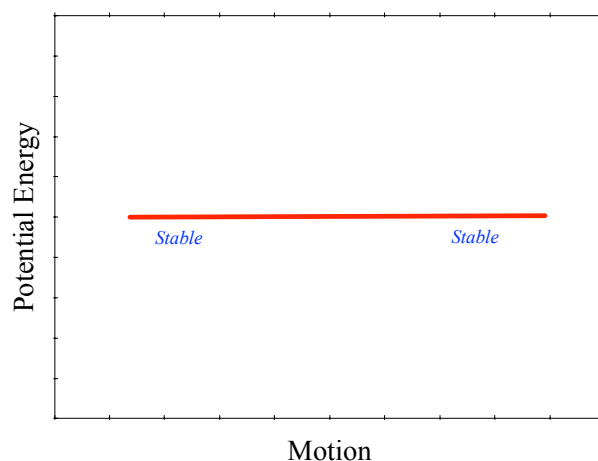


**Figure A1.4:** Energy graph of a neutrally stable mechanism.

Ultimately, the energy method that is based on the Lagrange-Dirichlet theorem states as well that at each local minimum in the potential energy a stable equilibrium occurs.

## A2. STATIC BALANCING [3]

Mechanisms that are statically balanced are also known as energy-free systems. The forces on these mechanisms are balanced or in a state of static equilibrium along the total range of motion. Consequently, the quasi-static operation of such mechanisms becomes therefore effortless. Typical applications of static balancing are the spring-to-spring balancer, the gravity balancer and the sliding balancer. Next, the spring-to-spring balancer is presented in further detail to give a clear explanation of static balancing.

A spring-to-spring zero stiffness balancer is a linkage with one degree-of-freedom composed of a rigid link hinged at one end, while having two springs attached along its body to the other end, see Figure A2.1. All members of this mechanism are pin-jointed. The used springs are zero-free-length springs, which mean that their elongation is equal to their lengths.

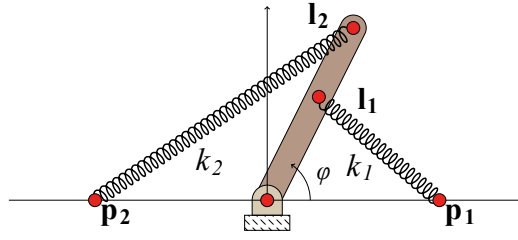


Figure A2.1: Spring-to-spring balancer [3].

The state of static balancing, for the spring-to-spring balancer, is guaranteed when the following condition is hold:

$$k_1 l_1 p_1 = -k_2 l_2 p_2 \quad (\text{A2.1})$$

Next, some general mathematical expressions are presented to show the static balancing conditions for the spring-to-spring balancer.

### A2.1. THE POTENTIAL ENERGY

The total elastic potential energy  $U$  that is stored by spring 1 and 2 in the mechanism is given by:

$$U = \frac{1}{2} k_1 (\mathbf{l}_1 - \mathbf{p}_1)^2 + \frac{1}{2} k_2 (\mathbf{l}_2 - \mathbf{p}_2)^2 \quad (\text{A2.2})$$

If we replace the vectors  $\mathbf{l}$  and  $\mathbf{p}$  by their coordinates in terms of rotation angle phi, we obtain:

$$U = \frac{1}{2} k_1 (l_1^2 - 2l_1 p_1 \cos \varphi + p_1^2) - \frac{1}{2} k_2 (l_2^2 - 2l_2 p_2 \cos \varphi + p_2^2) \quad (\text{A2.3})$$

Substituting Eq. (A2.1) into Eq. (A2.3) we obtain:

$$U = \frac{1}{2} k_1 (l_1^2 - 2l_1 p_1 \cos \varphi + p_1^2) - \frac{1}{2} \frac{k_1 l_1 p_1}{l_2 p_2} (l_2^2 - 2l_2 p_2 \cos \varphi + p_2^2) \quad (\text{A2.4})$$

Rearranging the terms yields:

$$U = \frac{1}{2} k_1 \left( l_1^2 + p_1^2 - \frac{l_1 l_2 p_1}{p_2} - \frac{l_1 p_1 p_2}{l_2} \right) \quad (\text{A2.5})$$

Eq. (A2.5) proves that the total potential energy is constant and does not depend on the link's orientation angle  $\varphi$ .

## A2.2. THE FORCE

To force is computed by taking the derivative of the total potential energy with respect to the corresponding degree-of-freedom, see Eq. (A2.6) and Eq. (A2.7).

$$F(x) = \frac{\partial U}{\partial x} \quad (\text{A2.6})$$

$$M(\varphi) = \frac{\partial U}{\partial \varphi} \quad (\text{A2.7})$$

By taking the derivative of Eq. (A2.3), we obtain the required external moment to keep the link in static equilibrium:

$$M_\varphi = \frac{dU}{d\varphi} = k_1 l_1 p_1 \sin \varphi + k_2 l_2 p_2 \sin \varphi \quad (\text{A2.8})$$

Implementing Eq. (A2.1) once again, we obtain:

$$M_\varphi = \frac{dU}{d\varphi} = k_1 l_1 p_1 \sin \varphi - k_1 l_1 p_1 \sin \varphi = 0 \quad (\text{A2.9})$$

The latter proves that there is no external force required to keep the mechanism in static equilibrium at any point along its range of motion. This is due to the fact that the potential energy is constant along the entire range of motion, and the internal forces are continuously kept in static equilibrium.

## A2.3. THE STIFFNESS

The stiffness is computed by taking the second derivative of the total potential energy with respect to the corresponding degree-of-freedom, see Eq. (A2.10) and Eq. (A2.11).

$$K(x) = \frac{\partial^2 U}{\partial x^2} \quad (\text{A2.10})$$

$$K(\varphi) = \frac{\partial^2 U}{\partial \varphi^2} \quad (\text{A2.11})$$

In case of the spring-to-spring balancer we apply Eq. (A2.11) and obtain:

$$K_\varphi = \frac{d^2 U}{d\varphi^2} = k_1 l_1 p_1 \cos \varphi + k_2 l_2 p_2 \cos \varphi \quad (\text{A2.12})$$

Once again applying Eq. (A2.1) we obtain:

$$K_\varphi = \frac{d^2 U}{d\varphi^2} = k_1 l_1 p_1 \cos \varphi - k_1 l_1 p_1 \cos \varphi = 0 \quad (\text{A2.13})$$

Thus, the latter proves that the stiffness of the system becomes zero. This implies that under the same condition, the system does not only have zero stiffness, but is also neutrally stable. The next figure presents, for the completeness of this section, the behaviour of the spring's energy functions with respect to the corresponding degree-of-freedom.

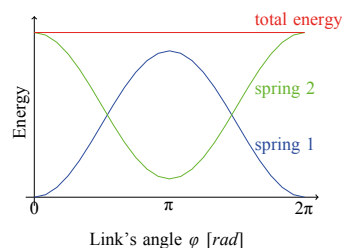


**Figure A2.2:** Energy graphs of the different springs. Added up lead to a constant energy path [3].

It is important to highlight an important aspect regarding the definitions of zero stiffness and neutral stability in static balancing. There is a subtle difference between the two definitions, yet quite meaningful. To guarantee the state of static balancing, zero stiffness is necessary but not sufficient. This is due to the fact that zero stiffness is also a necessary condition for systems with constant force. Meaning that zero stiffness does not imply that a mechanism is in equilibrium. Neutral stability, on the other hand, is a necessary and sufficient condition to guarantee a state of static balancing. Thus, neutral stability implies zero stiffness and equilibrium.

#### A2.4. GRAVITY BALANCER

For the Barrier in Motion it is more applicable to use a gravity balancing mechanism. The idea of gravity balancing is to compensate the weight of a mechanism in order to achieve an effortless actuation when no payload is present. Several designs are based on the use of external springs and/or stationary centres of gravity, see Figure A2.3.

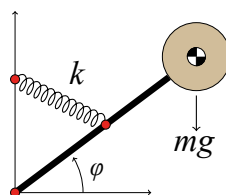


**Figure A2.3:** Gravity balancer [3].

As like for the spring-to-spring balancer, it is possible to set up equations and conditions that can lead to a statically balanced gravity balancer.

### A3. COMPLIANT MECHANISMS [1]

Mechanical devices are mechanisms that transfer or transform motion, force or energy. These consist, traditionally, of rigid links connected at movable joints. The energy of a mechanism is, for instance, transferred from the input to the output, while conserving the energy between the in- and output. This may lead to a much larger output force than at the input force. However, the output displacement will be much smaller than the input displacement.

Compliant mechanisms are also designed to transfer or transform motion, force, or energy. Yet, they gain their mobility from the deflection of flexible members rather than from movable joints like the ones from rigid-links mechanisms.

The main advantages of compliant mechanisms can be divided in two categories: cost reduction and increased performance. For the first category one may think of part-count reduction, reduced assembly time and simplified manufacturing processes. The second category incorporates increased precision, increased reliability, reduced wear, reduced weight, and reduced maintenance.

Compliant mechanisms have the potential to reduce the total number of required parts to accomplish a specific task dramatically. Some mechanisms can even be manufactured in monolithic manner. Consider for instance the mechanism shown in Figure A3.1. This figure depicts a pseudo-rigid-body and a compliant design of the same mechanism. There are considerably fewer components required for the compliant mechanism than for the rigid mechanism. Thus, reducing manufacturing, assembly time and cost.

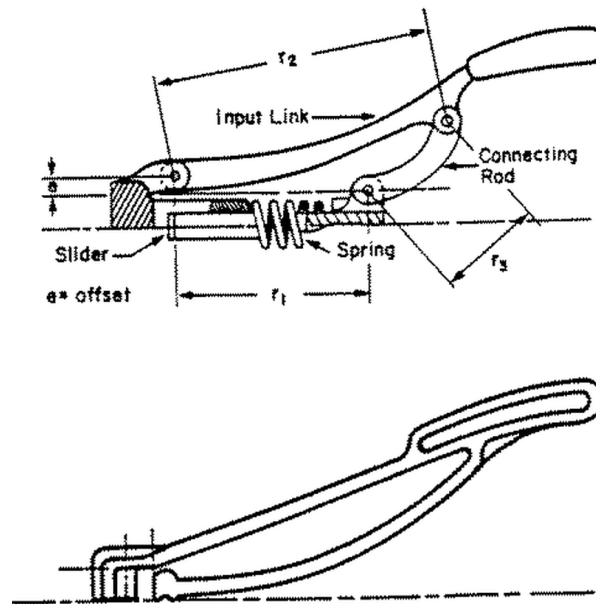


**Figure A3.1:** Rigid body model and its compliant model. (<https://compliantmechanisms.byu.edu/content/intro-compliant-mechanisms>).

The reduction of movable joints leads also to reduced wear and need for lubrication. This is especially desirable for applications in which certain mechanisms are not easily accessible, or for applications in harsh environments that may affect the joints.

In addition, reduced number of joints also increases mechanism precision, since backlash can be reduced or eliminated. On a small scale, it also reduces vibration and noise.

Also, using compliant mechanisms can reduce the weight significantly in comparison with rigid-body counterparts. This might be desirable in aerospace and other applications for instance.

Strain energy is stored in the flexural members of compliant mechanisms due to the deflection of these members. The effects of springs can be integrated into a compliant mechanism's design, since this stored strain energy is similar to the strain energy in a deflected spring. Meaning that the stored energy can be released at a later time or in a different manner.

Besides the advantages, compliant mechanisms do also present several challenges and disadvantages. The largest challenge is, perhaps, the relative difficult analysis and design process of compliant mechanisms. It is therefore required to have a proper knowledge of mechanism analysis, synthesis methods and the deflection of flexible members. It does not only require the understanding of the combination of these fields, but also an understanding of their interaction in complex situations. For instance, linearised beam equations are no longer valid, since many of the flexible members undergo large deflections. This forces designers to use nonlinear equations that account for geometric nonlinearities caused by large deformations.

The motion that results from the deflection of the compliant links is also limited by the strength of these deflecting members. Moreover, a continuous rotational motion such as possible with a pin joint cannot be produced by a compliant link.

The storage of energy in flexural members can also be disadvantageous in some applications. For example, not all of the energy might be transferred from the input to the output to the output, due to the fact that some energy is stored in the mechanism.

Fatigue analysis can also be more vital for compliant mechanisms than for rigid-body counterparts, since compliant members are often loaded cyclically. It is therefore important to design those members in such a way that they have sufficient fatigue life to perform their prescribed functions.

Furthermore, compliant links that are exposed to stress for long periods of time, or high temperatures, might experience stress relaxation or creep. Such phenomenon could influence the functionality of the mechanisms as well.

It is therefore helpful to have knowledge of such manner in order to determine which application will benefit most by use of compliant mechanism technology.

#### A4. SCALE AND GRAVITY CONTRIBUTION [4]

This section will describe important considerations that should be taken into account during weight balancing, since the volume, density, and gravity will have major influences on the total behaviour of the system.

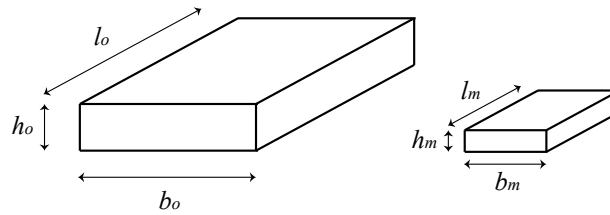


**Figure A4.1:** The original and scaled version of a three-dimensional rectangle.

The index  $o$  refers to the original scale. The index  $m$  refers to the model and scaled version of the original. The geometrical scale factor  $S_l$  between these two is defined as

$$S_l = \frac{l_m}{l_o} = \frac{b_m}{b_o} = \frac{h_m}{h_o}. \quad (\text{A4.1})$$

If  $S_l < 1$ , then it means that the model is smaller than the original geometry. On the other hand, if  $S_l > 1$ , then the model is larger than the original. Besides the geometrical scale factor, there exist also scale factors for time, speed, acceleration, mass, force, stress, pressure, energy, density, etcetera.

##### A4.1. STATIC SCALE LAWS

Consider the following figure.

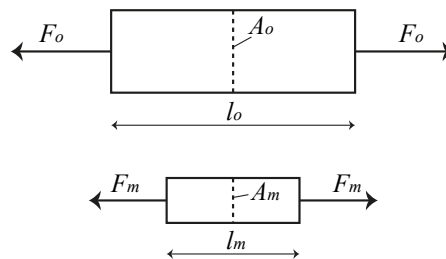


**Figure A4.2:** Scaling for applied forces.

When the length of the specimen is proportionally changed, we could write the following scale factor

$$S_l = \frac{l_m}{l_o}. \quad (\text{A4.2})$$

An arbitrary cross-section  $A$  would then change with

$$S_A = S_l^2. \quad (\text{A4.3})$$

The force and area stress would then be

$$S_F = \frac{F_m}{F_o}, \quad (\text{A4.4})$$

$$S_\sigma = \frac{S_F}{S_A} = \frac{S_F}{S_l^2}. \quad (\text{A4.5})$$

Keeping the occurring stress in the material the same means that  $S_\sigma=1$ . This can only be realized when  $S_F=S_l^2$ .

### A4.2. GRAVITY CONTRIBUTION

If a body is merely exerted to its own weight, then the contribution of earth gravity is proportional to the volume and thus to  $l^3$ . Furthermore, the gravity is also proportional to the density  $\rho$  and earth's acceleration  $g$ , which leads to  $S_F=S_g S_\rho S_l^3$ . Thus, the material stress scale factor can now be written as

$$S_\sigma = \frac{S_F}{S_l^2} = \frac{S_g S_\rho S_l^3}{S_l^2} = S_g S_\rho S_l. \quad (\text{A4.6})$$

In most cases will  $S_g$  be equal to 1. On the other hand, if the material density also stays the same, then the latter will reduce to

$$S_\sigma = S_l \quad (\text{A4.7})$$

Thus, equally formed structures that are exerted to self-weight, will experience stress change proportional to the geometrical change.

### A4.3. STIFFNESS

The stiffness of a structure can play a major role in the design process. This requires therefore a thorough understanding of the contribution of stiffness due to geometrical change. Let us consider Hooke's Law:

$$\varepsilon = \frac{\Delta l}{l} = \frac{\sigma}{E} = \frac{F}{AE} \quad (\text{A4.8})$$

in which  $\sigma$  is the material stress,  $E$  the elasticity modulus,  $F$  the applied force and  $A$  the stressed area. Thus, the stiffness  $c$  is caused by the applied force  $F$  and the deformation due to that force:

$$c = \frac{F}{\Delta l} = \frac{AE}{l}. \quad (\text{A4.9})$$



---


Incorporating this for scale change we obtain the following:

$$S_c = \frac{S_A S_E}{S_l} = \frac{S_l^2 S_E}{S_l} = S_l S_E. \quad (\text{A4.10})$$

Thus, if the material stays the same (same  $E$ ), the structure becomes proportionally stiffer due to geometrical change.

In case of the monolithic designs that are considered in the research of statically balanced sound barriers, it is important to realize the existing trade-off between the stiffness and the contribution of gravity to the system. Especially since the contribution of gravity is cubical  $S_F = S_l^3$  and the contribution of the stiffness linear  $S_c = S_l$ .





Appendix B  
Numerical



## B1. STRUCTURAL OPTIMIZATION [3]

In structural optimization are searches for the most desirable arrangement of parts under specific conditions carried out. This is done with the aid of optimization and search techniques. For compliant mechanisms, for instance, are these techniques used to obtain designs (topology, shapes and dimensions) that satisfy a certain objective function for a set of parameters and constraints.

Functions that are being minimized are called the objective functions. The variables in the functions are referred to as design variables and the domain of the design variables is known as the search space. Thus, the formulation of an optimization procedure contains the objective function  $f(\mathbf{x})$ , the  $p$  equalities  $h_i$ , the  $m$  inequalities  $g_j$ , the  $n$  design variables  $\mathbf{x}$  and the search space  $\Omega$ . The design variables  $x_1, x_2, \dots, x_n$  are normally clustered into the design vector  $\mathbf{x}$ .

$$\begin{aligned} & \min_{\mathbf{x} \in \Omega} f(\mathbf{x}) \\ & \text{subject to} \\ & \quad h_i(\mathbf{x}) = 0 \quad i = 1, 2, \dots, p \\ & \quad g_j(\mathbf{x}) \leq 0 \quad i = 1, 2, \dots, m \\ & \text{where} \\ & \quad \mathbf{x} = [x_1 \ x_2 \ \dots \ x_n] \end{aligned}$$

### B1.1. TOPOLOGY OPTIMIZATION

The first goal in structural optimization is to obtain the topology. The topology is a certain branch within mathematics that investigates how the properties of a certain space are preserved or changed when it is subjected to deformations. The topology can be defined as the connectivity of small elements with their neighbours. If the connections between the elements remain, then the topology is not affected. However, when a hole is introduced, there are connections that need to be broken, which means that the topology is adjusted. The next figure depicts an example of a topology with certain functionality. Thus, topology optimization refers to the process of finding the topology, or connectivity among constitutive elements, that satisfy the objective function best.

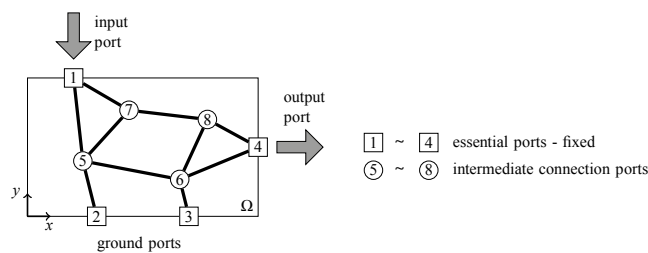


Figure B1.1: Topology optimization [3].

### B1.2. SHAPE OPTIMIZATION

The second goal in structural optimization is to obtain the shape. During shape optimization are the shapes of the constitutive elements altered and investigated. An example is given in Figure B1.2. Thus, shape optimization procedures refer to the process of finding the optimal shapes of the contour or surface that satisfy the objective function in a fixed topology best.

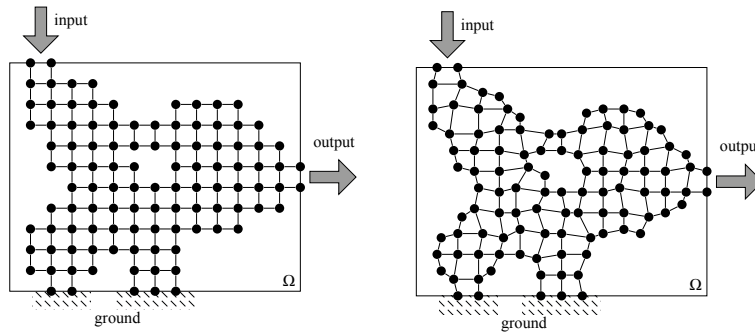


Figure B1.2: Shape optimization [3].

### B1.3. SIZE OPTIMIZATION

The third goal in structural optimization is to obtain the size of the constitutive elements. The design variables in this case is the sizing variables or the variables that define the dimensional properties of a model, i.e. thickness, cross sections, radii, diameters and so on. At this stage, the topology and the shape of the model are already defined. In Figure B1.3 is an example given of a size optimization with fixed topology.

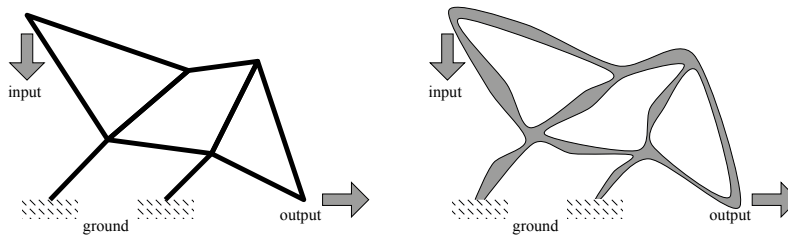


Figure B1.3: Size optimization [3].

## B2. ISOGEOMETRIC ANALYSIS [5]

A fundamental step in breaking the barriers down between engineering design and analysis is by focusing on one, and only one, geometric model that can be used directly as an analysis model, or a model which can be adjusted geometrically. This demanded the classical Finite Element Analysis to change to an analysis procedure based on CAD representations: the Isogeometric Analysis.

### B2.1. NURBS

The most widely used computational geometry technology in isogeometric analysis is NURBS (Non-Uniform Rational B-Splines). These are convenient for free form surface modelling, can exactly represent conic sections, and there are multiple efficient and numerically stable algorithms that generate NURBS geometries. In contrast with Finite Elements are the basis functions in NURBS usually not interpolatory. NURBS have two meshes: the control mesh and the physical mesh, Figure B2.1. The control points are used to define the control mesh, while the control mesh interpolates the control points. The control mesh is consisting of multilinear elements that are bilinear quadrilateral in two dimensions and trilinear hexahedra in three dimensions. Note, the control mesh does not conform the actual geometry. The control variables of the control polygon are the degrees-of-freedom and are located at the control points.

The physical mesh is a representation of the actual geometry. The physical mesh consists of patches and knot spans. The patches can be seen as macro-elements or subdomains. The knots are points, lines, and surfaces in one-, two- and three-

dimensional topologies, respectively. The knot spans are the smallest entities that are dealt with in isogeometric analysis approaches.

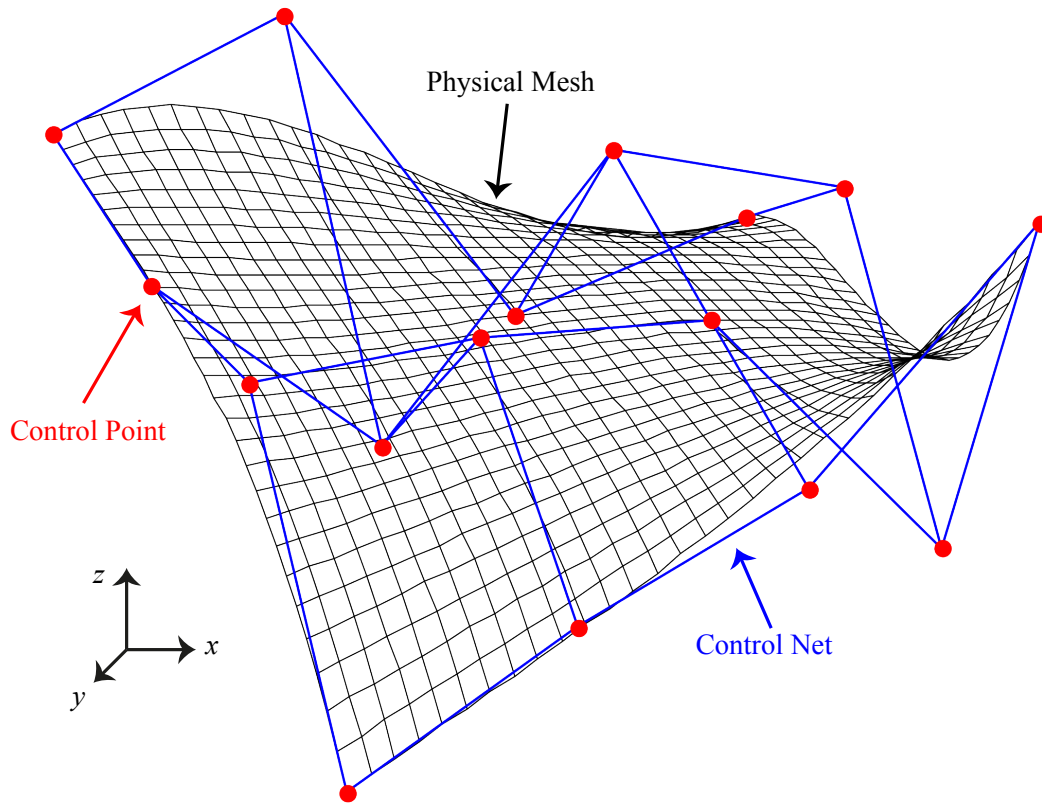


**Figure B2.1:** The control and physical mesh ([http://blogs.embarcadero.com/files/2012/04/beziersurface2000px\\_5857.png](http://blogs.embarcadero.com/files/2012/04/beziersurface2000px_5857.png)).

### B2.1.1. KNOT VECTORS

A knot vector is a set of coordinates in one dimension in the parameter space, written as  $\Xi = \{\xi_1, \xi_2, \dots, \xi_{n+p+1}\}$ , where  $\xi_i$  (element of Real space) is the  $i^{th}$  knot,  $i$  is the knot index,  $i = 1, 2, \dots, n+p+1$ ,  $p$  is polynomial order, and  $n$  is the number of the basis functions used to construct the B-Spline curve. The knots simply subdivide the parameter space into elements. Furthermore, the element boundaries are basically the images of knot lines under the B-Spline mapping in the physical space. The functions of the B-Splines are piecewise polynomials where the different pieces are joined along the knot lines.

Knot vectors are said to be uniform when knots are equally spaced in the parameter space. On the other hand, they are said to be non-uniform when the knots are unequally spaced. Also, a knot vector is known as to be open if the first and last knot values appear  $p+1$  times.

### B2.1.2. B-SPLINES

The B-Spline basis functions are defined recursively by starting with piecewise constants ( $p = 0$ ):

$$N_{i,0}(\xi) = \begin{cases} 1 & \text{if } \xi_i \leq \xi < \xi_{i+1}, \\ 0 & \text{otherwise.} \end{cases} \quad (\text{B2.1})$$

And for  $p=1,2,3,\dots,n$ , the basis functions are defined by

$$N_{i,p}(\xi) = \frac{\xi - \xi_i}{\xi_{i+p} - \xi_i} N_{i,p-1}(\xi) + \frac{\xi_{i+p+1} - \xi}{\xi_{i+p+1} - \xi_{i+1}} N_{i+1,p-1}(\xi). \quad (\text{B2.2})$$

The important properties of B-Spline basis functions are:

1. They constitute a partition of unity, which means, for all  $\xi$

$$\sum_{i=1}^n N_{i,p}(\xi) = 1 \quad (\text{B2.3})$$

2. The support of each  $N_{i,p}$  is compact and contained in the interval  $[\xi_i, \xi_{i+p+1}]$
3. Each basis function is non-negative, which means,  $N_{i,p}(\xi) \geq 0$  for all  $\xi$ . Thus, all of the coefficients of a mass matrix computed from a B-Spline basis are greater than, or equal to, zero.

The B-Spline curves are in Real dimensions constructed by taking a linear combination of B-Spline basis functions. The valued coefficients of the vector of basis functions are referred to as control points. If we have  $n$  functions,  $N_{i,p}$ ,  $i = 1, 2, \dots, n$ , and corresponding control points  $\mathbf{B}_i$  (element of Real dimensions),  $i=1, 2, \dots, n$ , a piecewise-polynomial B-Spline curve is then given by

$$C(\xi) = \sum_{i=1}^n N_{i,p}(\xi) \mathbf{B}_i. \quad (\text{B2.4})$$

The next figure depicts a piecewise quadratic B-Spline in two-dimensional space. The red dots  $\bullet$  represent the control points, once again. The blue and black lines represent the B-Spline curve and the control polygon, respectively.

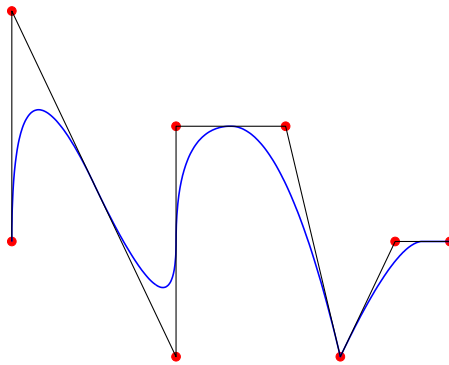


**Figure B2.2:** Piecewise quadratic B-spline [5].

Important properties of B-Spline curves are:

1. They have continuous derivatives of order  $p-1$  in the absence of repeated knots or control points.
2. If a knot or a control point is repeated  $k$  times, then it decreases the continuous derivatives by  $k$ .
3. Affine transformations of B-Spline curves are obtained by applying the transformation to the control points.

A new knot can always be inserted without changing a curve geometrically or parametrically. This is also known as  $h$ -refinement, see Figure B2.3. Furthermore, the polynomial order of the basis functions can be increased without changing the geometry or parametrization of a curve. This is known as  $p$ -refinement. A third procedure is known as  $k$ -refinement. This procedure only inserts a unique knot after the original curve polynomial is elevated with a certain value. Using the latter procedure leads to a more superior approach for high precision than  $p$ -refinement.



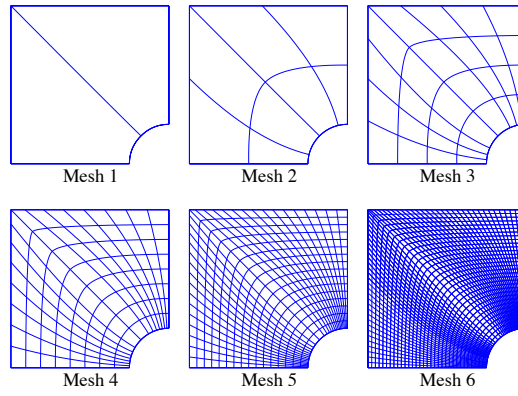


Figure B2.3:  $h$ -refinement [5].

### B2.1.3. B-SPLINE SURFACES

A control net is given by  $\{B_{i,j}\}$ ,  $i=1,2,\dots,n, j=1,2,\dots,m$ , with knot vectors  $\Xi = \{\xi_1, \xi_2, \dots, \xi_{n+p+1}\}$ , and  $H = \{\eta_1, \eta_2, \dots, \eta_{m+q+1}\}$ , the tensor product of a B-Spline surface is defined by:

$$S(\xi, \eta) = \sum_{i=1}^n \sum_{j=1}^m N_{i,p}(\xi) M_{j,q}(\eta) B_{i,j} \quad (B2.5)$$

where  $N_{i,p}$  and  $M_{j,q}$  are the basis functions of the B-spline curves.

### B2.1.4. B-SPLINE SOLIDS

The tensor product of B-spline solids is analogously defined to B-spline surfaces. A control net is given by  $\{B_{i,j,k}\}$ ,  $i=1,2,\dots,n, j=1,2,\dots,m, k=1,2,\dots,l$ , and knot vectors are given by  $\Xi = \{\xi_1, \xi_2, \dots, \xi_{n+p+1}\}$ ,  $H = \{\eta_1, \eta_2, \dots, \eta_{m+q+1}\}$ , and  $Z = \{\zeta_1, \zeta_2, \dots, \zeta_{l+r+1}\}$ . Thus, a B-spline solid is defined by

$$S(\xi, \eta) = \sum_{i=1}^n \sum_{j=1}^m \sum_{k=1}^l N_{i,p}(\xi) M_{j,q}(\eta) Z(\zeta) B_{i,j} \quad (B2.6)$$

### B2.1.5. RATIONAL B-SPLINES

The projective transformation of a B-spline gives a rational polynomial of the form  $f/g$ , where  $f$  and  $g$  are piecewise polynomials. A rational B-spline in Real dimensions is constructed as follows. Let  $\{B_i^w\}$  be a set of control points for a B-spline curve in Real dimension+1 with knot vector  $\Xi$ . These are also known as the ‘projective’ control points for the desired NURBS curve in Real dimension. The following relations derive these control points:

$$(B_i)_j = (B_i^w)_j / w_i, \quad j = 1, \dots, d, \quad (B2.7)$$

$$w_i = (B_i^w)_{d+1} \quad (B2.8)$$

where  $(B_i)_j$  is the  $j^{th}$  component of the vector  $B_i$ , and  $w_i$  is referred to as the  $i^{th}$  weight.

The rational basis functions and NURBS are given by

$$R_i^p(\xi) = \frac{N_{i,p}(\xi)w_i}{\sum_{i=1}^n N_{i,p}(\xi)w_i}, \quad (\text{B2.9})$$

$$C(\xi) = \sum_{i=1}^n R_i^p(\xi)B_i \quad (\text{B2.10})$$

The rational surfaces and solids are defined in terms of rational basis functions as follows

$$R_{i,j}^{p,q}(\xi,\eta) = \frac{N_{i,p}(\xi)M_{j,q}(\eta)w_{i,j}}{\sum_{i=1}^n \sum_{j=1}^m N_{i,p}(\xi)M_{j,q}(\eta)w_{i,j}}, \quad (\text{B2.11})$$

$$R_{i,j,k}^{p,q,r}(\xi,\eta,\zeta) = \frac{N_{i,p}(\xi)M_{j,q}(\eta)Z_{k,r}(\zeta)w_{i,j,k}}{\sum_{i=1}^n \sum_{j=1}^m \sum_{k=1}^l N_{i,p}(\xi)M_{j,q}(\eta)Z_{k,r}(\zeta)w_{i,j,k}}. \quad (\text{B2.12})$$

The next figure depicts a control net and its corresponding NURBS surface description of a torus.

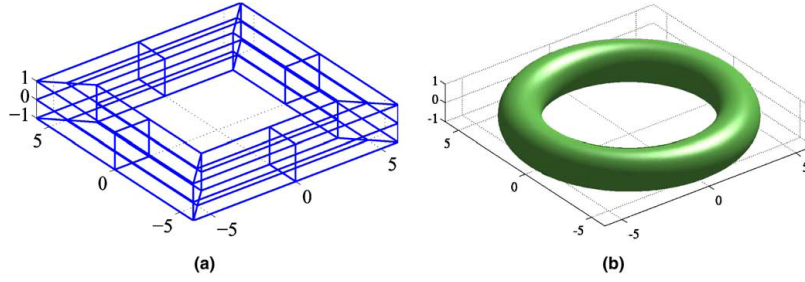


**Figure B2.4:** A torus [5].

Thus, the important properties of NURBS are:

1. NURBS basis functions form a partition unity.
2. The continuity and support of NURBS basis functions are the same as for B-splines.
3. Affine transformations in physical space are obtained by applying the transformation to the control points, which is, NURBS possess the property of affine covariance.
4. If the weights are equal, NURBS become B-splines (i.e. piecewise polynomials).
5. NURBS surfaces and solids are the projective transformations of tensor product, piecewise polynomial entities.

### B3. ELEMENT FORMULATION

#### B3.1. KIRCHHOFF-LOVE PLANAR BEAMS [6]

This approach employs the Kirchhoff-Love plate theory, which is an extension of the Euler-Bernoulli beam theory. It assumes that a two-dimensional mid-surface plane can represent a three-dimensional plate. The kinematic assumptions are as follows:

1. Straight lines that are normal to the mid-surface remain straight after deformation.
2. Straight lines that are normal to the mid-surface remain normal to the mid-surface after deformation.
3. The thickness of the plate does not undergo any change during deformation.

Beam formulations are presented next.

For an arbitrary conservative system we can formulate the total potential energy functional as

$$\Pi = U + T \quad (\text{B3.1})$$

in which  $U$  and  $T$  represent the elastic strain energy stored in the deformed body and the potential energy of applied external forces, respectively. These energy functions of Euler-Bernoulli beam can be written as

$$U(\tilde{\mathbf{u}}) = \frac{1}{2} \int \left[ EA(\lambda - \lambda_0)^2 + EI(\kappa - \kappa_0)^2 \right] ds_0, \quad (\text{B3.2})$$

$$T(\tilde{\mathbf{u}}) = - \int \left[ p_0 \mathbf{n}^T \tilde{\mathbf{u}} + \mathbf{q}_0^T \tilde{\mathbf{u}} \right] ds_0 - \mathbf{f}^T \tilde{\mathbf{u}}, \quad (\text{B3.3})$$

in which  $\mathbf{u}$  represents the continuous displacement field. The terms  $\lambda$  and  $\kappa$  denote the stretch and the curvature of the beam's centroid axis in the deformed configurations, respectively, which are obtained by

$$\lambda = \frac{ds}{ds_0}, \quad (\text{B3.4})$$

$$\kappa = \frac{\dot{\mathbf{r}} \times \ddot{\mathbf{r}}}{\|\dot{\mathbf{r}}\|^3} \cdot \frac{ds}{ds_0}, \quad (\text{B3.5})$$

in which  $ds$ ,  $ds_0$  and  $\mathbf{r}$  represent the initial arch lengths, current arch lengths, and the current configuration, respectively. The dots over the symbols denote successive differentiation with respect to  $\zeta$ , the variable of parametrization. The variables  $p_0$ ,  $\mathbf{q}_0$ ,  $\mathbf{f}$ , and  $\mathbf{n}$ , represent the pressure and distributed loads per unit lengths, the vector of concentrated loads, and the normal vector of the NURBS curve, respectively.

With the implementation of the linear isotropic constitutive law and geometrical non-linear structural response, the derivation of the strain energy function with respect to the vector of degree-of-freedom results in the internal force vector and the stiffness matrix of the following form

$$\mathbf{f}_i(\mathbf{u}) = \frac{\partial U}{\partial \mathbf{u}} = \int \mathbf{D}^T \mathbf{C} \mathbf{G} ds_0, \quad (\text{B3.6})$$

$$\mathbf{K}(\mathbf{u}) = \frac{\partial^2 U}{\partial \mathbf{u}^2} = \int \mathbf{D}^T \mathbf{C} \mathbf{D} ds_0 + \int \left[ EA(\lambda - \lambda_0) \frac{\partial^2 (\lambda - \lambda_0)}{\partial \mathbf{u}^2} + EI(\kappa - \kappa_0) \frac{\partial^2 (\kappa - \kappa_0)}{\partial \mathbf{u}^2} \right] ds_0, \quad (\text{B3.7})$$

with

$$\mathbf{C} = \begin{bmatrix} EA & 0 \\ 0 & EI \end{bmatrix}, \quad (\text{B3.8})$$

$$\mathbf{D} = \begin{bmatrix} \frac{\partial(\lambda - \lambda_0)}{\partial \mathbf{u}} & \frac{\partial(\kappa - \kappa_0)}{\partial \mathbf{u}} \end{bmatrix}^T, \quad (\text{B3.9})$$

$$\mathbf{G} = \begin{Bmatrix} \lambda - \lambda_0 \\ \kappa - \kappa_0 \end{Bmatrix}. \quad (\text{B3.10})$$

A similar approach can be used to obtain the external force vector

$$\mathbf{f}_e(\mathbf{u}) = \frac{\partial T}{\partial \mathbf{u}} = - \int [p_0 \mathbf{R}^T \mathbf{n} + \mathbf{R}^T \mathbf{q}_0] ds_0 - \mathbf{R}^T \mathbf{f}. \quad (\text{B3.11})$$

Note that the internal and external force vectors and the stiffness matrix are computed at knot span level using Gaussian quadrature. The assembly is similar to the procedures employed in standard FEA.

### B3.2. KIRCHHOFF-LOVE SHELLS [7], [8]

As in the previous, the orthogonality of the director field to the mid-surface is enforced and the transverse shear effects are left out in the formulation of Kirchhoff-Love shell theory. The strain energy function  $U$  of Kirchhoff-Love shells is written as

$$U = \frac{1}{2} \int_{\Omega_0} (\mathbf{n} \cdot \boldsymbol{\varepsilon} + \mathbf{m} \cdot \boldsymbol{\rho}) d\Omega_0, \quad (\text{B3.12})$$

with  $\boldsymbol{\varepsilon}$  and  $\boldsymbol{\rho}$  as the relative strain measures, i.e. the membrane and bending strain tensors,  $\mathbf{n}$  and  $\mathbf{m}$  represent the membrane force and bending moment resultant tensors per unit reference length, and  $\Omega_0$  is the reference area of the shell's mid-surface. More, the strain measures are defined as

$$\boldsymbol{\varepsilon} = \varepsilon_{\alpha\beta} \mathbf{G}^\alpha \otimes \mathbf{G}^\beta \quad \text{with} \quad \varepsilon_{\alpha\beta} = \frac{1}{2} (\mathbf{g}_{\alpha\beta} - G_{\alpha\beta}), \quad (\text{B3.13})$$

$$\boldsymbol{\rho} = \rho_{\alpha\beta} \mathbf{G}^\alpha \otimes \mathbf{G}^\beta \quad \text{with} \quad \rho_{\alpha\beta} = \kappa_{\alpha\beta} - K_{\alpha\beta}, \quad (\text{B3.14})$$

in which the kinematic variable  $\mathbf{G}$ ,  $\mathbf{g}$ ,  $\mathbf{K}$  and  $\kappa$  refer to the metric and curvature tensors of the mid-surface in the reference and current configurations, respectively. These fundamental forms are, in the reference configuration, given as

$$G_{\alpha\beta} = \mathbf{G}_\alpha \cdot \mathbf{G}_\beta, \quad (\text{B3.15})$$

$$K_{\alpha\beta} = \mathbf{G}_{\alpha,\beta} \cdot \mathbf{N}, \quad (\text{B3.16})$$

in which  $\mathbf{G}_\alpha = \partial \mathbf{R} / \partial \theta^\alpha$  are known as the covariant basis vectors and the comma indicates partial differentiation with respect to a curvilinear co-ordinate  $\theta^\beta$ .

The covariant basis vectors span the tangent plane  $T_{\mathbf{r}}\Omega_0$  and the dual basis  $\mathbf{G}^\alpha$  is constructed using the standard relation  $\mathbf{G}_\alpha \cdot \mathbf{G}^\beta = \delta_\alpha^\beta$ , with  $\delta_\alpha^\beta$  as the Kronecker delta. The symbol  $\mathbf{N}$  is the unit surface normal defined as

$$\mathbf{N} := \|\mathbf{G}^3\| = \frac{1}{J} \mathbf{G}_1 \times \mathbf{G}_2, \quad (\text{B3.17})$$

in which  $J$  is the reference surface Jacobian

$$J = \|\mathbf{G}_1 \times \mathbf{G}_2\| \quad (\text{B3.18})$$

The vectors  $(\mathbf{G}_1, \mathbf{G}_2, \mathbf{N})$  are described as the surface convected basis. The membrane force and the bending moment resultant tensors are obtained by integrating the Saint Venant-Kirchhoff constitutive law for orthotropic materials through the thickness of the shell, which gives

$$\mathbf{n} := n^{\alpha\beta} \mathbf{G}^\alpha \otimes \mathbf{G}^\beta = \mathbf{A} \cdot \boldsymbol{\varepsilon} + \mathbf{B} \cdot \boldsymbol{\rho}, \quad (\text{B3.19})$$

$$\mathbf{m} := m^{\alpha\beta} \mathbf{G}^\alpha \otimes \mathbf{G}^\beta = \mathbf{B} \cdot \boldsymbol{\varepsilon} + \mathbf{D} \cdot \boldsymbol{\rho}, \quad (\text{B3.20})$$

in which  $\mathbf{A}$ ,  $\mathbf{B}$  and  $\mathbf{D}$  are the membrane, coupling and bending stiffness tensors in the surface convected basis. Although an orthotropic approach is implemented, when the material characteristics are equal in all directions, then an isotropic material is achieved.

Furthermore, using a Saint Venant-Kirchhoff material model to describe an isotropic and linear elastic material, we can write the second Piola-Kirchhoff stress tensor in Voigt notation:

$$\begin{bmatrix} \bar{S}^{11} \\ \bar{S}^{22} \\ \bar{S}^{12} \end{bmatrix} = \frac{E}{1-\nu^2} \begin{bmatrix} 1 & \nu & 0 \\ \nu & 1 & 0 \\ 0 & 0 & (1-\nu)/2 \end{bmatrix} \cdot \begin{bmatrix} \bar{E}_{11} \\ \bar{E}_{22} \\ 2\bar{E}_{12} \end{bmatrix} \quad (\text{B3.21})$$

The  $S^{\alpha\beta}$  and  $E_{\alpha\beta}$  represent the stress and strain coefficients in a local Cartesian basis, respectively. The  $E$  represents the elasticity modulus and  $\nu$  the Poisson's ratio.

By separating the stresses into a membrane and a bending part and integrating through the thickness  $t$ , we can define the stress resultant tensor  $\mathbf{n}$  as follows:

$$\begin{bmatrix} \bar{n}^{11} \\ \bar{n}^{22} \\ \bar{n}^{12} \end{bmatrix} = \frac{Et}{1-\nu^2} \begin{bmatrix} 1 & \nu & 0 \\ \nu & 1 & 0 \\ 0 & 0 & (1-\nu)/2 \end{bmatrix} \cdot \begin{bmatrix} \bar{\varepsilon}_{11} \\ \bar{\varepsilon}_{22} \\ 2\bar{\varepsilon}_{12} \end{bmatrix} \quad (\text{B3.22})$$

and the bending moment tensor  $\mathbf{m}$

$$\begin{bmatrix} \bar{m}^{11} \\ \bar{m}^{22} \\ \bar{m}^{12} \end{bmatrix} = \frac{Et^3}{12(1-\nu^2)} \begin{bmatrix} 1 & \nu & 0 \\ \nu & 1 & 0 \\ 0 & 0 & (1-\nu)/2 \end{bmatrix} \cdot \begin{bmatrix} \bar{\kappa}_{11} \\ \bar{\kappa}_{22} \\ 2\bar{\kappa}_{12} \end{bmatrix} \quad (\text{B3.23})$$

Thus, both  $\mathbf{n}$  and  $\mathbf{m}$  are symmetric and the notation  $(-)$  refers to local Cartesian basis.

According to Kiendl et al. the internal stiffness matrix is equal to

$$K^{\text{int}} = \int_A \left( \frac{\partial \mathbf{n}}{\partial u_j} : \frac{\partial \boldsymbol{\varepsilon}}{\partial u_i} + \mathbf{n} : \frac{\partial^2 \boldsymbol{\varepsilon}}{\partial u_i \partial u_j} + \frac{\partial \mathbf{m}}{\partial u_j} : \frac{\partial \boldsymbol{\kappa}}{\partial u_i} + \mathbf{m} : \frac{\partial^2 \boldsymbol{\kappa}}{\partial u_i \partial u_j} \right) dA \quad (\text{B3.24})$$

in which the first and last two terms represent the membrane and the bending stiffness, respectively.

Nagy et al. used components of the linear stiffness matrix and a trilinear operator used to form the geometric stiffness matrix  $\mathbf{k}_g$  of classical linear buckling as

$$K_{ij} = \int_{\Omega_0} \left( \frac{\partial \boldsymbol{\varepsilon}}{\partial u_i} \cdot \frac{\partial \mathbf{n}}{\partial u_j} + \frac{\partial \boldsymbol{\rho}}{\partial u_i} \cdot \frac{\partial \mathbf{m}}{\partial u_j} \right) d\Omega_0 \quad (\text{B3.25})$$

$$L_{ij} = \int_{\Omega_0} \left( \frac{\partial^2 \boldsymbol{\varepsilon}}{\partial u_i \partial u_j} \cdot \frac{\partial \mathbf{n}}{\partial u_k} + \frac{\partial^2 \boldsymbol{\rho}}{\partial u_i \partial u_j} \cdot \frac{\partial \mathbf{m}}{\partial u_k} \right) d\Omega_0 \quad (\text{B3.26})$$

$$\mathbf{k}_g = \mathbf{L} \cdot \mathbf{u} \quad (\text{B3.27})$$

with  $i, j, k = d \cdot K$  and  $\mathbf{u}$  is the discrete displacement vector corresponding to static equilibrium.

## B4. NUMERICAL PROCEDURE

For the most updated version of the Matlab code, it is recommended to contact Giuseppe Radaelli ([g.radaelli@tudelft.nl](mailto:g.radaelli@tudelft.nl)). This section will briefly describe some key parts of the codes.

### B4.1. PLANAR BEAMS

The knot vector is defined by

```
c.knots = [0 0 0 0.2 0.4 0.6 0.8 1 1 1];
```

The  $h$ - or  $k$ -refinement is defined by

```
% h- or k-refinement
uins = 0: (1/30) :1; % Knot insertion
uins = setdiff(uins, unique(c.knots));
deg_el = 2; % Degree elevation
cc = k_refinecurve(c, deg_el, uins);
```

The material properties are defined by

```
% MATERIAL PROPS PETG (SI-Units, kg-m-s)
E = 2.3225e+9; % N/m2, Pa (Young's modulus)
cross.rho = 1270; % kg/m3 (density)
cross.h = 0.0015; % m (thickness)
cross.w = .2; % m (width)
cross.A = cross.h*cross.w; % m2 (cross-section)
cross.maxstrain = 3.5; % maximum strain
cross.yieldstress = 0.45e+8; % Yield stress
cross.yieldstrain = 0.04; % Yield strain
```

The application of the actuation point on the body of the beam is defined by

```
dofs.mp=ceil(m.geo.number*0.5);
```

The value 0.5 is taken from the origin, and means halfway the body. Choosing a value larger or smaller than 0.5 will shift the point of actuation further or closer to the origin, which is  $(x,y)=(0,0)$ .

The optimization input vector and its constraints are defined as follows

```
%startpoint (length is in meters and angles in radians)
x=[0 0 2 0.5*pi 2 0 0.5 -0.5*pi 0.5 0 2 -0.5*pi 2 0];

lb=x-.2; % Lower bound
ub=x+.2; % Upper bound

% Aeq*x=beq
Aeq=diag([1 1 0 0 0 0 0 0 0 0 0 0 0 0]); %constraint to which the
optimization is hold (matrix)
beq=zeros(14,1); %vector
```

The Sequential Programming optimization toolbox is used as follows

```
% Sequential Programming
ms = MultiStart('UseParallel','always','Display','iter')
options=optimset('Algorithm','sqp','GradObj','on','Hessian',
'off',...
'tolX',1e-7,'TolFun',1e-9,'MaxIter',500,'MaxFunEvals',5000,...
'PlotFcns',@optimplotfval,'UseParallel','never')
problem = createOptimProblem('fmincon','lb',lb,'ub',ub,'Aeq',Aeq,...
'beq',beq,'objective',@NesObjFun,'x0',x,'options',options);
[x, Objbest,exitflag,output,solutions] = run(ms,problem,1)
save('filename.mat')
```

The Nelder-Mead Simplex algorithm is used as follows

```
% Nelder-Mead Simplex search method
options=optimset('tolX',1e-5,'TolFun',1e-6,'MaxIter',250,'MaxFunEvals',1000,
'PlotFcns',@optimplotfval);
[x,fval,exitflag,output]= fminsearch(@NesObjFun,x, options)
save('filename.mat')
```

The boundary conditions are defined as follows

```
dofs.ep1 =[0 0]; dofs.ep2 =[0 0];
dofs.theta1 =[0]; dofs.theta2 =[0];

dofs.mp1=[nan -.4]; dofs.phil=[nan];
```

The `dofs.ep` represent the  $x$  and  $y$  constraints of the beam-ends. The `dofs.theta` represent the rotational constraints of the beam-ends. The `dofs.mp` and the `dofs.phi` represent the  $x$  and  $y$  actuation and the rotational actuation at the actuation application point on the body of the beam, respectively.

## B4.2. SHELL STRUCTURES

The thickness of the structural element is defined in

```
h = 0.04; %thickness in meters
```

The different boundary conditions are given in

```
dofs.ep1    = [0 0 0]; dofs.ep2    = [0 0 0];
dofs.theta1 = [0 0 0]; dofs.theta2 = [nan 2 nan];
```

The `dofs.ep` represent the  $x,y,z$  displacement of the corresponding beam-end. The `dofs.theta` represent the rotational conditions  $\varphi_x, \varphi_y, \varphi_z$  of each corresponding beam-end.

The initial optimization vector is defined by

```
ObjVars=[1 4 3 5 -0.5 0.5 pi/2 pi*.75 1 1 1 1 1 -1.4 -1 0 0 -1];
```

The optimization options are defined as follows

```
options=optimset('tolX',1e-5,'TolFun',1e-6,'MaxIter',1000,'MaxFunEvals',4000,
'PlotFcns',@optimplotfval_log)
[x,fval,exitflag,output]= fminsearch(@ObjectiveFunction,ObjVars, options)
save('filename')
```

The mesh refinements are given in

```
o    = [0;0];
nelu = 10;
nelv = 80;
```

The `o` represents the order elevation. The standard polynomial order of the basis functions is equal to 3. This order is elevated by the value between the brackets. The refinement of the mesh is given by `nelu` and `nelv`. The `nelu` stands for  $n$  elements in  $u$  direction, while `nelv` stands for  $n$  elements in  $v$  direction.

The objective for optimization procedure is given by

```
Objective= sum(abs(RM(10:end,4)))
Objective= sum(abs(RF(20:end,5)-mean(RF(20:end,5))))
```

The first objective is used when it is aimed to obtain zero actuation force. The second objective leads to a constant actuation force.

The knot vector is defined as follows

```
surf.knots={ [0 0 0 1 1 1] [0 0 0 0.333333 0.666666 1 1 1]};
```

The positions of the beam sliders at each beam-end are defined by

```
m_beams.pil1X=[((c(1,1,1)+c(1,3,1))/2)+0.01 (c(2,1,1)+c(2,3,1))/2
(c(3,1,1)+c(3,3,1))/2 0 0 0];
m_beams.pil2X=[((c(1,1,4)+c(1,3,4))/2)+0.01 (c(2,1,4)+c(2,3,4))/2
(c(3,1,4)+c(3,3,4))/2 0 0 0];
```



The material properties are stated in (SI-Units)

```
m.mat = setIsotropicMat('PETg',2e9,0.3,1270); % ('name',Emodulus [Pa],
Poissons ratio, density [kg/m3])
```

The pressure load, distributed load and gravity force are defined in the following lines

```
m.load.p0 = [0]; % pressure load [Pa]
m.load.d1 = [0 0 0]'; % distributed load along x, y, and z [Pa]
m.load.g = [0 0 -9.81]'; % acceleration along x, y and z [m/s^2]
```

The properties of the beam sliders are given by

```
breedte = h*10; % h is equal to the thickness of the shell structure.
hoogte = h*10;
m_beams.E = m.mat.E;
m_beams.G = m.mat.E/(2*(1+ m.mat.nu12));
m_beams.A = breedte*hoogte;
m_beams.Iyy = hoogte*breedte^3/12;
m_beams.Izz = breedte*hoogte^3/12;
m_beams.J = (breedte*hoogte/12) * (breedte^2+hoogte^2);
```

## B5. NUMERICAL RESULTS

This section present several other obtained geometries. Also, some failure and non-convergence will be discussed. Note, these topics will be discussed for the planar beam situations. And these discussions are the same for shell structures and are therefore not presented here.

### B5.1. OTHER POTENTIAL GEOMETRIES

As is discussed in the papers, the user of the numerical code should be well aware of the conditions and boundaries that are chosen. Here are two examples, which had different search spaces in comparison to those presented in Paper I.

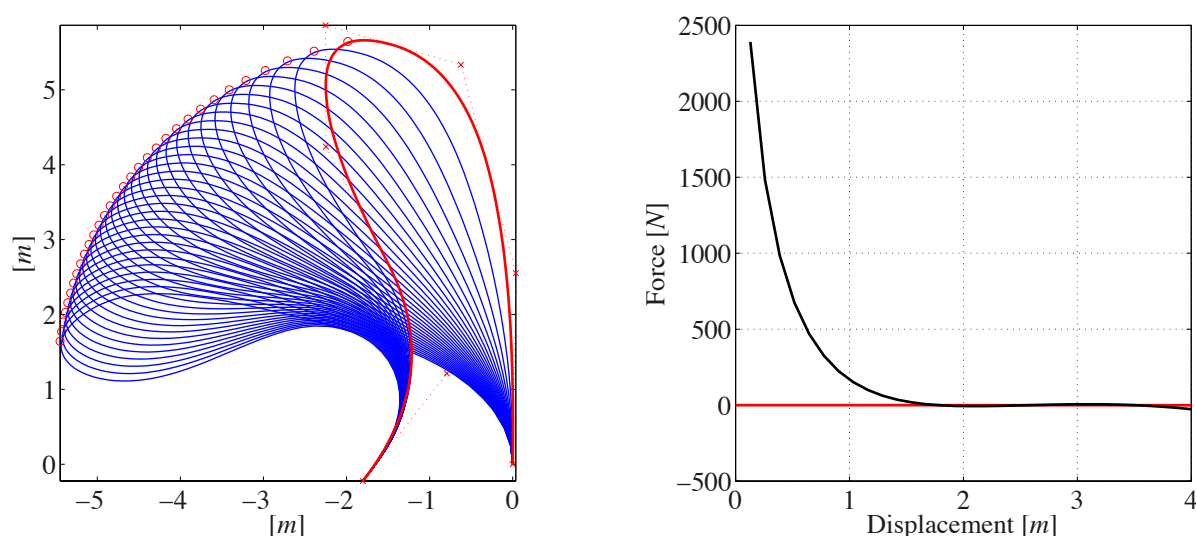


**Figure B5.1:** Vertical displacement applied at the top (left). The corresponding force at point of actuation application (right).

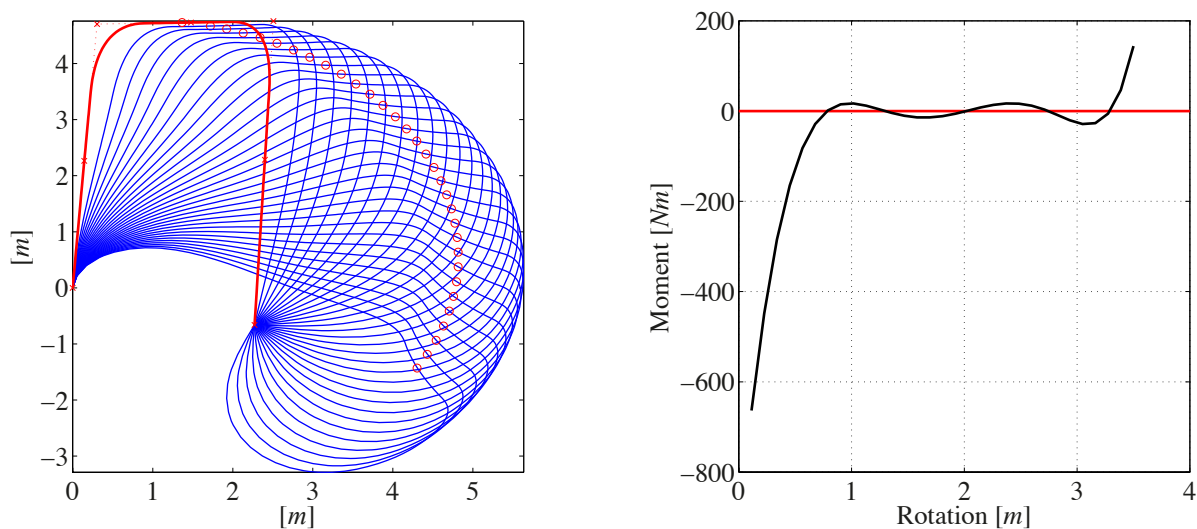


**Figure B5.2:** Rotational actuation applied at the righter boundary (left). The corresponding force at point of actuation application (right).

On the other hand, wide ranges might also lead to impractical geometries for real life applications. The following figure is an excellent example of the latter case. This geometry is obtained after optimization procedure. It can also be seen from the force graph that the required actuation goes to zero after a short while. Thus, the system finds itself in the statically balanced range.

Yet, as can be seen from the geometrical graph, the beam crosses itself, which is an impractical configuration. Note that the geometry is not rigid or attached at the crossing point. The numerical program just considers the geometry to be a geometrical line without any physical characteristics, which makes crossing possible.

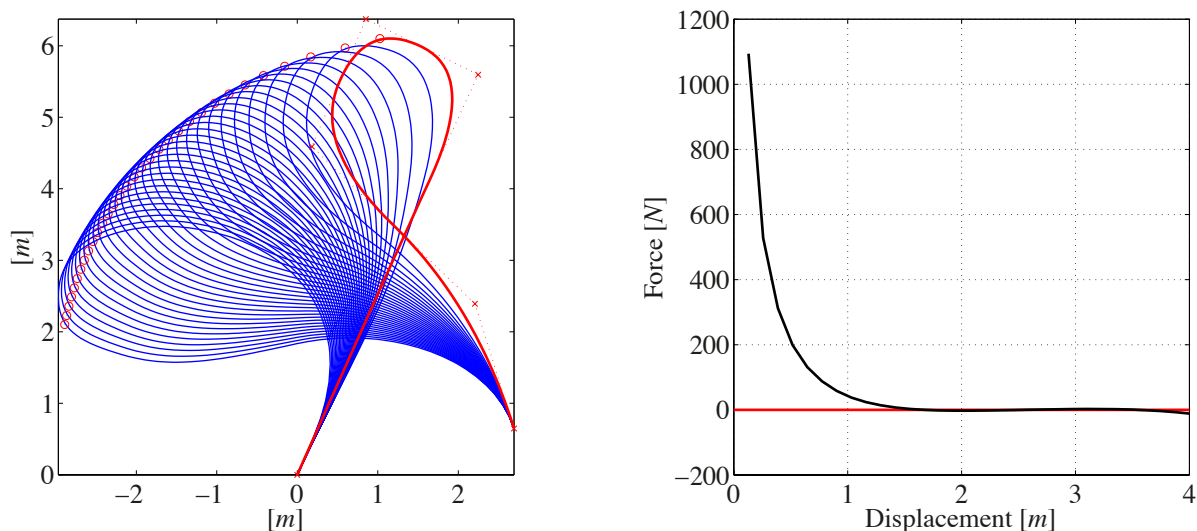


**Figure B5.3:** An example of a structure that crosses itself (left), the applied actuation is a downwards vertical displacement. The corresponding force at point of actuation application (right).

The next figure depicts another statically balanced impractical geometry, which crosses itself and has a sharp local geometrical change halfway its geometrical length. The interesting side issue for this case is the occurring strain in the material, see Figure B5.4. A clear increasing strain peak is depicted due to deformation.

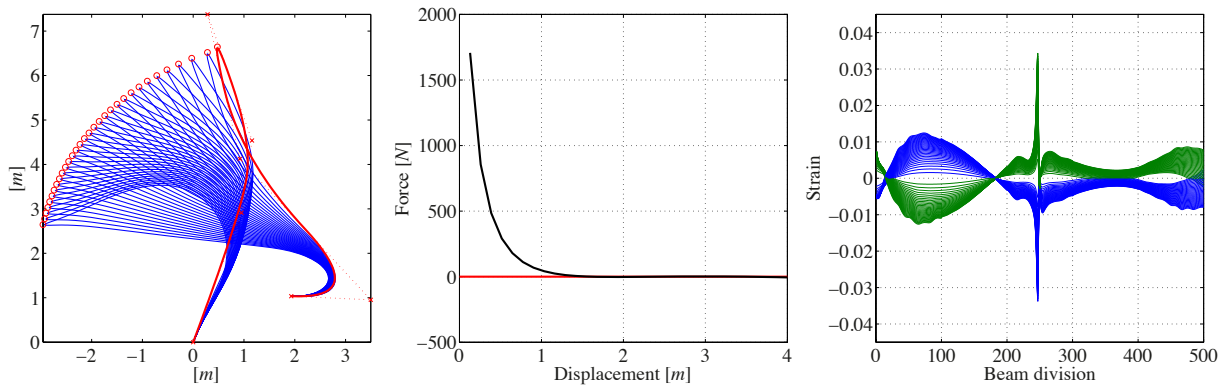


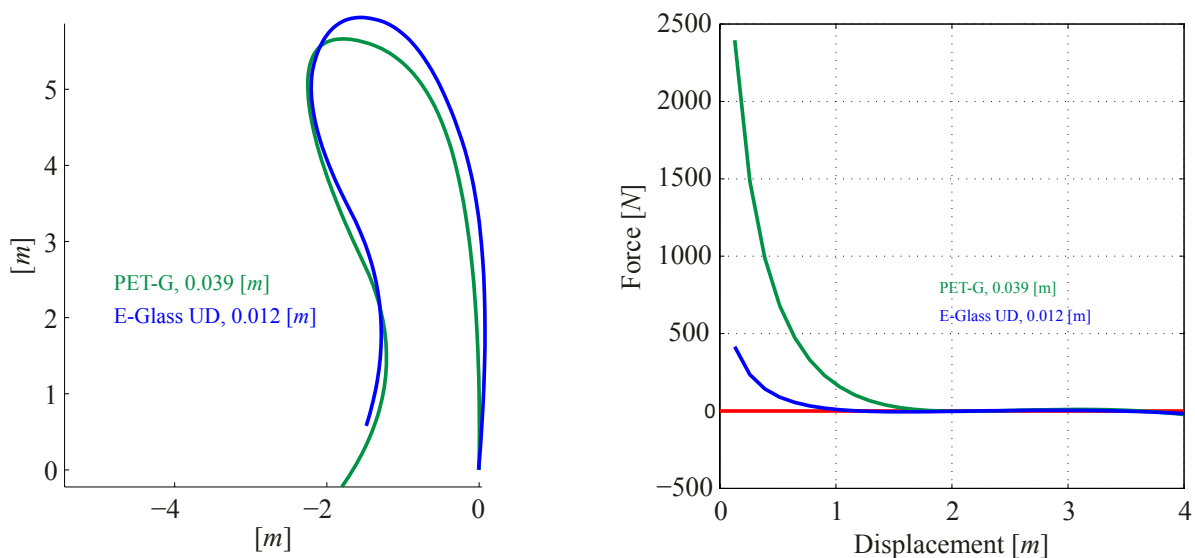
**Figure B5.4:** An example of a sharply shaped topology (left). The corresponding force at point of actuation application (middle). The corresponding strains are given in the righter figure.

Concluding, it is important that the user of this approach is aware of the implemented upper and lower bound conditions of the search space during optimization procedure. These are defined by the `ub` and `lb` in the numerical code for the planar beams. Note that the lengths and angles of the control polygon can have relative different upper and lower boundaries.

### B5.2. DIFFERENT MATERIAL APPLICATION

It is also possible to apply other materials than PET-G during numerical simulations. The only requirement is that they should be elastic. Note also that when applying a material like steel, the deformation in the material does not pass the yield strain. This would lead to plastic deformation, which is highly undesirable in these cases.

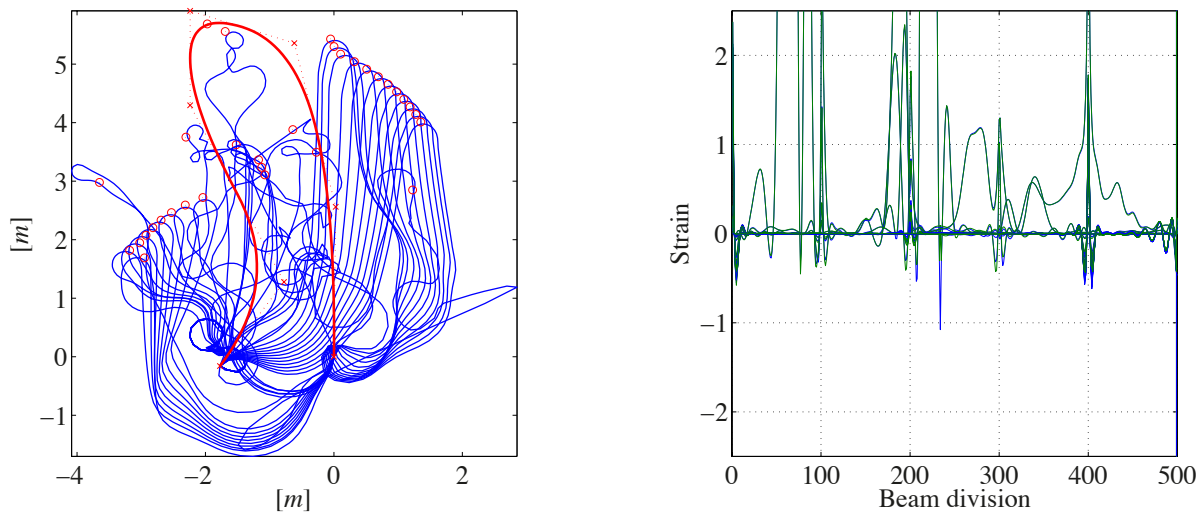
The following figure presents two results of geometries after optimization. Both had equal boundary and initiation conditions. The only difference is the applied material. The green results represent PET-G, and the blue results represent an E-Glass laminated material. An important remark is the fact that the thickness of the laminated material is significantly less than the PET-G one. This is due to the different mechanical properties of the materials. If the thickness is kept the same, then the laminated configuration would result in significantly larger geometries. Thus, with the applied thickness, we were able to obtain fairly similar geometrical sizes for the two configurations.



**Figure B5.5:** Two fairly similar configurations, yet made from different materials (left). The corresponding force at point of actuation application, vertical displacement (right).

### B5.3. FAILURE

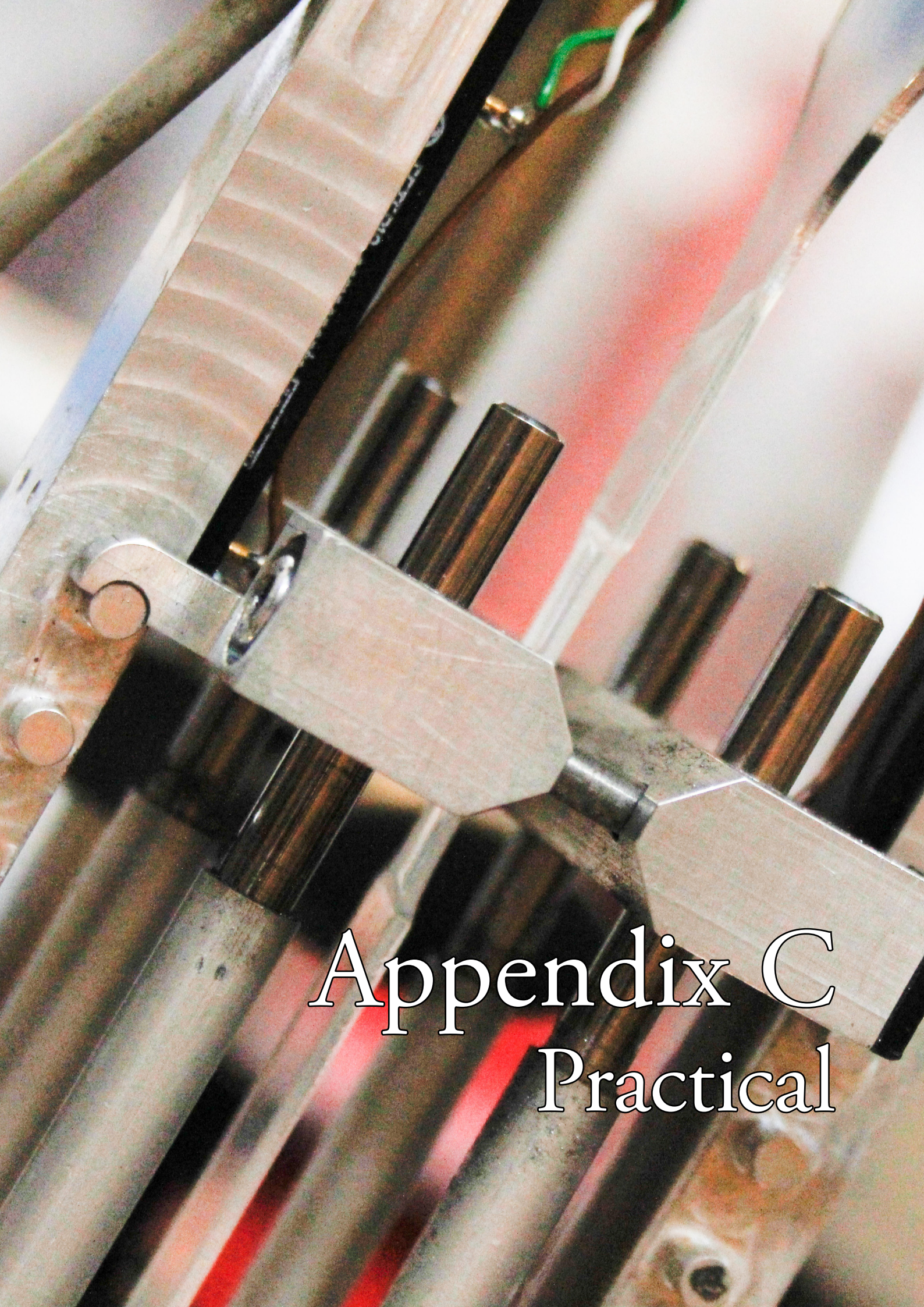
Simulations can also lead to failure due to several reasons. ‘Wrongly’ applied actuation and boundary conditions can be a reason. Yet, a more important factor is the consideration of the scaling factors as discussed in Appendix A4. Choosing the appropriate thickness is essential to obtain converged solutions. The next figure depicts a configuration that did not have sufficient beam thickness, and thus stiffness, to perform the required deformation. It was not able to keep itself into balance since the contribution of gravity was larger than the stiffness. Obtaining converged solutions is therefore a trade-off between the contribution of the stiffness, which is due to the chosen material and its thickness, and the contribution of gravity. The choices in this research are based on trial-and-error approaches.



**Figure B5.6:** A configuration that did not reach convergence along its actuation path due to insufficient stiffness (left). The material strain due to the deformation of the structure (right).





A close-up photograph of a mechanical assembly, likely a laser cutting head. The image shows several cylindrical metal components, possibly nozzles or guides, arranged in a row. A bright red laser line is visible, passing through the assembly. The background is blurred, showing more of the machinery and a red light source. The text "Appendix C Practical" is overlaid on the bottom right of the image.

Appendix C  
Practical





## C1. EXPERIMENTS

### C1.1. PLANAR BEAM EXPERIMENT

This section describes the experiment of a statically balanced planar beam. The specific geometry is obtained from optimization procedures. The control polygon  $\mathbf{q}$  that describes the geometry is given in the following table:

Parameter	Value	Unit
$A_x$	0.0	[m]
$A_y$	0.0	[m]
$l_1$	0.250000000000000	[m]
$\theta_1$	1.41484539201484	[rad]
$l_2$	0.250000000000000	[m]
$\theta_2$	0.157080000000000	[rad]
$l_3$	0.158743118996969	[m]
$\theta_3$	-1.256640000000000	[rad]
$l_4$	0.050000000000000	[m]
$\theta_4$	-0.157080000000000	[rad]
$l_5$	0.250000000000000	[m]
$\theta_5$	-1.884960000000000	[rad]
$l_6$	0.250000000000000	[m]
$\theta_6$	-0.255465376585968	[rad]

**Table C1.1:** Control polygon  $\mathbf{q}$  for the physical model made of a planar beam.

The numerical and physical geometries are depicted in the following figures.

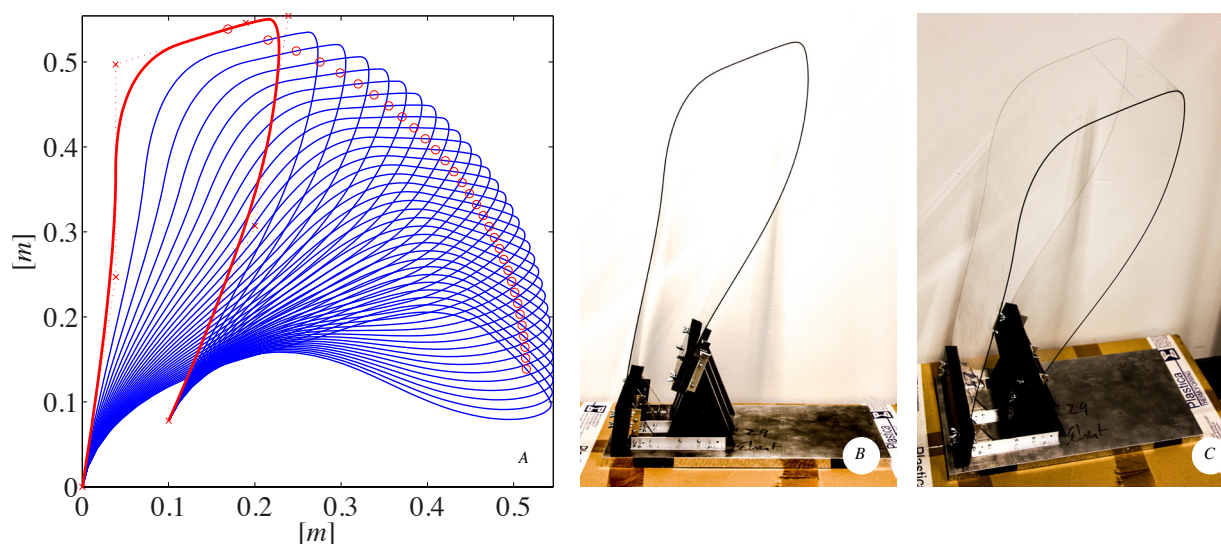


**Figure C1.1:** The numerically obtained configuration (A). The physical model is depicted in (B) and (C). In (C) it is also possible to see the point of application at the top due to the drawn line on the model.

The specific shape is obtained by means of thermoforming. The company *Plastica-Thermoforming* realized this (<http://www.plastica-thermoforming.nl/nl/home.html>).

The deformed configuration and the knife edge that is used to apply the vertical displacement are depicted in the following figure.



**Figure C1.2:** The deformed configuration (left) and the knife edge that is used to apply the vertical displacement (right). The knife edge is kept in its place due to double-sided tape.

The foundation that held the structure in its place is presented in the following figure.

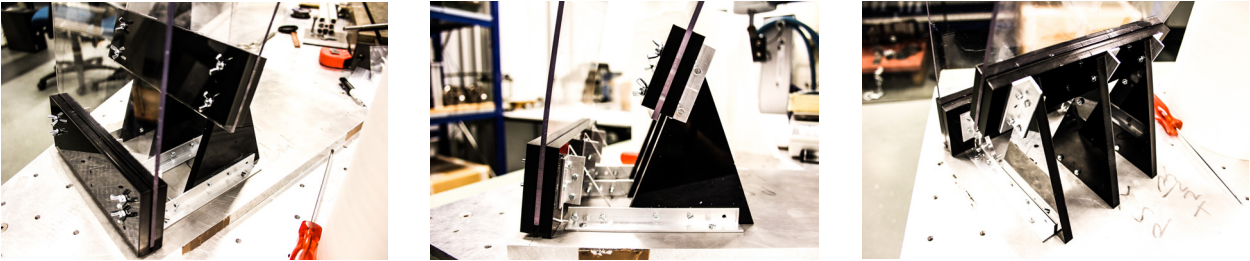


**Figure C1.3:** The specifically designed foundation that keeps the structure in its place. Each figure is taken from a different angle.

## C1.2. SHELL BEAM EXPERIMENT

This section describes the experiment of a statically balanced shell beam. The specific geometry is obtained from optimization procedures. The control polygon  $\mathbf{q}$  that describes the geometry is given in the following table:

Parameter	Value	Unit
$l_{s,1}$	0.05	[m]
$l_{s,2}$	0.05	[m]
$l_{s,3}$	0.1	[m]
$l_{s,4}$	0.4	[m]
$\theta_{s,1}$	3.25195278466510e-05	[rad]
$\theta_{s,2}$	2.95437264663154e-05	[rad]
$\theta_{s,3}$	0.306367318527785	[rad]
$\theta_{s,4}$	1.28900274815564e-05	[rad]
$l_{w,1}$	0.0838301660398948	[m]
$l_{w,2}$	0.0867951073193820	[m]
$l_{w,3}$	0.0907991490727126	[m]
$l_{w,4}$	0.139419259209913	[m]
$l_{w,5}$	0.179550436253061	[m]
$\theta_{w,1}$	-1.21455533214775	[rad]
$\theta_{w,2}$	-1.25820381682529	[rad]
$\theta_{w,3}$	-0.826420248770186	[rad]
$\theta_{w,4}$	-0.631554857739950	[rad]
$\theta_{w,5}$	-0.753436410190118	[rad]

**Table C1.2:** Control polygon  $\mathbf{q}$  for the physical model made of a planar beam.

The specific shape is obtained by means of vacuum forming. A mould is milled and used to obtain the shape. The following figures depict the numerical and physical model. The mould is presented as well.

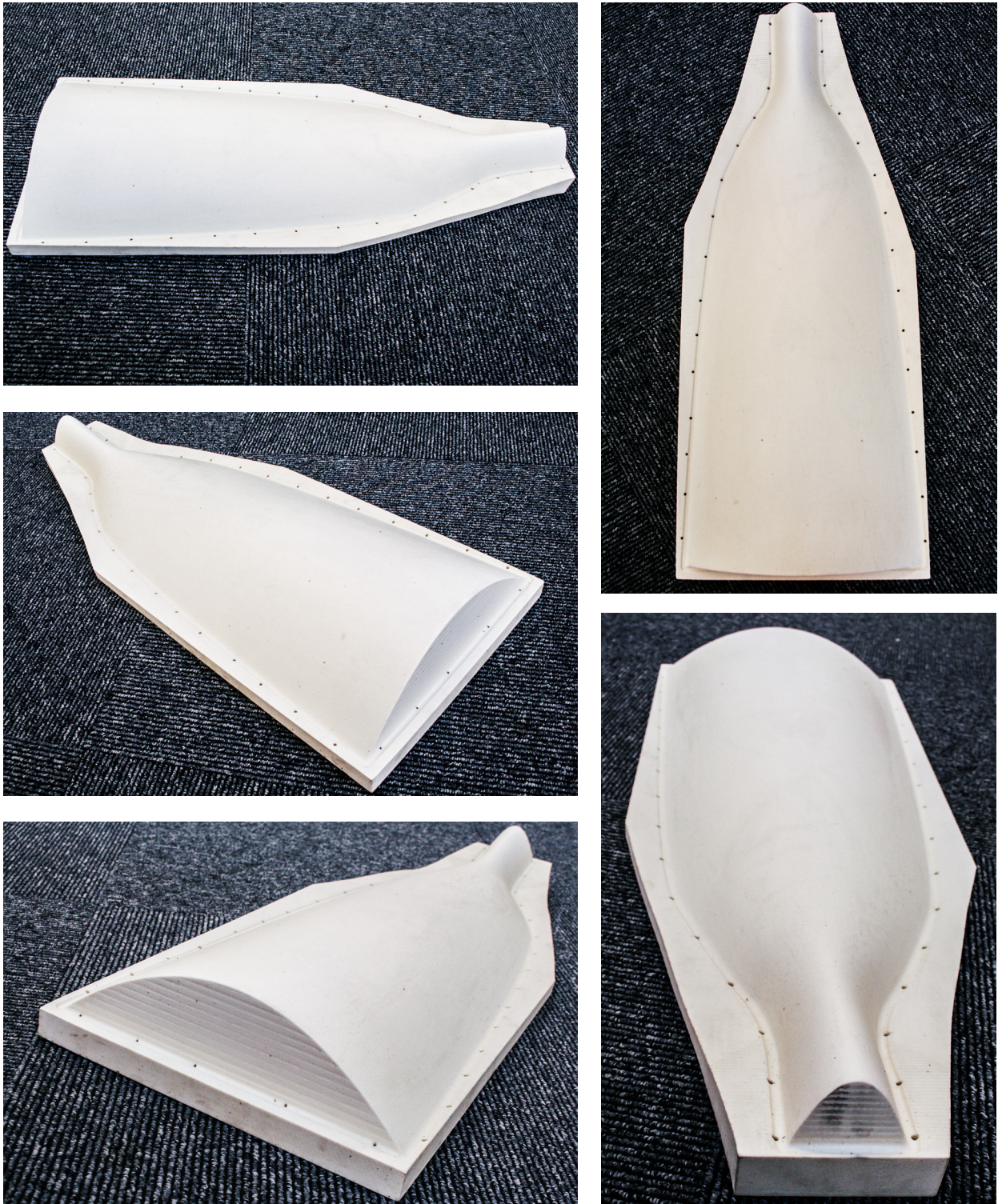


**Figure C1.4:** The mould that is used to obtain the eventual shape of the physical model. This is obtained by using a drill machine at the faculty of Architecture. Each figure is taken from a different angle.

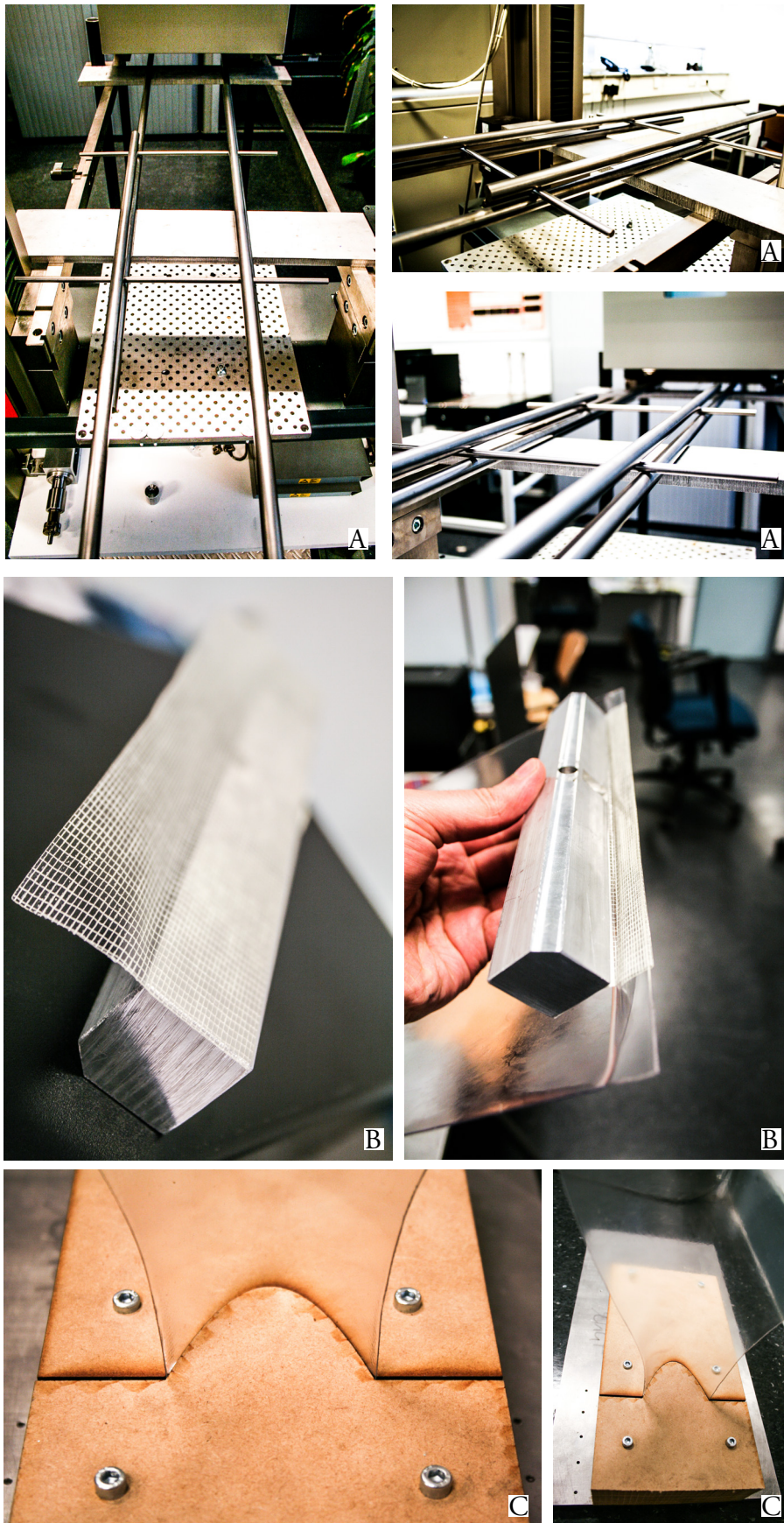


**Figure C1.5:** **A:** Straight rods on which the model is placed in order to be displaced in horizontal sense. **B:** A bar which is used as a knife-edge to apply the displacement at the top of the structure. The double-sided tape is used to keep the knife-edge in its place. **C:** The clamped fixation at the bottom of the model. This is made out of 9 MDF plates of which each is 6mm thick.



**Figure C1.6:** The physical model is being tested by a compression bench, which measures the vertical displacement and the required force simultaneously.

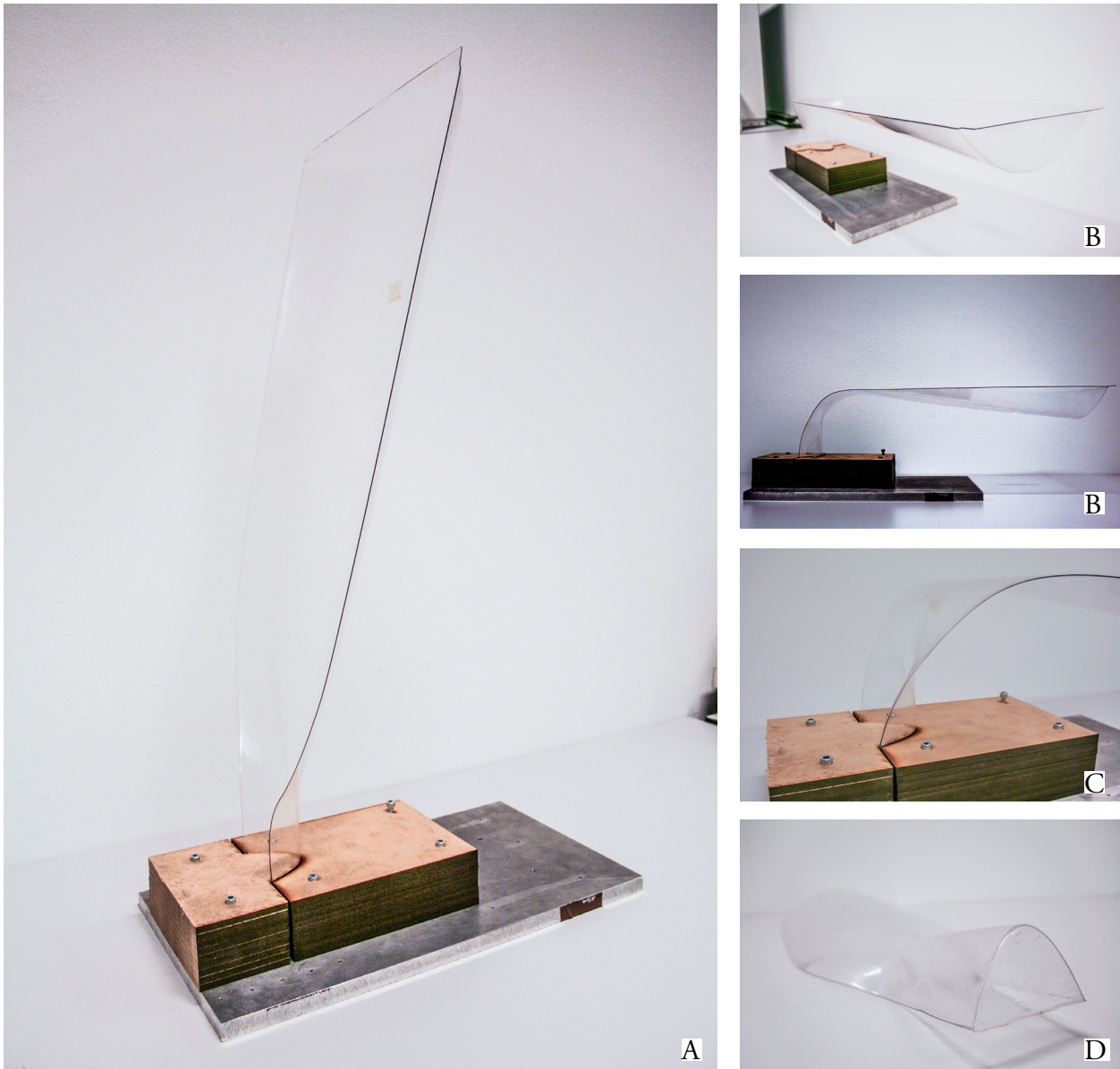


**Figure C1.7:** **A:** The physical model in its erected state. **B:** The physical model is positioned in a stable position without the addition of an external weight or force. **C:** The deforming region of the physical model. **D:** The physical model shown from the bottom.

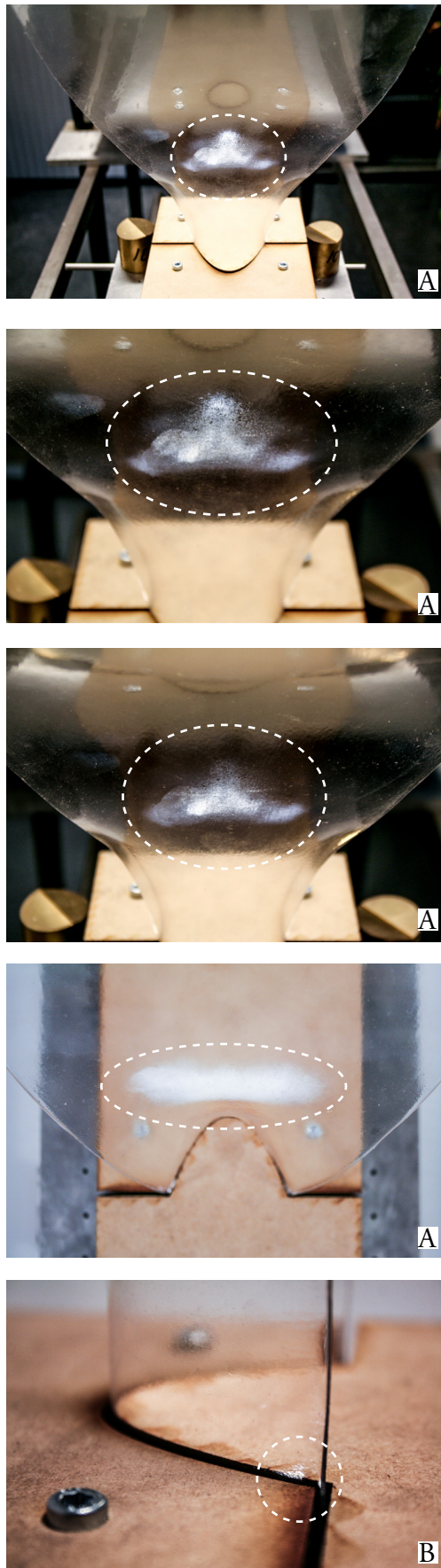


**Figure C1.8:** A: Material strain at the deforming region. B: Material strain at the clamped fixation.

### C1.3. PET-G PULL TEST

After the planar beam physical model was tested on the compression bench, it seemed smart to investigate what kind of mechanical properties the material had. Therefore, a pull test was carried out to obtain the elasticity modulus of the material. The following figures depict the pull test of the specimens. The next page presents the mechanical properties shared by the company that delivered the material. This is followed by the results from the tension test.

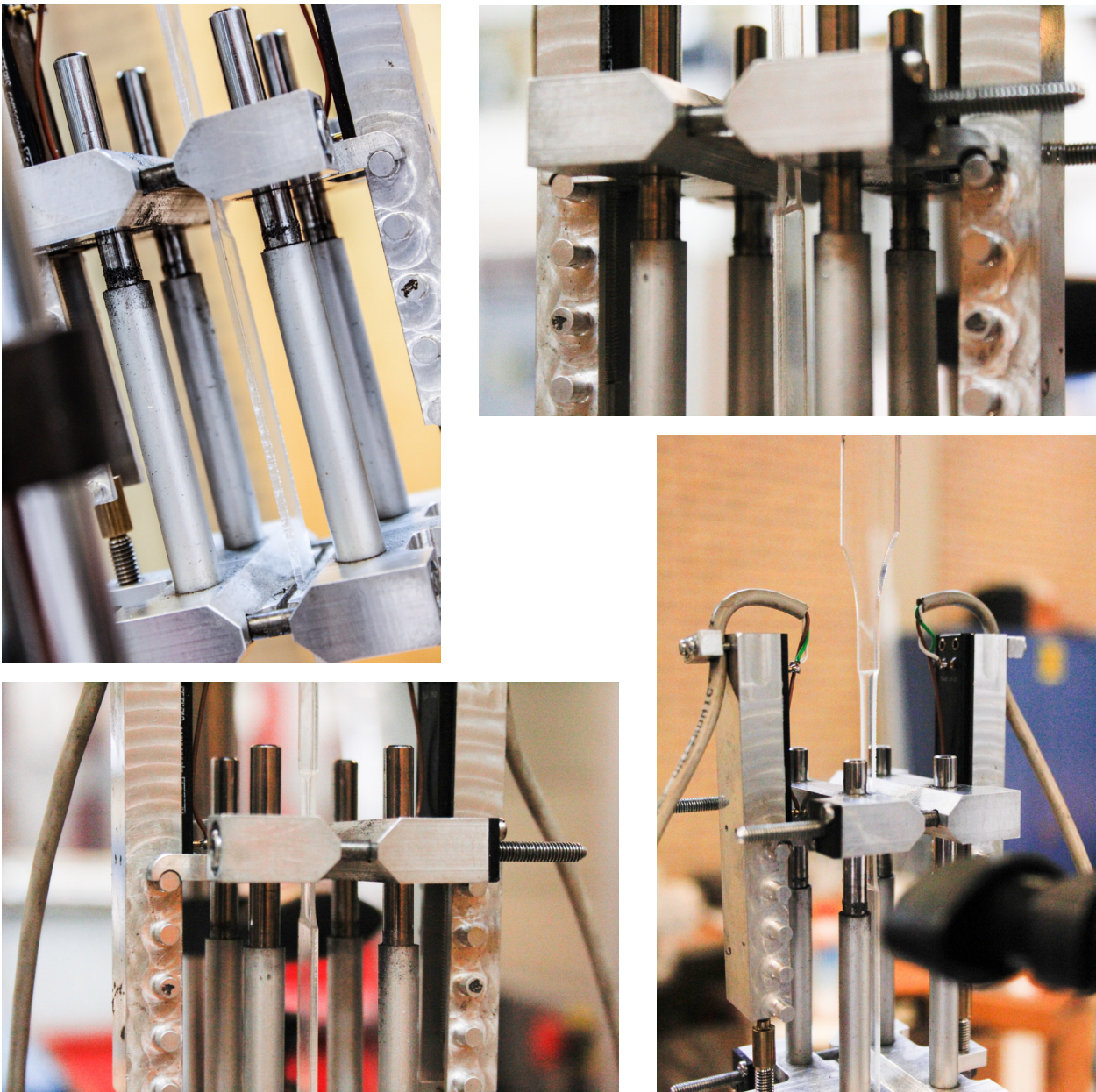


**Figure C1.9:** PET-G pull tests. The pulling direction is vertical in this case.





Product Data Sheet, February 2006

## Vivak® UV Solid Copolyester Sheets.

Your benefits:

- good weather resistance
- excellent thermoformability
- good impact strength
- good fire rating

Solid **Vivak® UV** sheets are made of thermoplastic copolyester. They offer high impact strength, a good fire rating and good weather resistance. These properties are demonstrated by our 10-year guarantee on mechanical strength and optical properties.

**Vivak® UV** sheets can be rapidly thermoformed at low energy consumption, short production times, extreme degrees of stretching and accurate mold surface reproduction, without predrying. The sheets are easy to screen print and machine.

**Vivak® UV clear 2099** is a grade of clear transparent sheet with extremely high light transmission and high gloss.

**Vivak® UV white 2130** sheets are translucent white sheets with good light diffusion and a pleasant hue.

### Applications:

Ideal fields of application for Vivak® UV are: Outdoor P.O.S., displays, poster pillars, vending machines, poster boards and outdoor posters, advertising boards.

	Test Conditions	Typical Values	Unit	Test Method
<b>PHYSICAL</b>				
Density		1.27	g/cm <sup>3</sup>	ISO 1183-1
Moisture absorption	after storage in standard climate 23 °C/ 50 % RH	0.2	%	ISO 62-4
Refractive index	after storage in water at 23 °C until saturation	0.6	%	ISO 62-1
	20 °C	1.567	–	ISO 489
<b>MECHANICAL</b>				
Tensile stress at yield		> 45	MPa	ISO 527-2/1B/50
Elongation at yield		4	%	ISO 527-2/1B/50
Tensile strength		> 45	MPa	ISO 527-2/1B/50
Elongation at break		> 35	%	ISO 527-2/1B/50
Elastic modulus		2000	MPa	ISO 527-2/1B/1
Limiting flexural stress		ca. 80	MPa	ISO 178
Impact strength	Charpy, unnotched	no break	kJ/m <sup>2</sup>	ISO 179/1fU
	Charpy, notched	ca. 7	kJ/m <sup>2</sup>	ISO 179/1eA
	Izod, notched	ca. 6	kJ/m <sup>2</sup>	ISO 180/1A
<b>THERMAL</b>				
Vicat softening temperature	Method B50	80	°C	ISO 306
Thermal conductivity		0.2	W/m K	DIN 52612
Coeff. of linear thermal expansion		0.05	mm/m K	DIN 53752-A
Heat deflection temperature under load	Method A: 1.80 MPa	63	°C	ISO 75-2
	Method B: 0.45 MPa	70	°C	ISO 75-2
<b>ELECTRICAL</b>				
Dielectric strength		20	kV/mm	IEC 60243-1
Volume resistivity		10 <sup>15</sup>	Ohm-cm	IEC 60093
Surface resistivity		10 <sup>18</sup>	Ohm	IEC 60093
Dielectric constant	at 10 <sup>3</sup> Hz	2.6		IEC 60250
	at 10 <sup>6</sup> Hz	2.4		IEC 60250
Dissipation factor	at 10 <sup>3</sup> Hz	0.005		IEC 60250
	bei 10 <sup>6</sup> Hz	0.02		IEC 60250

The mechanical properties were measured on sheets of 4 mm thickness.

**Product Liability Clause:** This information and our technical advice – whether verbal, in writing or by way of trials – are given in good faith but without warranty, and this also applies where proprietary rights of third parties are involved. Our advice does not release you from the obligation to verify the information currently provided – especially that contained in our safety data and technical information sheets – and to test products as to their suitability for the intended processes and uses. The application, use and processing of our products and the products manufactured by you on the basis of our technical advice are beyond our control and, therefore, entirely your own responsibility. Our products are sold in accordance with the current version of our General Conditions of Sale and Delivery.





Figure C1.10: The pull test specimens after the pull test. The righter figure enlarges the critical area.

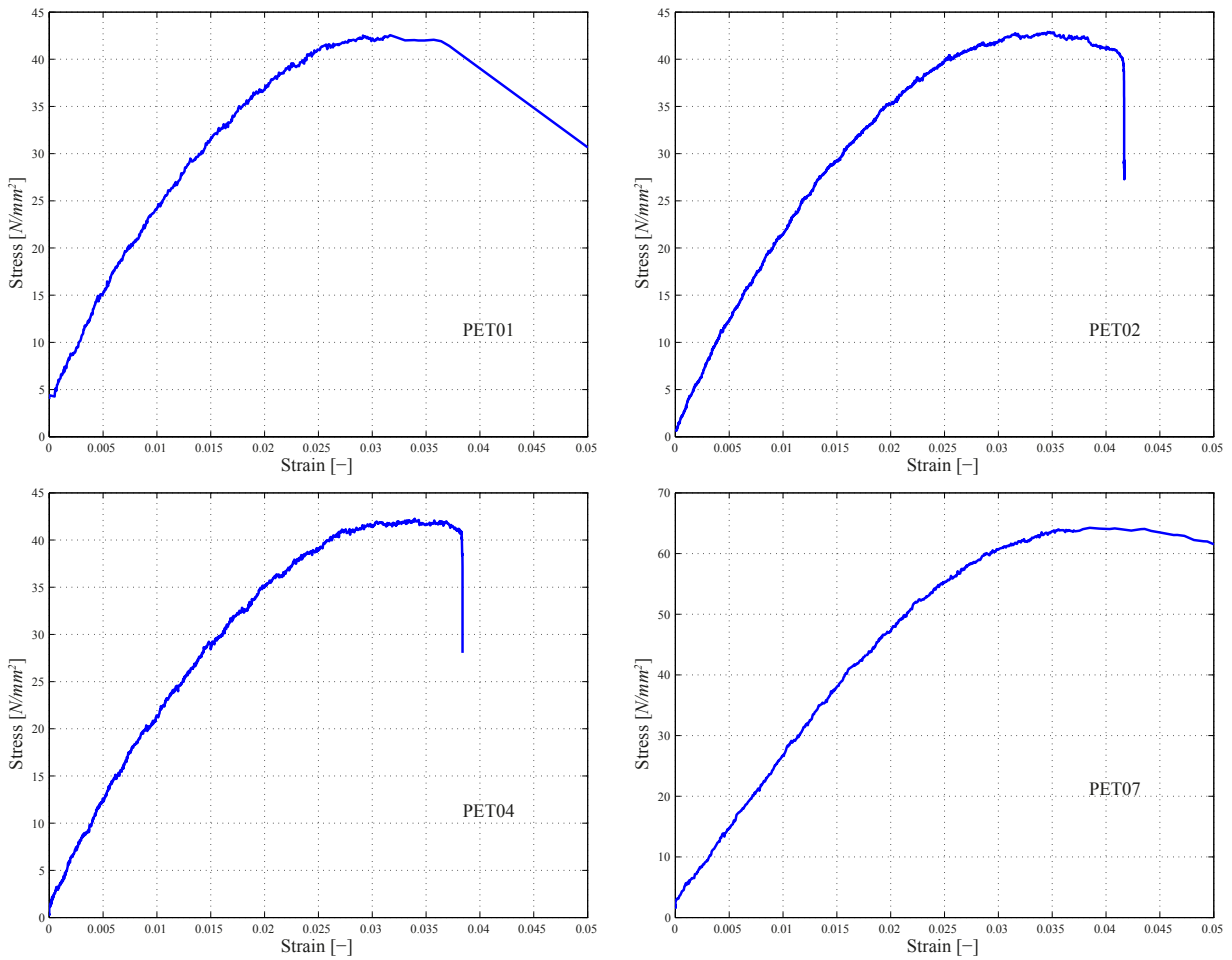


Figure C1.11: The pull test results.

The elasticity modulus of each graph is calculated by taking the slope between the 0.05% and the 0.25% strain. The elasticity moduli of the graphs are:

$$\text{PET01} = 2.3501\text{e}+03 \text{ N/mm}^2$$

$$\text{PET02} = 2.4786\text{e}+03 \text{ N/mm}^2$$

$$\text{PET04} = 2.2371\text{e}+03 \text{ N/mm}^2$$

$$\text{PET07} = 2.2400\text{e}+03 \text{ N/mm}^2$$

The average results in  $E = 2.32\text{e}+03 \text{ N/mm}^2$ . Thus, higher than stated by the company ( $2.0\text{e}3 \text{ N/mm}^2$ ) that delivered the material.

## C2. ACTUATION

There are several configurations found for the Barrier in Motion, with each a specific type of actuation. This section will give an overview of how these actuations could be realized in practice.

There are three major approaches to actuate the Barrier in Motion: fluidic muscles, linear drives and slides, and rotary drives.

Muscle Tower II [9] was actuated by means of fluidic muscles in order to be positioned in specific configurations, see Figure C2.1. This could also be applied to the Barrier in Motion. These muscles could be attached on the inside of the planar designs, or the two sided shell beam. Yet, the pathways that they realize during actuation might be different than the ones described in the two papers. Therefore, new optimization runs should be carried out in order to obtain energy-free actuation.



Figure C2.1: Muscle-Tower II [9].

The fluidic muscles (FESTO) are depicted in the following figure. Both muscles come in different sizes and can have a nominal length between the 40 and 9000 *mm*. The piston force they are able to deliver lies between the 480 and 6000 *N*. The difference is that the first muscle is built as a pressed connection, and the second as screwed one.

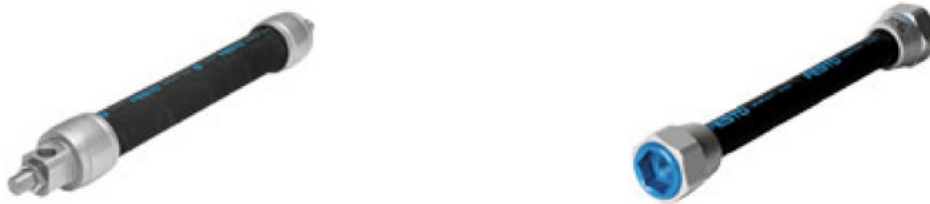


**Figure C2.2:** DMSP and MAS FESTO ([http://www.festo.com/cat/nl\\_nl/products\\_010606](http://www.festo.com/cat/nl_nl/products_010606)).

The second mechanical actuation is the linear drive or slider and the direct drive. These are available in electric, pneumatic and hydraulic versions. An illustration is given in the following figure. These have basically one degree-of-freedom. They come in different sizes and can have a stroke length between the 1 and 8500 *mm* and between the 1 and 5750 *mm* for the linear and direct drive, respectively. The force that they are able to deliver lies between the 15 and 3000 *N* and the 93.7 and 202 *N* for the both, respectively. This actuation could be applied for the cases in which vertical actuation is applied. One should only not forget that these should then have an own rail at foundation level on which it displaces itself in the horizontal direction, see Figure C2.4. This could also be applied to the single shell beam element designs.



**Figure C2.3:** Linear drive or slider (left) and the direct drive (right) ([http://www.festo.com/cat/nl\\_nl/products\\_011100](http://www.festo.com/cat/nl_nl/products_011100)).

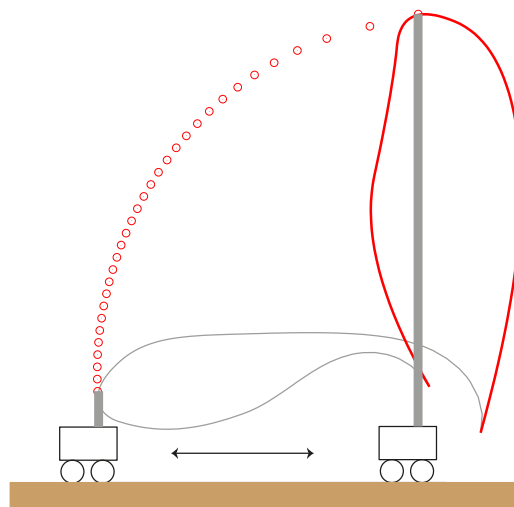


**Figure C2.4:** A practical solution by implementing the sliders and linear drives of FESTO.

Another and more robust solution is the use of rotary actuators. These could be placed at one of the boundary conditions without the need of an extra rail construction or whatsoever. Furthermore, they can have continuous actuation or moment to a fixed angular position. The next figure gives examples of electrical rotary actuators.

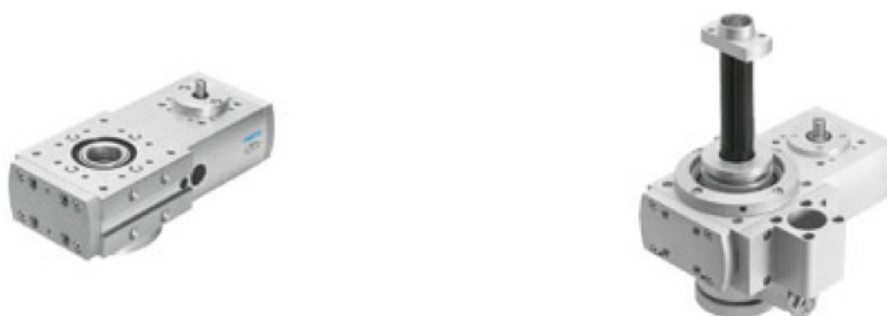


**Figure C2.5:** Rotary actuation ([http://www.festo.com/cat/nl\\_nl/products\\_011100](http://www.festo.com/cat/nl_nl/products_011100)).

A last option is the application of a tendon. Such tendon could be attached on the in- or outside of a Barrier in Motion. At the foundation level it could then have a mechanism that rolls up the tendon, which causes the structure simultaneously to deform. Thus leading to a robust solution as well.

Of course, more thorough research is needed to actually apply these actuation types and configurations in the natural environment. Especially on withstanding the change in weather conditions.

### C3. NOISE

An important aspect that needs to be investigated more thoroughly is the aspect of noise reduction. Conventional sound barriers and other sound reducing applications have great stature and a lot of weight per unit of volume. In most of the cases they also hinder the sight of by passers. As is proposed in this research, the Barrier in Motion resolves this issue by making the sound barrier disappear when it is not needed. The first issue that arises is the fact that since the structure is compliant and deformable, the sound reducing elements should also deform accordingly. Some propositions are made here that could achieve this.

The material itself could be perforated so that the noise waves would enter and get dissipated. However, the mechanical properties of the material might get changed due to this perforation. Also, it is not clear whether the material would be able to withhold the large deformations while having perforations in its body, since these perforations might cause stress concentrations that could lead to plastic deformation in the material.

To find more information about the Dutch regulations concerning noise along roads and train tracks, it is advised to consult '*Richtlijnen geluidbeperkende constructies langs wegen*'. This publication presents the minimal requirements for structures that tend to reduce the noise along roads and train tracks. Furthermore, Dutch governmental laws concerning this topic can be consulted through the following link:

([http://wetten.overheid.nl/BWBR0031722/volledig/geldigheidsdatum\\_31-08-2015](http://wetten.overheid.nl/BWBR0031722/volledig/geldigheidsdatum_31-08-2015)).

#### C3.1. NOISE BARRIER MATERIALS

The consulted website for this section is:

([http://www.fhwa.dot.gov/environment/noise/noise\\_barriers/design\\_construction/design/design05.cfm](http://www.fhwa.dot.gov/environment/noise/noise_barriers/design_construction/design/design05.cfm))

In practice are several standard materials and surface treatments applied to reduce the noise of traffic. Some of these will be presented here.

The first and most common used material is concrete, see Figure C3.1. It is considered as one of the most durable materials currently for many highways is formulated, cast, and cured properly. It is able to withstand all kinds of different

weather conditions. Due to its high density is not much thickness demanded to meet the requirements of noise reduction. Concrete lends itself also perfectly to the purpose of esthetical goals.



**Figure C3.1:** Concrete noise walls.

### C3.1.1. BRICK AND MASONRY BLOCK

Brick and masonry block walls either can be either hand-laid or pre-assembled by machines. These walls have greater versatility in general and in comparison with concrete walls. Yet, all brick and masonry wall require a continuous concrete foundation. The walls should then be anchored to the foundation with reinforcing bars. Just like concrete, brick and masonry easily meet the requirements for sound reduction.



**Figure C3.2:** Brick and masonry block barriers.

### C3.1.2. METALS

Most common used metals are steel, aluminium and stainless steel. The least expensive type is the first one. Most constructed panels, posts and girts are coated with plastisols, bonded powders, enamel paints, or galvanizing material. Or they are manufactured as self-protecting.

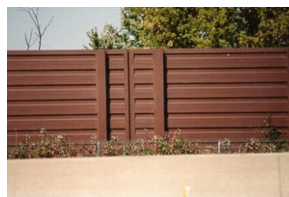


**Figure C3.3:** Steel barriers.

Aluminium is a lightweight alloy, which is typically coated with a bonded powder.

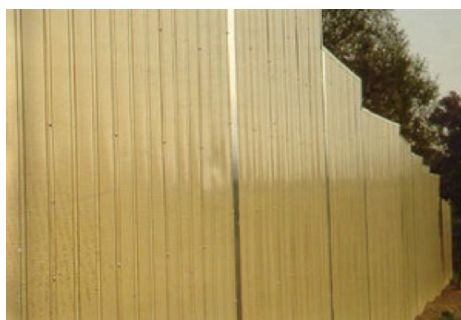


**Figure C3.4:** Aluminium barriers.

Stainless steel is a highly durable and corrosion resistant metal alloy and requires therefore no coating. Metal panels have a weight advantage and are therefore highly applicable for sound reducing applications.

### C3.1.3. WOOD

Most applied wood types for noise barriers are pressure preservative treated lumber, plywood (Figure C3.5a), and glue laminated products (Figure C3.5b).



**Figure C3.5:** Ply and GL wood barriers.

### C3.1.4. TRANSPARENT PANELS

Typical transparent noise barriers are constructed of glass or clear plastic panels. Glass panels are typically made of single tempered or laminated tempered glass sheets. Plastics as well as glass can be tinted and etched to give a frosted appearance. These transparent applications are ideal in reducing or virtually eliminating the visual impact of noise barriers. Yet, these can also be as much as 20 times more expensive in comparison with the common concrete or steel panels. Also, the plastic panels might be affected by ultraviolet light.



**Figure C3.6:** Transparent barriers.

### C3.1.5. PLASTICS

There exist several plastic materials types that are used as barrier material. Think of Polyethylene, PVC and fibreglass (Figure C3.7 left). These are extremely versatile, mouldable and most of them are recyclable. The recycled plastics can also be used as barrier material, see Figure C3.7 right.



**Figure C3.7:** Fibreglass (left) and recycled plastic (right) barriers.

### C3.1.6. COMPOSITES

A composite noise barrier material is in general terms a product that is composed of two or more primary materials.



**Figure C3.8:** Plywood with fibreglass skin barriers.

For more information on different types of barrier surface treatment it is wise to consult the following link: ([http://www.fhwa.dot.gov/environment/noise/noise\\_barriers/design\\_construction/design/design05.cfm](http://www.fhwa.dot.gov/environment/noise/noise_barriers/design_construction/design/design05.cfm))



## C3.2. MISCELLANEOUS

The Barrier in Motion can also be implemented with different applications to reduce noise. The first possibility is by applying surface treatment to the structure of the Barrier in Motion, see Figure C3.9. By attaching honeycomb or hexagonal elements to the outside of the structure, we might achieve noise reduction.

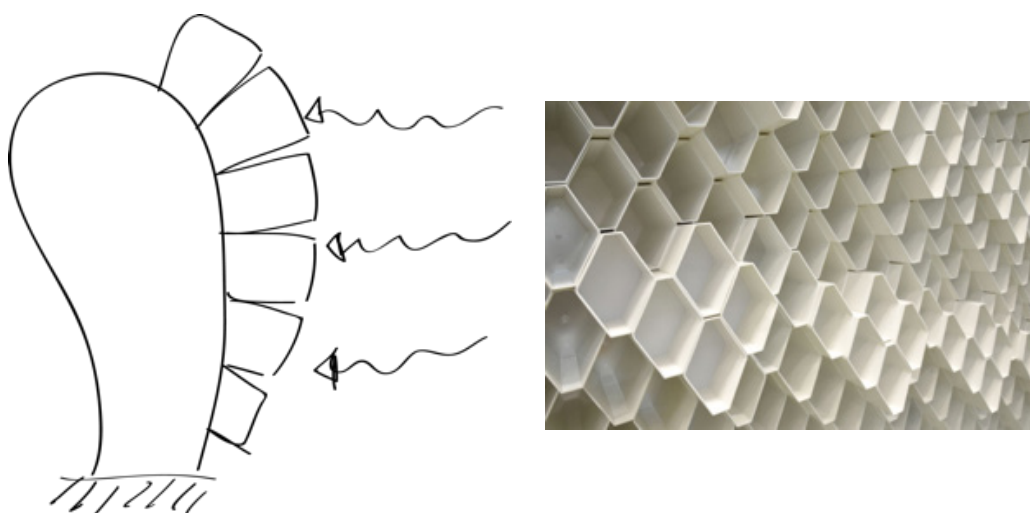


Figure C3.9: Surface treatment by applying hexagonal elements.

Other applications could be the application of aero-gels or sponges. Yet, the application of these types of materials needs further research.

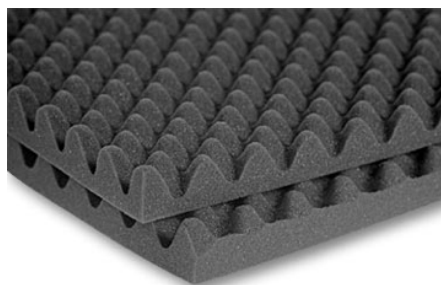


Figure C3.10: Sponges.

On the other hand, several companies are trying to produce sound reducing membranes. These membranes could be used to be placed between two interactive elements, see Figure C3.11a. These membranes could also be used to create inflatable cushions that are attached to the body of the Barrier in Motion, see Figure C3.11b.



Figure C3.11: Different combinations with interactive sound barriers.

**REFERENCES**

- [1] Larry L. Howell, *Compliant Mechanisms*. Wiley, 2002.
- [2] H. Alkisaiei, G. Radaelli, J. L. Herder, H. Bier, and L. J. Sluys, “An Energy Approach to the Design of Large-Scale Compliant and Monolithic Gravity Balancers For Deformable Walls,” Delft University of Technology, MSc Thesis, 2016.
- [3] J. A. Gallego Sanchez, “Statically Balanced Compliant Mechanisms,” Delft University of Technology, PhD Thesis, 2013.
- [4] J. C. Cool, *Werktuigkundige Systemen*. 1992.
- [5] T. J. R. Hughes, J. A. Cottrell, and Y. Bazilevs, “Isogeometric analysis: CAD, finite elements, NURBS, exact geometry and mesh refinement,” *Comput. Methods Appl. Mech. Eng.*, vol. 194, no. 39–41, pp. 4135–4195, Oct. 2005.
- [6] A. P. Nagy, M. M. Abdalla, and Z. Gürdal, “Isogeometric sizing and shape optimisation of beam structures,” *Comput. Methods Appl. Mech. Eng.*, vol. 199, no. 17–20, pp. 1216–1230, Mar. 2010.
- [7] A. P. Nagy, S. T. IJsselmuiden, and M. M. Abdalla, “Isogeometric design of anisotropic shells: Optimal form and material distribution,” *Comput. Methods Appl. Mech. Eng.*, vol. 264, pp. 145–162, Sep. 2013.
- [8] J. Kiendl, K.-U. Bletzinger, J. Linhard, and R. Wüchner, “Isogeometric shell analysis with Kirchhoff–Love elements,” *Comput. Methods Appl. Mech. Eng.*, vol. 198, no. 49–52, pp. 3902–3914, Nov. 2009.
- [9] S. Yiannoudes, “Kinetic Digitally-Driven Architectural Structures as ‘ Marginal ’ Objects - a Conceptual Framework,” *Footprint*, vol. 6, pp. 41–54, 2010.







Appendix D  
Patent



# TU Delft

Delft University of Technology

## Invention Disclosure Form

This document has been created with the interactive Inventor Portal.

### CONFIDENTIAL

Title of invention

**Statically Balanced Compliant Sound Barriers**

Involved faculties and departments

Please assign the faculties and departments involved in this invention, at least the faculty AND department you and your co-inventors are working for.

Faculty / Department\*

**SE Structural Engineering**

Faculty / Department

**PME Precision and Microsystems Engineering**

Faculty / Department

I want to register

**a NEW INVENTION in order to file a patent application**

To protect inventions made at TU Delft by filing a patent application the TU Delft Patent Department asks you to fill out the questions below. This information will be treated confidentially.

#### 1. Description

1a) Describe the invention briefly, in such a way that an educated non-expert may understand the invention\*

**The idea is to come up with soundbarriers that are interactive. They disappear when not needed and erect when needed. You might know that ordinary sound barriers are big, heavy and rigid. Deforming such a structure costs a lot of energy and therefore also force. In order to make this structure deform with the least amount of energy, we intend to make it statically balanced. This basically means that there is one part that is contributing as positive stiffness, while the other part is contributing as negative stiffness. These two quantities cancel each other out and result in zero stiffness. Statically balanced mechanism are applied on a very small scale. This is the first time that this method is applied on a scale of 6 meters high. Besides, conventional sound barriers are made of different particles, hinges etc. This solution offers a monolithic approach, which looks very elegant. See the attached picture.**

1b) Do you have a scientific description and/or drawings of the invention?\*

**Yes (Please attach)**

Scientific description and/or drawings

**IMG\_9863.JPG**

**IMG\_9874.JPG**

**10.png**

1c) State key words\*

**Underactuated, Static Balancing, Zero stiffness, Monolithic, Sound Barrier, Compliant Mechanism, Interactive Building**

1d) In which phase of development is the invention?\*

**Model**

What will be the development phase over 6 months? And what will it be over 11 months?\*

**MSc Graduation**

1e) Which (scientific) results have been achieved applying the invention?\*

**Depends on whether we continue with this topic after I graduate or not.**

1f) How can patent infringement be detected?\*

**I don't really know**

2. Novelty and Inventive step

2a) Which aspects of the product or steps in the method are new and improve on the current state of the art?\*

**The novelty is that we are able to deform large structures with the least amount of energy. Besides this, we are able to make large monolithic structures out of plastic for instance.**

2b) For which problem has a solution been found and how does the invention solve this problem? Which significant advantages does the invention offer?\*

**The problem was that large deformations of large structures cost a lot of energy. This is solved by making this large structure monolithic and statically balanced.**

2c) How has this problem been resolved till now, are there alternative solutions?\*

**This problem has not been solved until now.**

**Alternatives can be something like Pseudo Rigid Body Mechanisms (PRBM). However, this is also not checked and done before. Although, Hyperbody tried to make an interactive tower by using pneumatic muscles (google: Hyperbody Muscle Tower)**

2d) What is not obvious in the invention?\*

**It is not obvious that the shape acts like two opposite springs that cause a constant energy field. It is also not obvious that we could design or invent such an application in a monolithic sense.**

2e) In which respect is the invention better than the alternatives? (Is the invention for example more accurate, faster, cheaper etc.) What are the drawbacks of the invention for the user (in terms of quality and quantity)?\*

**It is cheaper, less parts are needed, made of one sheet plastic for instance, speed depends on actuation, lightweight.**



2f) How do you evaluate the impact or size of the invention? Explain.\*

**This approach will change the whole design of interactive buildings. It will have an influence in the fields of structures, architectures, mechanisms, aesthetics and many more. Imagine we could invent a bridge, which can change of shape, made of one sheet plastic or so, and requires almost zero energy. Or imagine to invent one flat sheet of plastic that could change into a chair. Or a door that changes its shape in order to open or close.**

2g) Has the invention been disclosed? \*

**No**

Are there any plans to disclose the invention in the near future?\*

**No**

2h) State of the art: \*

Any publication (paper, patent, thesis, conference presentation, etc.) on the same topic as your invention or which come close to it, including your own, may jeopardise the novelty and/or inventiveness of your invention and consequently its patenting. We therefore ask you to perform a search on patents and publications in the field of your invention.

Please list all relevant publications found. Briefly summarise the main points of each publication and describe and discuss the differences and similarities with your invention.

**Statically balanced mechanisms**

3. Industrial and/or commercial applicability

3a) What are potential fields of commercial application and what are your expectations with regard to market potential? \*

**Well, of course rail way engineering. Besides this, the building industry, like architecture or so. Other fields who deal with furniture for instance and probably many more that I can't foresee now.**

3b) When is competition from next-generation technology reasonably likely?\*

**I don't understand this question?**

3c) Which development is needed to arrive at a tradable product or commercially applicable method? Please state how, what and by whom? Describe important and significant steps in the development process and (estimates of) related costs and timeframes.\*

**There needs to be a thorough investigation about applying the specific materials, like plastic, outside in the environment. Next to this, a thorough investigation on how to actuate it in the best manner. Besides this, a thorough investigation on how to absorb or reflect sound that originated from passing trains. The latter is only applicable if we are planning to use this method for determining sound barriers.**

3d) Are partners/co-financiers willing to contribute to the further development and/or patent application?\*

**Not identified**

3e) Identify potential developers, producers and users\*

**ProRail, NS, Festo...**

4. Funding

These questions are meant to clarify the funding of the research from which the patent was a result and by whom the inventor's salary (inventors' salaries) is (are) paid. This may have consequences for IP property rights and, hence, for sharing of costs and/or revenues.

4a) How is the research funded from which the invention is a result?\*

**Contract funding (derde geldstroom)**

4b) Please list the persons, companies or organisations involved in the research which led to the invention, for example the EU KP7, Senternovem, IOP, NWO, STW, SON, FOM, Marie Curie etc. and/or companies like DSM, Philips, Shell etc.

Person / organisation / company

Type of involvement

Extent of involvement

---

Person / organisation / company

Type of involvement

Extent of involvement

---

Person / organisation / company

Type of involvement

Extent of involvement

For providing further information please use the text box in the additional information section.

4c) Do any of these third parties hold any rights to the invention?\*

**Not applicable**

4d) Is a third party stated above involved in payment of (part of) the salary of one or more inventor(s)?\*

**Not applicable**

5. Patent attorney

Do you prefer a specific patent attorney?

**No**

What is the required technical or scientific field of expertise?

**Structural Engineering, Architecture, Mechanical Engineering, Material Engineering, Acoustic Engineering**

Further attachments and other remarks

Please state any further comments and/or questions

Further attachments

## Details on person of inventor(s)

Surname	Alkisaiei	Herder	Sluys	Bier	Radaelli
First name	Hussen	Justus	Lambertus Johannes	Henriette Hildegard	Giuseppe
external co-inventor	no	no	no	no	yes
Salutation					
Initials	H.	J.L.	L.J.	H.H.	
E-Mail	h.alkisaiei@tudelft.nl	j.l.herder@tudelft.nl	l.j.sluys@tudelft.nl	h.h.bier@tudelft.nl	G.Radaelli@tudelft.nl
Employer					
Nationality					
Street address:					
Zip/Postal code, Town					
Country					
Comment					
What is your share of the invention?	20%	20%	20%	20%	20%
I agree that personal data will be used and forwarded for patent administration purposes (e.g. to external patent attorneys, etc.).					
To my knowledge, no other persons are involved in the invention.					
	(Date, Signature)	(Date, Signature)	(Date, Signature)	(Date, Signature)	(Date, Signature)

**This invention has been disclosed to the TU Delft patent department on 28/04/2015 .**



Rijksdienst voor Ondernemend  
Nederland

## Ontvangstbevestiging

Ontvangstbevestiging van uw verzoek om een aanvraag om een octrooi bij Octrooi Centrum Nederland:

Behandelingsnummer	500140587	
(voorlopig) aanvraagnummer	N2015722	
Datum ontvangst	04 november 2015	
Ontvangend bureau	Octrooi Centrum Nederland, Den Haag	
Uw referentie	016504 NL-PD	
Aanvrager	Technische Universiteit Delft	
Aantal aanvragers	1	
Land van herkomst	NL	
Korte aanduiding	Barrier	
Meegestuurde documenten	package-data.xml application-body.xml UITTR.pdf\151104 LS 016504 NL-PDabstract.pdf (1 p.) CONCL.pdf\151104 LS 016504 NL-PDconclnedeneng.pdf (4 p.) 4001UITV-1.pdf (1 p.) 4001UITV-3.pdf (1 p.) 4001UITV-5.pdf (1 p.)	nl-request.xml nl-request.pdf (2 p.) BESCHR.pdf\151104 LS 016504 NL-PDdescription.pdf (5 p.) TEK.pdf\151104 LS016504 NL- PDfigsind.pdf (1 p.) 4001UITV-2.pdf (1 p.) 4001UITV-4.pdf (1 p.)
Ingediend door	CN=Jacques van Breda 11746	
Methode van indiening	Online	
Datum en tijd aanmaak ontvangstbevestiging	04 november 2015, 16:56:50 (CET)	
Unieke reeks tekens	D3:65:DE:F6:DD:76:DE:50:3C:7F:3C:6C:D3:D6:77:8B:95:52:C9:0C	

/Octrooi Centrum Nederland, Team Octrooi register, tel. 088-6026000/

**ABSTRACT**

Barrier, for instance suitable for use as barrier along rail-ways or traffic ways, comprising an assembly of a barrier body and supports for said barrier body, wherein the assembly is statically balanced and provided with a collapsed configuration and an erected configuration, wherein the erected  
5 configuration is stable and movement of the barrier body out of the erected configuration causes gravity to operate as a driver moving the assembly to the collapsed or flattened configuration.

## Barrier

The invention relates to a barrier, for instance suitable for use along rail-ways or traffic ways, comprising  
5 an assembly of a barrier body and a support for said barrier body.

Such a barrier is commonly applied to reduce the noise of traffic, in particular moving trains on railways and moving cars on motorways. A disadvantage of the known barrier  
10 that it spoils the view since it is always present, even when its presence is not necessary in situations of low traffic conditions.

It is an object of the invention to provide a barrier in which the disadvantage of the known barrier is countered or  
15 reduced, and wherein further advantages are achieved as will become apparent from the following disclosure.

The barrier of the invention has the features of one or more of the appended claims.

First and foremost the barrier of the invention is  
20 characterized in that the assembly is stable in a fully erected configuration and statically balanced in a range of positions between a collapsed or flattened configuration up to the fully erected configuration, wherein movement of the barrier body out of the erected configuration causes gravity to oper-  
25 ate as a main driver moving the assembly to the collapsed configuration. This provides a solution to the problem of the ever present barrier of the prior art. Of course the term 'statically balanced' as used in this application also includes the situation that not a perfect static balancing of the barrier  
30 is achieved, but also an almost perfect static balancing which is reflected in the term "essentially" in the appended claims. The barrier of the invention can be moved to the collapsed or flattened configuration when it serves no purpose. Advantageously then only little energy will be required to move the  
35 barrier from the erected configuration into the collapsed or flattened configuration, since only the erected configuration is stable and once the barrier is moved out of the erected configuration, essentially gravity suffices to move the assembly gently through a range of statically balanced positions to

the collapsed or flattened configuration.

In an alternative embodiment according to the invention it is possible that the assembly is also statically balanced in the fully erected configuration, wherein stability of the assembly in the fully erected configuration is provided by additional stability means securing the assembly in the fully erected configuration. Of course the operation of the stability means must be interrupted once it is desired to have the assembly move from the erected configuration into the collapsed or flattened configuration. Suitable stability means for securing the assembly in the fully erected configuration can for instance be provided in the form of an appropriate lock.

It is advantageous that the barrier of the invention comprises drive means for moving the assembly out of or back to the erected configuration. Moving of the barrier out of or back to the erected configuration is relatively effortless and does not require much additional energy input from the drive means.

There are many ways in which the drive means can operate, but preferably the drive means operate on the support and/or on the barrier body.

There are also many possible embodiments that may be applied for the drive means. Preferably the drive means are selected from the group comprising a motor, a winch, pneumatics, hydraulics, cables. The drive means may then operate directly on the barrier body or on the support for the barrier body, depending on what best suits the requirements of the situation. Consistent therewith the support may be selected to be fixed, rotatable, or translatable.

In another aspect of the invention the barrier body is monolithic. In this manner the assembly can be embodied to be compliant and statically balanced with notable advantages, i.e. inherently no friction or backlash, inherently no lubrication required, and obviously no assembly of separate components.

Preferably the barrier body is an elastic body. The elastic body can absorb potential energy when the barrier body deforms going from the erected configuration to the collapsed

configuration, and release said potential energy going back from the collapsed or flattened configuration to the erected configuration. Obviously this is very beneficial for restricting energy consumption. Suitably the barrier body is embodied  
5 in a plastic or artificial material.

Further it is preferable that the barrier body is transparent. Even when the barrier is in the erected configuration, the view to the environment is then only moderately impaired.

10 The invention is also embodied in an assembly of a series of barriers according to the invention, wherein each single barrier of the series of barriers is independently operable.

This is advantageous particularly when the assembly  
15 also has one or more sensors, and operation of each single barrier of the series of barriers is determined by a parameter or parameters monitored by said one or more sensors. In an exemplary embodiment for instance the parameter can be a local noise level or a mass of a passing train at a predetermined  
20 distance of said single barrier. This opens up the possibility that the single barriers of the series of barriers are operated consecutively in accordance and in synchronicity with a moving train to absorb or reflect the sound of said moving train.

25 The invention will hereinafter be further elucidated with reference to the drawing of an exemplary embodiment of an apparatus according to the invention that is not limiting as to the appended claims.

In the drawing:

30 -figure 1 shows a laboratory scale barrier according to the invention in an erected configuration; and

-figure 2 shows the laboratory scale barrier of figure 1 in a collapsed or flattened configuration.

35 Whenever in the figures the same reference numerals are applied, these numerals refer to the same parts.

Making reference to both figure 1 and figure 2, an exemplary barrier 1 according to the invention is shown in respectively an erected configuration and in a collapsed or flattened configuration. It is remarked that the said figures



1 and 2 show the barrier 1 on a laboratory scale, yet in practice the barrier may be for instance 6 m high when in the erected configuration to make it suitable for use as barrier along rail-ways or traffic ways.

5           Figures 1 and 2 show that the barrier 1 comprises an assembly of a barrier body 2 and supports 3, 4 for said barrier body 2. The assembly of said barrier body 2 and supports 3, 4 is statically balanced in a range of positions between a collapsed or flattened configuration as shown in figure 2 up  
10 to but excluding the fully erected configuration shown in figure 1 which is stable. A slight movement of the barrier body 2 out of the erected configuration shown in figure 1 causes gravity to operate as a driver moving the assembly gently through a range of statically balanced positions starting  
15 slightly out of the erected configuration and ending in the collapsed configuration shown in figure 2. Although it is not shown in the figures it is also feasible to configure the assembly as being statically balanced also in the fully erected configuration, wherein stability of the assembly in the fully  
20 erected configuration is then provided by additional stability means securing the assembly in the fully erected configuration.

          Figure 2 shows an example of the barrier 1 comprising additional drive means 5 for moving the assembly out of the  
25 erected configuration. Likewise the drive means can be configured to move the assembly back from the collapsed or flattened configuration to the erected configuration.

          In the laboratory setting of figure 2 the drive means 5 operate on the barrier body 2, yet it is envisaged that in a  
30 full-scale barrier the drive means will be applied to operate on the supports 3, 4 of the barrier body 2. Depending on the configured actual situation the drive means are preferably selected from the group comprising a motor, a winch, pneumatics, hydraulics, cables, whereas the supports 3, 4 are selected to  
35 be either fixed, rotatable, or translatable.

          Preferably the barrier body 2 is an elastic body. As is shown in figure 1 and figure 2 the barrier body 2 is preferably monolithic, and more preferably it is embodied in a plastic or artificial material. It can also be seen that pref-

5

erably the barrier body 2 is transparent.

Although not further shown in the figures, the invention is also embodied in an assembly of a series of barriers 1 according to the invention, wherein each single barrier 1 of  
5 the series of barriers is independently operable. Particularly in that situation it is preferred that the assembly has one or more sensors 6 (see figure 1), wherein operation of each single barrier 1 of the series of barriers is determined by a parameter or parameters monitored by said one or more sensors 1.  
10 Preferably the sensor is a sound pressure level sensor or a load cell, wherein the parameter is a local noise level or a mass of a passing train at a predetermined distance of said single barrier 1. This makes for instance possible that the single barriers of the series of barriers are operated consec-  
15 utively in accordance and in synchronicity with a moving train to absorb or reflect the sound of said moving train as monitored with the one or more sensors 1.

Although the invention has been discussed in the foregoing with reference to an exemplary embodiment of the apparatus of the invention, the invention is not restricted to  
20 this particular embodiment which can be varied in many ways without departing from the invention. The discussed exemplary embodiment shall therefore not be used to construe the appended claims strictly in accordance therewith. On the contrary,  
25 the embodiment is merely intended to explain the wording of the appended claims without intent to limit the claims to this exemplary embodiment. The scope of protection of the invention shall therefore be construed in accordance with the appended  
30 claims only, wherein a possible ambiguity in the wording of the claims shall be resolved using this exemplary embodiment.

**CONCLUSIES**

1. Wal (1), bijvoorbeeld geschikt voor gebruik langs het spoor of verkeerswegen, omvattende een samenstel van een wallichaam (2) en een drager (3, 4) voor genoemd wallichaam (2), **met het kenmerk**, dat het samenstel stabiel is in een volledig opgerichte configuratie en in hoofdzaak statisch gebalanceerd in een bereik van posities tussen een ingeklapte of vlakke configuratie tot aan de volledig opgerichte configuratie, waarbij een beweging van het wallichaam (2) uit de volledig opgerichte configuratie veroorzaakt dat zwaartekracht werkzaam is als een drijvende kracht die het samenstel door het bereik van statisch gebalanceerde posities brengt naar de ingeklapte configuratie.

2. Wal volgens conclusie 1, **met het kenmerk**, dat het samenstel tevens statisch gebalanceerd is in de volledig opgerichte configuratie, waarbij stabiliteit van het samenstel in de volledig opgerichte configuratie voorzien is door additionele stabiliteitsmiddelen die het samenstel zekerstellen in de volledig opgerichte configuratie.

3. Wal volgens conclusie 1 of 2, **met het kenmerk**, dat deze aandrijfmiddelen (5) bezit voor het bewegen van het samenstel uit of terug naar de volledig opgerichte configuratie.

4. Wal volgens conclusie 3, **met het kenmerk**, dat de aandrijfmiddelen werkzaam zijn op de drager (3, 4) en/of op het wallichaam (2).

5. Wal volgens conclusie 3 of 4, **met het kenmerk**, dat de aandrijfmiddelen geselecteerd zijn uit de groep omvattende een motor, een lier, pneumatiek, hydraulica, kabels.

6. Wal volgens één der conclusies 1 - 5, **met het kenmerk**, dat de drager (3, 4) geselecteerd is met de eigenschap gefixeerd, roteerbaar, transleerbaar.

7. Wal volgens één der conclusies 1 - 6, **met het kenmerk**, dat het wallichaam (2) monolithisch is.

8. Wal volgens één der conclusies 1 - 7, **met het kenmerk**, dat het wallichaam (2) een elastisch lichaam is.

9. Wal volgens één der conclusies 1 - 8, **met het kenmerk**, dat het wallichaam (2) is uitgevoerd in een kunststof of kunstmatig materiaal.

10. Wal volgens één der conclusies 1 - 9, **met het kenmerk**, dat het wallichaam (2) transparant is.

11. Samenstel van een reeks wallen (1) volgens één der conclusies 1 - 10, **met het kenmerk**, dat iedere afzonderlijke wal (1) van de reeks wallen onafhankelijk werkzaam is.

12. Samenstel volgens conclusie 11, **met het kenmerk**, dat deze één of meer sensoren (6) bezit, waarbij werkzaamheid van iedere afzonderlijke wal (1) van de reeks wallen bepaald wordt door een parameter of parameters die bewaakt worden door genoemde één of meer sensoren (6).

13. Samenstel volgens conclusie 12, **met het kenmerk**, dat de parameter een lokaal geluidsniveau of een massa op een vooraf bepaalde afstand van genoemde afzonderlijke wal (1) is.

14. Samenstel volgens conclusie 12 of 13, **met het kenmerk**, dat de enkele wallen van de reeks wallen achtereenvolgens werkzaam zijn in overeenstemming met en in synchroniciteit met een bewegende trein voor het absorberen of reflecteren van het geluid van genoemde bewegende trein.

CLAIMS

1. Barrier (1), for instance suitable for use along railways or traffic ways, comprising an assembly of a barrier body (2) and a support (3, 4) for said barrier body (2), **characterized in that** the assembly is stable in a fully erected configuration and essentially statically balanced in a range of positions between a collapsed or flattened configuration up to the fully erected configuration, wherein a movement of the barrier body (2) out of the erected configuration causes gravity to operate as a driver moving the assembly through the range of statically balanced positions to the collapsed configuration.

2. Barrier according to claim 1, **characterized in that** the assembly is also statically balanced in the fully erected configuration, wherein stability of the assembly in the fully erected configuration is provided by additional stability means securing the assembly in the fully erected configuration.

3. Barrier according to claim 1 or 2, **characterized in that** it comprises drive means (5) for moving the assembly out of or back to the fully erected configuration.

4. Barrier according to claim 3, **characterized in that** the drive means operates on the support (3, 4) and/or on the barrier body (2).

5. Barrier according to claim 3 or 4, **characterized in that** the drive means are selected from the group comprising a motor, a winch, pneumatics, hydraulics, cables.

6. Barrier according to any one of claims 1 - 5, **characterized in that** the support (3, 4) is selected to be fixed, rotatable, translatable.

7. Barrier according to any one of claims 1 - 6, **characterized in that** the barrier body (2) is monolithic.

8. Barrier according to any one of claims 1 - 7, **characterized in that** the barrier body (2) is an elastic body.

9. Barrier according to any one of claims 1 - 8, **characterized in that** the barrier body (2) is embodied in a plastic or artificial material.

10. Barrier according to any one of claims 1 - 9,

7

**characterized in that** the barrier body (2) is transparent.

11. Assembly of a series of barriers (1) according to any one of claims 1 - 10, **characterized in that** each single barrier (1) of the series of barriers is independently operable.

12. Assembly according to claim 11, **characterized in that** it has one or more sensors (6), wherein operation of each single barrier (1) of the series of barriers is determined by a parameter or parameters monitored by said one or more sensors (6).

13. Assembly according to claim 12, **characterized in that** the parameter is a local noise level or a mass at a predetermined distance of said single barrier (1).

14. Assembly according to claim 12 or 13, **characterized in that** the single barriers of the series of barriers are operated consecutively in accordance and in synchronicity with a moving train to absorb or reflect the sound of said moving train.

1/1

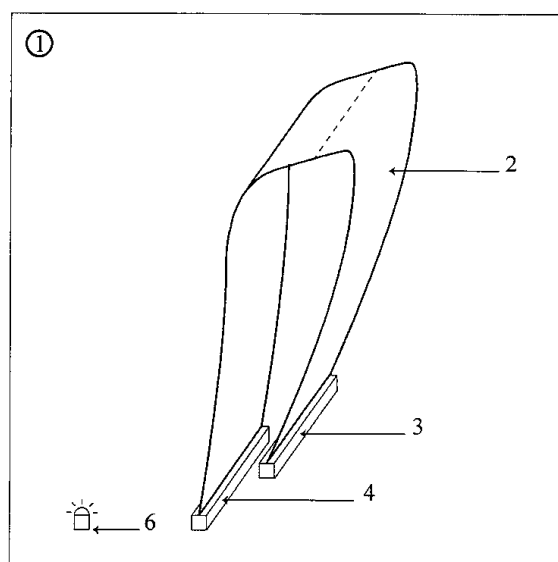


Figure 1

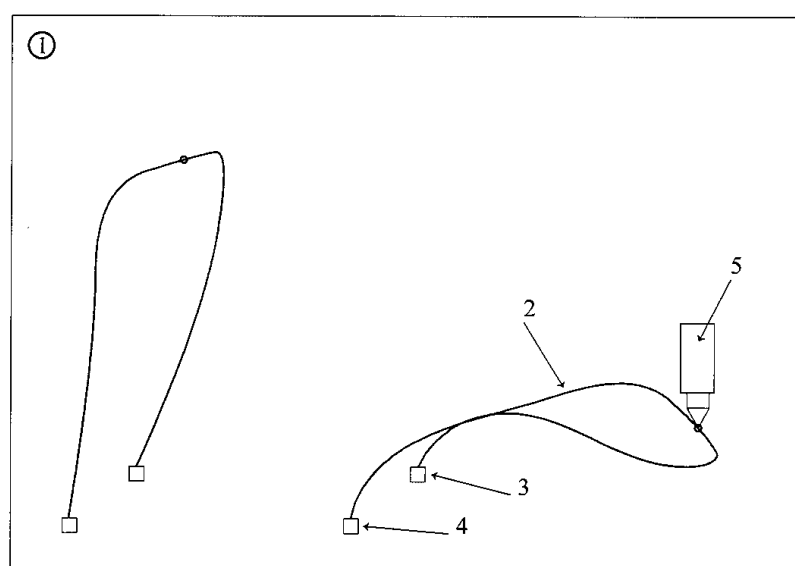


Figure 2

## Technische Universiteit Delft

Corporate and Legal Affairs

P.O. Box 5                      Stevinweg 1  
2600 AA Delft                  2628 CN Delft  
The Netherlands              The Netherlands

### Patent claim transfer agreement

#### The parties signing,

Technische Universiteit Delft, Established at Delft, Stevinweg 1, 2628 CN Delft, duly represented by the dean of the faculty of **Civil Engineering and Geosciences, Bert M. Geerken** [*name dean*], hereinafter named "TU Delft", on the one hand,

and

**Hoessein Alkisaie** [*name student*], living at **Rijswijkseplein 322, 2516 LJ, Den Haag, NL** [*adres*], born d.d. **17-12-1988**, student at the faculty **Civil Engineering and Geosciences**, supervised by **L.J. (Bert) Sluys** [*name supervisor*], hereinafter named "Student", on the other hand,

#### Consider that:

- Student works or worked at the research project entitled: **Statically Balanced Compliant Sound Barrier** "hereinafter called "the Project";
- Co-workers of the Project are the inventors of a potential patentable invention concerning the Project;
- Student is one of the inventors of the invention entitled: **Statically Balanced Compliant Sound Barrier**, hereinafter called "the Invention";
- TU Delft wishes to get the full ownership of the intellectual property rights regarding the Project.
- TU Delft, as the sole applicant, files an application for a patent on the Invention.

#### Agree as follows:

1. Student delegates to TU Delft his/her patent rights on the Invention by undersigning of this agreement.
2. TU Delft assumes the patent rights on the Invention.
3. At the moment TU Delft earns revenues related to the Invention, in accordance with the rules of TU Delft Student will receive earnings in recompense for the transfer of his/her rights on the potential patent application c.q. granted patent regarding the Invention as if he/she is or was a staff member of TU Delft.
4. The potential patent application will state the name of Student if he/she is an inventor or one of the inventors.

#### Drawn up and subscribed in duplicate at Delft,

##### TU DELFT:

Date: .....

Name supervisor: **L.J. (Bert) Sluys**

Initial supervisor: .....

Signature dean: .....

##### Student:

Date: **20-5-2015**

Name: **Hoessein Alkisaie**

Signature:

